Modelling the Impact of Total Stress Changes on Groundwater Flow

A thesis
Submitted to the College of Graduate Studies and Research
In Partial Fulfillment of the Requirements for the Degree of
Master of Science
In the
Department of Civil and Geological Engineering
University of Saskatchewan
Saskatoon, SK, Canada

By

Dissanayake Nalinda Laksiri Dissanayake

Permission to Use

In presenting this thesis in partial fulfillment of the requirements for a postgraduate degree from the University of Saskatchewan, I agree that the Libraries of this University may make it freely available for inspection. I further agree that permission for copying of this thesis in any manner, in whole or in part, for scholarly may be granted by the professor or professors who supervised my thesis work or, in their absence, by the Head of the Department or the Dean of the College in which my thesis work was done. It is understood that any copying, publication, or use of this thesis or parts thereof for financial gain shall not be allowed without my written permission. It is also understood that due recognition shall be given to me and to the University of Saskatchewan in any scholarly use which may be made of any material in my thesis.

Requests for permission to copy or to make other use of material in this thesis in whole or part should be addressed to:

Head of the Department of Civil and Geological Engineering
University of Saskatchewan
Saskatoon, Saskatchewan
S7N 5A9
Canada

ABSTRACT

The research study involved using the modified FEMWATER code to investigate the impact of total stress changes on groundwater flow in the vicinity of a salt tailings pile. Total stress and pore-pressure data observed at the Lanigan and Rocanville potash-mine sites were used to assist the development of a generic FEMWATER model. The original 3-D mesh considered for model study covers a region of 7.6 km x 7.6 km x 60 m. The simulated pile itself covers a surface area of 1.6 km x 1.6 km within the region. Symmetry of the idealized system allowed half of the system to be modelled to reduce the size of the mesh. The model was layered to facilitate different materials representing different hydrostratigraphic scenarios. The GMS-release of the FEMWATER code (version 2.1) was modified to simulate the pore-pressure response to total stress changes caused by tailings pile loading at the ground surface to be modelled. The modified code was verified before applying to present study.

Long-term pore pressure generation and dissipation due to pile construction was investigated for eleven hydrostratigraphic scenarios consisting of plastic clays, stiff till and dense sand layers commonly found in Saskatchewan potash mining regions. The model was run for two distinctive pile loading patterns. Model results indicated that the loading pattern has a significant influence on pore pressure generation beneath the pile. The model was initially run for 30 year pile construction period and later simulated for 15, 25 and 35 year construction periods to investigate the impact of loading rate. These results showed that, as expected, the peak pore water pressure head is proportional to the pile construction rate. A sensitivity analysis, which was carried out by changing hydraulic conductivity of stiff till, revealed that the lower the hydraulic conductivity, the greater the pore pressure generation beneath the pile.

Overall, the research study helped to understand and predict the influence of pile construction and hydrostratigraphy on pore-pressure changes beneath salt tailing piles. Low K/S_s or c_v materials (compressible tills) demonstrate a slow dissipation rate and

high excess pressures. Compared to dense sand which has very high K/S_s, till has very low K/S_s which causes in high excess pore pressure generation. Sand layers act as drains, rapidly dissipating pore pressures. Thicker low K/S_s units result in slower dissipation and higher pressures. As the thickness of the low K/S_s layer increases, the peak pressures increase as the drainage path lengthens. Thin plastic clay layers give rise to the highest pressures.

The model study showed that hydrostratigraphic scenarios similar to those found at Saskatchewan potash mine sites can generate the high pore pressures observed in the vicinity of salt tailings piles as a result of pile loading. Peak pressures are very sensitive to pile construction rates, loading patterns and hydrostratiagraphy of the region. Peak pressures can reach levels that would be of concern for pile stability on the presence of adverse geological conditions.

ACKNOWLEDGEMENTS

I find this as a great opportunity to acknowledge for those who assisted and encouraged me for the accomplishment of my graduate studies and research.

First I would like to declare my sincere gratitude to my supervisor Prof. Malcolm Reeves for his invaluable support and amicable guidance throughout the course of study. I would also like to thank Assistant Professor Chris Hawkes and Associate Professor Ian Fleming; graduate advisory Committee members, Michelle Uwiera; the external examiner for their valuable inputs and constructive criticism during the progress of this work. Associate Professors Doug Milne and Jitendra Sharma are also appreciated for chairing my final defense and committee meetings respectively.

My very special thanks go to Dr. Sumith P. Kahanda and Dr. Chandima Karunanayake for their help, encouragement and guidance throughout my studies and even before. My sincere gratitude is extended to Dr. Lal Samarasekera who helped and guided me in many ways during my studies.

I foremost owe a very special debt of gratitude to my beloved wife Kishari Sooriya Arachchilage, whose unfailing support, understanding and encouragement shown during difficult times.

Timely help provided by the library staff and the Engineering computer Centre staff is also appreciated. I am grateful to all my colleagues and friends at the University of Saskatchewan and in Saskatoon for making my stay, a wonderful and memorable experience.

Financial assistance provided by Prof. Malcolm Reeves together with Saskatchewan Potash Produces Associations is greatly appreciated.

DEDICATION

This thesis is dedicated to my beloved parents who gave unwavering support, constant encouragement and paid immense sacrifice for the success in my academic career.

TABLE OF CONTENTS

LIST OF TABLES

LIST OF FIGURES

1. INTRODUCTION

1.1 General Background

Potash mining in Saskatchewan has been operating for over four decades. Saskatchewan's potash industry is one of the largest in the world and produces a considerable volume of mining waste annually. Management of this massive amount of tailings require engineering expertise as the pile stability and the groundwater flow in the vicinity of tailings piles can have adverse consequences.

During potash mining, solid waste products (mainly salt) are stored in large piles on surface at the mine sites. Liquid wastes (brine) are stored in tailings ponds before disposal by deep well injection. Currently, 10 tailings piles and ponds of various sizes are in operation in Saskatchewan Tailing Management Areas (TMAs). Pile construction is a long-term process. Pile life can vary from 15-40 years depending on the amount of waste to be stacked and the area available. Salt tailings piles cover large areas and these areas are underlain by both local and/or regional aquifers. Brine migration from the TMAs to these subsurface aquifers is unavoidable and its control and mitigation is a challenging environmental problem.

Proper management schemes for controlling contaminant transport through these aquifers are essential for a tailings facility. In the study of the influence of salt tailing piles on groundwater flow, field-monitoring systems can provide useful data such as pressure head and brine concentration at a given time at a known location. However, the prediction of long-term impact of pile construction is of primary importance for TMAs. Due to the complexity of the hydrostratigraphy, three-dimensional (3-D), density dependent groundwater flow and transport models are perhaps the only feasible method of predicting the long-term impact of pile loading on regional groundwater flow.

1.2 Pile Loading Effect on Aquifers

Over the past years much research has been conducted to investigate the long-term impact of pile construction on regional groundwater flow. The pile construction rate, the geometry of the pile, the properties of the tailings as well as the hydrostratigraphy can be identified as influential factors on groundwater flow in the vicinity of a tailings pile.

During construction, the aquifer and aquitards beneath the pile are subjected to loading and the total stress can significantly change with time. Research related to the impact of total stress changes due to potash pile construction on groundwater flow and transport is limited. Aquitards beneath the pile undergo consolidation settlement with the pile construction over a long period. The loading effect of the pile on pore pressure generation and dissipation during pile construction is the key factor to be considered.

Depending on the geological conditions, significant pressure head can be generated in aquitards. The dissipation of these pressures by drainage to the aquifers influences regional groundwater flow and can extend for several kilometres. Outward radial gradients created by pile loading can provide the driving force for migration of contaminants in shallow and deep aquifers. Natural regional gradients in these aquifers are usually very small, consistent with low natural recharge rates. The brine migrations due to radial driving force and subsequent impact are out of the scope of the present study.

Most groundwater flow and transport codes are not developed to model time-dependent total stress changes, which is the focus of the current research. The study is an attempt to approximately model the impact of total stress changes during salt tailings pile construction on groundwater flow. Prediction of the influence of pile loading is made using the modified version of the FEMWATER code that incorporates total stress changes as a result of pile loading.

1.3 Geometry of Potash Tailing Piles

The pile geometry is an important factor in the development of pile loading. A typical tailings pile is roughly triangular in cross-section with height varies from 40 to 70 m. Under pressure from regulators, the mining companies attempt to minimize the area impacted by tailing piles by building them as high as possible on the smallest possible

footprint. The height is restricted by stability considerations and by the capital and energy costs associated with pumping tailing to greater heights (Landine, 1993).

A cross section of a typical tailings pile is illustrated in Figure 1.1. Major components of a TMA are the tailings pile, brine pond, berm and the drainage ditch. During pile construction, the long slope of a pile is maintained at a slope angle 2-3^0. If the long slope is kept flat, fine material can settle out on the pile rather than in the brine pond. Typical slope angles for the steep scarp slope of the pile can vary from 30-40^0. This construction geometry increases the useful life of the pond. The berm prevents brine spreading on the surface outside the TMA.

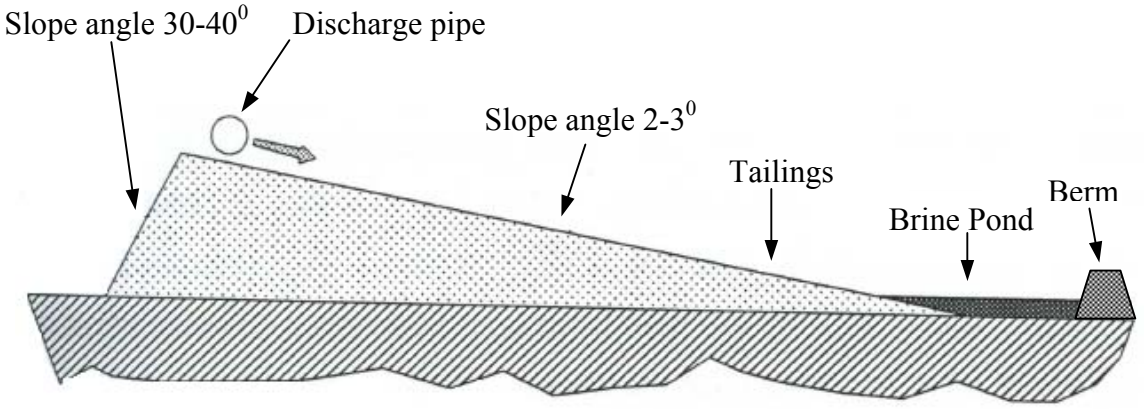

Figure 1.1: Typical cross section of a salt tailings pile (after Loi, 1988)

1.4 Hydrostratigraphy

The hydrostratigraphy varies considerably from place to place and has significant influence on the groundwater flow behaviour. Sands, stiff tills and plastic clay units are

commonly found in the shallow subsurface in Saskatchewan potash mining regions. Model investigations were carried out for various combinations of these materials for better understanding of pore pressure development and dissipation.

Sands have relatively high hydraulic conductivities; for example, in the 10^{-5} to 10^{-4} m/s range. Significant pore pressure generation caused by loading in such permeable units is not possible at loading rates that may reasonably be achieved in the field. In tills, hydraulic conductivity is lower (e.g., typically 10^{-8} to 10^{-10} m/s). Till units have much slower pore pressure dissipation rates, compared to sand units, and can build up significant excess pressures as a result of loading. Clayey units of moderate to high plasticity tend to have very low hydraulic conductivities. The pore pressure response to surface loading in such thin plastic clay units can be very large.

Figure 1.2 illustrates a typical hydrostratigraphic sequence with sand and till layers. Tailings pile construction results in pore pressure build-up in the till layers because of their low hydraulic conductivity. Possible pore pressure contour patterns are shown in till layers. Eleven hydrostratigraphic scenarios were considered for the present study. They are summarized in section 4.5.

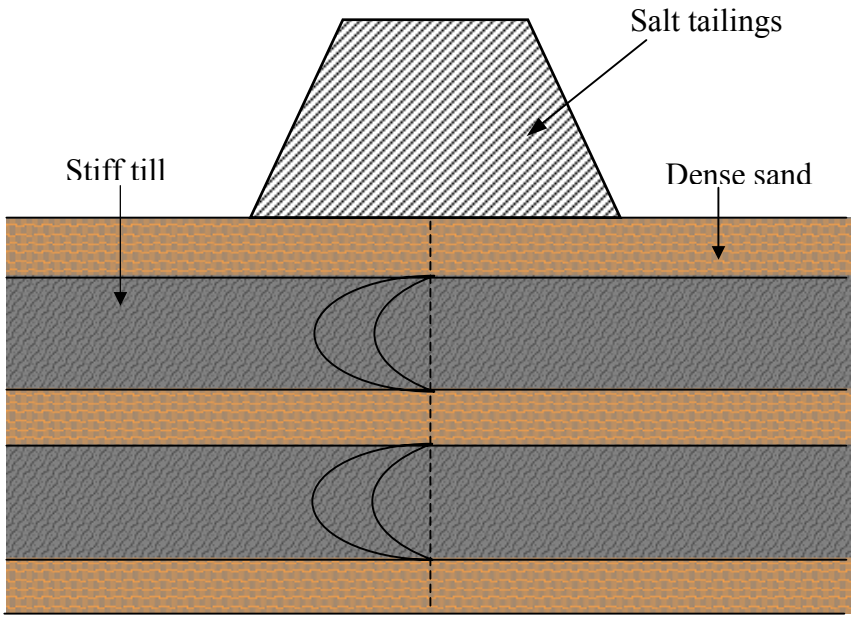

Figure 1.2: Layout Diagram of a Typical Hydrostratigraphic Scenario

1.5 Pile Loading Analysis using the FEMWATER Code

The groundwater flow and transport code FEMWATER (Lin et al., 2001) is a 3-D finite element computer code for simulating density dependent flow and transport in variably saturated media. This code has been selected for modelling saturated-unsaturated, variable-density flow and brine transport at the ten tailings management areas (TMA) associated with potash mining in Saskatchewan. The present study focuses only on an application of the code for modelling saturated flow under constant density conditions.

FEMWATER was originally developed for the U.S. Environmental Protection Agency and later updated by the U.S Army Corps of Engineers, Waterways Experiment Station (Lin et al., 2001). It is one of the codes supported by the U.S. Department of Defence

groundwater modelling system (GMS). For application to TMA problems, the GMS-release of the FEMWATER code was modified to allow pore-pressure response to total stress changes as a result of pile loading at the surface (Reeves, 2005).

As a result of the modifications made to the code, a study was conducted to independently verify the modified code (FEMWATER 2.1m). A series of benchmark solutions was undertaken to verify the modified code for a wide range of problems. Problems selected for the verification study included steady state and transient flow, variable-density flow, variably saturated flow and problems involving pore-pressure dissipation and generation and soil consolidation.

The verification study is out of the scope of the current research. The benchmark problems used for verification study are listed in Appendix A. Terzaghi's consolidation problem is discussed in details in Appendix A as it discusses the total stress changing in groundwater flow. In this problem, numerical model results are compared with the analytical solution of the Terzaghi's 1-D consolidation equation. A detailed verification study report was submitted to Saskatchewan Potash Producers Association (SPPA) to support the use of the model for brine transport predictions (Reeves and Dissanayake, 2006).

1.6 Research Objectives and Scope

The primary objective of the research is to apply the modified FEMWATER code to predict the influence of pile loading on groundwater flow. Long-term pore pressure generation and dissipation due to pile construction are investigated for eleven different hydrostratigraphic scenarios. The specific objective of the study is to investigate the pore water pressure development beneath a pile for a variety of loading rates and loading patterns.

Localized sand lenses within tills (not modeled in this study) can extend high pore-pressure zones beyond the toe of the slope with serious consequences for pile stability. The current study develops an understanding of the circumstances in which high pore-pressures can arise as a consequence of loading rate and hydrostratigraphy.

The model was run for four loading rates to identify the influence of loading rate on pore pressure development. Layered structures with single drainage and double drainage cases are considered. Pore pressure development is investigated for two distinctive loading patterns.

A sensitivity analysis was carried out to help understand the influence of material properties on pore pressure generation. Material properties including hydraulic conductivity (K) and specific storage (S_s) for generic hydrostratigraphic sand and till units are investigated. Existing thin clayey layers of high plasticity, which represent potential shear zones, are also considered in the study.

2. LITERATURE REVIEW

2.1 Introduction

Investigations related to groundwater response to total stress changes are relatively limited. In many practical situations, the assumption that total stress remains constant is not valid but most groundwater modelling codes are developed assuming this to be the case. Studies directly related to modelling total stress changes during salt tailings pile construction are limited. In this chapter, a few previous studies carried out in the area of total stress changes are briefly reviewed.

2.2 Total Stress Change Problems

It is possible to find a quite number of case histories related to total stress change. Gibson (1958) discusses the effect of changing total stress due to increasing clay thickness on the consolidation of a clay unit. In this study, increasing weight of superincumbent materials leads to pore pressure generation as the drainage path varies (Gibson, 1958). Similar pore pressure generation behavior that leads to change in total

stress can be observed during the construction of an earth dam (Eisenstein et al., 1977), and during sediment accumulation (Neuzil, 1993; 1995).

Thibodeau et al. (1998) describe a salt marsh system in which the total stress applied to the ground surface changes as the tidal load is applied and released periodically. In this study, the effective stress acting on the soil matrix does not change significantly and the majority of the domain of interest remains saturated. Neglecting effective stress changes, complex soil deformation models are not required to investigate ground water flow systems. Traditional groundwater flow models can be modified to approximate the effects of total stress changes and account for effective stress variation. A detailed discussion of the modifications that can be made can be found in the discussion of the USGS numerical model SUTRA (Reeves et al., 2000). FEMWATER was modified in a similar manner for the current study.

Hemond et al. (1984) discuss the importance of changing total stress on the observed pore water behavior in salt marsh peat sediments. Hemond and Fifield (1982) describe the importance of considering total stress changes to match model results to pore-pressure field data using a 1-D finite difference model study.

Bredehoeft and Hanshaw (1968) and Neuzil (1993, 1995) discuss overpressure and underpressure effects in aquifers and oil reservoirs. For these cases, sedimentation and erosion of the soil surface causes changes in total stress applied to the system.

Provost et al. (1998) discuss the change in total stress due to glaciations on crystalline rock aquifers. In this study, a long-term model investigation was conducted for a proposed nuclear waste repository in Sweden in order to investigate rock deformation.

Eigenbrod and Issigonis (1996) discuss a different situation. The study describes pile driving through a soft sensitive clay, and into very dense sand and gravel and resultant total stress changes. Piles were driven in soft clay and a very small pore pressure development was observed during the initial stage. During the second stage, a very high pore pressure was observed while penetrating into dense sand through soft clay. The reason is that the clay layer was loaded from below as the pile was driven into the dense sand layer. In this case, total stress changes and resulting pore water pressure changes in the clay layer was analyzed assuming the pile driving load is equivalent to a flexible load acting on the surface of an elastic half-space which represents the soft clay deposit (Eigenbrod and Issigonis, 1996).

Eisentein et al. (1977) discuss the total stress changes during earth dam construction. Embankments, in general, contain slowly draining materials that lead to simultaneous generation and dissipation of pore pressures. During dam construction, total stresses within a soil mass change during the consolidation process, even without a change in external load in order to maintain strain compatibility (Eisentein et al., 1977). A finite-element model was used to analyze the pore pressure generation and dissipation and hence the subsequent total stress changes during consolidation process. For the modelling analysis, the dam was assumed to be constructed in layers of soils and after each layer was placed, the model was run to investigate the total stress changes.

In this study, new loading and total stress conditions were represented by adding new layers to the model. This is similar to salt tailings pile construction in which the tailings are sequentially placed to increment total stress.

All the above case histories deal with the significance of taking total stress into consideration in groundwater flow modelling and pore pressure prediction. The present research focuses on modelling the long-term impact of total stress changes on groundwater flow.

3. THEORETICAL BACKGROUND

3.1 Introduction

This chapter discusses the theoretical background relevant to the modelling study. Firstly, incorporation of the total stress changes into the original FEMWATER (Lin et al., 2001) code is discussed in detail. The procedure used for FEMWATER is exactly analogous to the total stress incorporation procedure used by Reeves et al. (2000) for SUTRA (Voss, 1984). Secondly, the theoretical background relevant to the approximation of total stress distribution with depth is discussed.

3.2 Incorporation of Total Stress

3.2.1 Introduction

According to Reeves et al. (2000), most groundwater flow and transport models are developed on the assumption that the total stress imposed on the aquifer remains constant with time. This assumption is not valid for many practical situations in which aquifers are subjected to time-varying total stress.

In such situations, codes require the facility to model the pore pressure and total head response to the loading of the aquifer or aquitards and take the deformations of such units into consideration. The traditional groundwater flow equation can be modified to facilitate total stress changes if some simplifying assumptions are made.

The changes made to the FEMWATER code are exactly analogous to the changes reported by Reeves et al. (2000) for the SUTRA code. Pore pressure response due to surface loading in the groundwater flow equation can be accounted for considering the storativity term. The load is incorporated as a "pseudo" source-term.

3.2.2 Total Stress

In soil mechanics, total stress is defined as the sum of the effective stress and the pore pressure. For a given control volume, the general equation for total stress can be written as:

$$\sigma = \sigma' + P \qquad [3.1]$$

where

σ = Total stress, [$ML^{-1}T^{-2}$];

σ' = Effective stress, [$ML^{-1}T^{-2}$];

P = Pore pressure, [$ML^{-1}T^{-2}$].

In most situations, total stress remains constant while effective stress and pore water pressure vary. Considering a system in which the total stress remains constant, a mathematical expression for stress change could be written as:

$$d\sigma = d\sigma' + dP \qquad [3.2]$$

When total stress remains constant, $d\sigma$=0 and hence:

$$-d\sigma' = dP \qquad [3.3]$$

There are many practical situations in which the total stress does, to a reasonable approximation, remain constant. It is also common in many groundwater flow applications for pore pressure changes in aquifers to result in effective stress changes with no change in total stress. In such circumstances, equation [3.1] is approximately valid.

An example of a problem in which total stress obviously changes is the construction of an embankment. In such circumstances, the total stress clearly increases and changes in pore pressures are induced as a result of loading.

The ability to model the total stress changes and consequential pore pressure development is an important factor in selecting a groundwater flow and transport code for such a problem. Many codes do not allow for changes in total stress and this limits

their application to many problems dealing with total stress changes. In such situations, modifications to the original codes are often necessary to incorporate total stress change.

3.2.3 Incorporation of Total Stress Changes into FEMWATER Model

Voss (1984) expresses the mass balance equation, which describes flow in an aquifer as:

$$\frac{\partial}{\partial t}\left(n\rho g S_w\right) = \nabla.\left[\frac{k k_{rw}\rho g}{\mu}\left(\nabla P - \rho g\right)\right] + Q_p g \qquad [3.4]$$

where

S_w = Saturation of water, [ ];

ρ = Density of water, [ML^{-3}];

n = Porosity of the aquifer, [ ];

∇ =Del-operator, $\left(\frac{\partial}{\partial x}, \frac{\partial}{\partial y}, \frac{\partial}{\partial z}\right)$;

k =Intrinsic permeability tensor, [L^2];

k_{rw} = Relative permeability, [ ];

μ = Viscosity of water, [$ML^{-1}T^{-1}$];

P = Pore water pressure, [$ML^{-1}T^{-2}$];

g = Acceleration due to gravity, [LT^{-2}];

Q_p = A source term, [$ML^{-3}T^{-1}$].

Equation [3.4] can be rewritten by expanding the left hand side as:

$$ngS_w \frac{\partial \rho}{\partial t} + \rho g S_w \frac{\partial n}{\partial t} + n\rho g \frac{\partial S_w}{\partial t} = \nabla.\left[\frac{kk_{rw}\rho g}{\mu}\left(\nabla P - \rho g\right)\right] + Q_p g \qquad [3.5]$$

Using the chain rule, equation [3.5] can be further expanded as:

$$ngS_w \frac{\partial \rho}{\partial P}\frac{\partial P}{\partial t} + \rho g S_w \frac{\partial n}{\partial \sigma'}\frac{\partial \sigma'}{\partial t} + n\rho g \frac{\partial S_w}{\partial t} = \nabla.\left[\frac{kk_{rw}\rho g}{\mu}\left(\nabla P - \rho g\right)\right] + Q_p g \qquad [3.6]$$

where

σ' = Effective stress acting on the aquifer matrix, [$ML^{-1}T^{-2}$].

If matrix and water compressibilities are defined respectively as:

$$\alpha = -\frac{dn}{d\sigma'} \text{ and } \frac{dn}{d\sigma'} = -\alpha \qquad [3.7]$$

$$\beta = \frac{1}{\rho}\frac{d\rho}{dP} \text{ and } \frac{d\rho}{dP} = \rho\beta \qquad [3.8]$$

For a system with constant total stress, by substituting equations [3.7] and [3.8] in [3.6], the final form is obtained:

$$nS_w\rho g\beta\frac{\partial P}{\partial t}-S_w\alpha\rho g\frac{\partial \sigma'}{\partial t}+n\rho g\frac{\partial S_w}{\partial t}=\nabla.\left[\frac{kk_{rw}\rho g}{\mu}\left(\nabla P-\rho g\right)\right]+Q_p g \qquad [3.9]$$

Equation [3.9] is derived by neglecting the movement of soil particles and assumes a non-deformable control volume.

The impact of changing total stress on the surface can be incorporated into the governing equation as follows. The change of effective stress can be written in terms of total stress and pore pressure as:

$$\frac{d\sigma'}{dt}=\frac{d\sigma}{dt}-\frac{dP}{dt} \qquad [3.10]$$

Substitution of equation [3.10] into the mass balance equation [3.6] gives:

$$ngS_w\frac{\partial\rho}{\partial P}\frac{\partial P}{\partial t}+\rho gS_w\frac{\partial n}{\partial \sigma'}\left[\frac{\partial\sigma}{\partial t}-\frac{\partial P}{\partial t}\right]+n\rho g\frac{\partial S_w}{\partial t}=\nabla.\left[\frac{kk_{rw}\rho g}{\mu}\left(\nabla P-\rho g\right)\right]+Q_p g \qquad [3.11]$$

Rearranging the terms and substituting equations [3.7] and [3.8] in [3.11]:

$$ngS_w\rho\beta\frac{\partial P}{\partial t}-\rho gS_w\alpha\left[\frac{\partial\sigma}{\partial t}-\frac{\partial P}{\partial t}\right]+n\rho g\frac{\partial S_w}{\partial t}=\nabla.\left[\frac{kk_{rw}\rho g}{\mu}\left(\nabla P-\rho g\right)\right]+Q_p g \qquad [3.12]$$

Equation [3.12] can be further simplified as:

$$S_w(\alpha + n\beta)\rho g \frac{\partial P}{\partial t} + n\rho g \frac{\partial S_w}{\partial t} = \nabla.\left[\frac{kk_{rw}\rho g}{\mu}(\nabla P - \rho g)\right] + S_w \alpha \rho g \frac{\partial \sigma}{\partial t} + Q_p g \qquad [3.13]$$

The specific storage of the aquifer is defined by:

$$S_s = (\alpha + n\beta)\rho g \qquad [3.14]$$

Substituting specific storage term in Equation [3.13], the mass balance equation can be written:

$$S_s S_w \frac{\partial P}{\partial t} + n\rho g \frac{\partial S_w}{\partial t} = \nabla.\left[\frac{kk_{rw}\rho g}{\mu}(\nabla P - \rho g)\right] + Q_p g + S_w \alpha \rho g \frac{\partial \sigma}{\partial t} \qquad [3.15]$$

Equation [3.15] is the final form of the mass balance equation used in SUTRA (Voss, 1984) incorporating a term arising due to the change in total stress imposed on the matrix. The changes made to FEMWATER model is exactly analogous to the changes made in SUTRA. The right hand side (RHS) total stress term can be written in terms of loading efficiency; $\xi = \frac{\alpha}{\alpha + n\beta} = \frac{\alpha \rho g}{S_s}$ giving:

$$S_s S_w \frac{\partial P}{\partial t} + n\rho g \frac{\partial S_w}{\partial t} = \nabla.\left[\frac{kk_{rw}\rho g}{\mu}(\nabla P - \rho g)\right] + Q_p g + S_s S_w \xi \frac{\partial \sigma}{\partial t} \qquad [3.16]$$

For saturated flow when S_w=1 and k_{rw} =1, Equation [3.15] reduces to:

$$S_s \frac{\partial P}{\partial t} = \nabla . \left[\frac{k\rho g}{\mu} \left(\nabla P - \rho g \right) \right] + Q_p g + S_s \xi \frac{\partial \sigma}{\partial t} \qquad [3.17]$$

The source term $Q_p g$ and the total stress term $S_s \xi \frac{\partial \sigma}{\partial t}$ appear on the RHS of the equation, which leads to the treatment of the total stress term as an equivalent source term in SUTRA and FEMWATER:

$$S_s \frac{\partial P}{\partial t} = \nabla . \left[\frac{k\rho g}{\mu} \left(\nabla P - \rho g \right) \right] + Q_p g + Q_\sigma g \qquad [3.18]$$

where

$$Q_\sigma g = S_s \xi \frac{\partial \sigma}{\partial t} = \alpha \rho g \frac{\partial \sigma}{\partial t}$$

It is clear that if α is large (the porous medium skeleton is very compressible), then the equivalent source term Q_σ is large. If the hydraulic conductivity is low, the fluid increment cannot be expelled quickly and pore pressure builds up as loading occurs. If α is small (deformation of the porous medium skeleton is small), only a small volume of excess fluid generated by the reduction in storage resulting from loading. If the hydraulic conductivity is relatively high this fluid can easily be expelled with minimal pore-pressure build up.

3.3 Stress Distribution

3.3.1 Introduction

When a soil is loaded, the associated changes in stresses that may lead to failure are of interest. To estimate total stresses, the soil is treated as an elastic continuum and deformations are calculated using the theory of elasticity. This method provides reasonably accurate estimates when applied stresses are small compared with the stresses that would cause failure.

In order to apply the general theory of elasticity, a series of assumptions are made. The soil is considered to be an elastic, homogeneous and isotropic material. These assumptions provide a reasonable approximation in most aquifer-aquitard sequences under load. In the present study, long-term pile construction results in deformation beneath the pile. The stress distribution is required to investigate the impact of pile loading on pore pressure.

3.3.2 Boussinesq Theory

Theories for determining the stress distribution in an elastic continuum were developed over one hundred years ago. Boussinesq (1885) first predicted the stresses due to a vertical concentrated load applied to the surface for a homogeneous, elastic, isotropic

solid of semi-infinite extent, bounded by a horizontal plane surface. This is the fundamental solution for stress distribution calculation.

Consider a plane surface XY of a body and a load P is applied at the point with coordinates x, y as shown in Figure 3.1.

The normal and shear stresses on an elemental cube of the material at a distance z beneath the surface can be written:

$$\sigma_Z = \frac{3P}{2\pi}\frac{z^3}{R^5} \qquad [3.18]$$

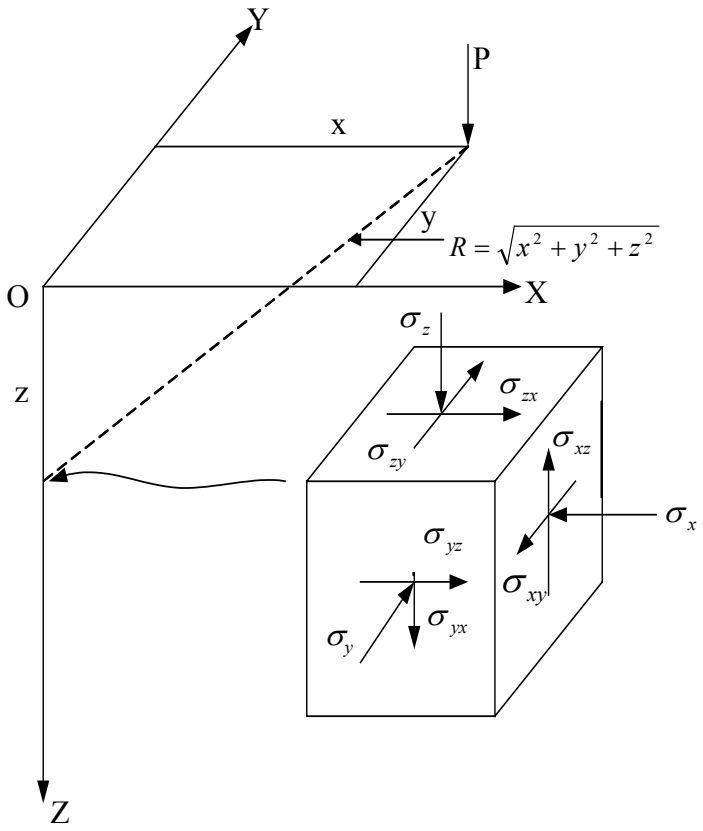

Figure 3.1: Schematic Diagram of Stresses (after Boussinesq, 1885)

$$\sigma_{ZX} = -\frac{3P}{2\pi}\frac{xz^2}{R^5} \qquad [3.19]$$

$$\sigma_{ZY} = -\frac{3P}{2\pi}\frac{yz^2}{R^5} \qquad [3.20]$$

$$\sigma_X = \frac{3P}{2\pi}\left[\frac{x^2 z}{R^5} + \frac{1-2\upsilon}{3}\left(\frac{1}{R(R+z)} - \frac{(2R+z)x^2}{R^3(R+z)^2} - \frac{z}{R^3}\right)\right] \qquad [3.21]$$

$$\sigma_Y = \frac{3P}{2\pi}\left[\frac{y^2 z}{R^5} + \frac{1-2\upsilon}{3}\left(\frac{1}{R(R+z)} - \frac{(2R+z)y^2}{R^3(R+z)^2} - \frac{z}{R^3}\right)\right] \qquad [3.22]$$

$$\sigma_{XY} = \frac{3P}{2\pi}\left[\frac{xyz}{R^5} + \frac{1-2\upsilon}{3}\frac{(2R+z)xy}{R^3(R+z)^2}\right] \qquad [3.23]$$

υ is Poisson's ratio and normal and shear stress components listed above are defined as shown in figure 3.1. In the present study, the stress distribution below a pile is required in order to estimate pore pressure. The solution for stresses as a result of a uniformly loaded rectangular area at the surface can be estimated from the Boussinesq point solution. The fundamental Boussinesq point solution can be integrated to obtain estimates of stress for various loading cases.

3.3.3 Newmark Method

The stresses and deformations generated in an elastic half space by a uniform, normal, surface pressure applied over a rectangular area are considered. Any rectangular area can be divided into sufficiently small blocks and the stress applied by each block is treated as a point load applied to the four corners of the block. Newmark (1940) obtained the following equation for the vertical normal stress beneath a corner of the rectangular area with a uniform applied pressure P:

$$\frac{\sigma_z}{p} = \frac{1}{4\pi}\left[F\left(1+\frac{z^2}{R^2}\right)+\sin^{-1}F\right] \qquad [3.24]$$

where

$$F = \frac{2ABzR}{z^2R^2+A^2B^2} = \frac{2nmz^3R}{z^2R^2+z^4n^2m^2} = \frac{2nmzR}{R^2+z^2n^2m^2}$$

$$R = \sqrt{A^2+B^2+z^2} = z\sqrt{m^2+n^2+1}$$

The uniform vertical pressure (P) is applied over a rectangular area with dimensions A by B on a horizontal plane surface. The stress at depth z is σ_z. The entire RHS of equation [3.24] can be considered as an influence factor depending on two dimensionless factors: m=A/z and n=B/z. A and B can be interchanged in equation [3.24] without changing the stress. Therefore m and n are also interchangeable.

Equation [3.24] can be simply rewritten as:

$$\sigma_z = Ip \qquad [3.25]$$

Where I is the influence factor or stress intensity factor which depend on the shape, position and orientation of the loaded area and the depth to the point where the stress is to be calculated.

I can be written as:

$$I = \frac{1}{4\pi}\left[F\left(1 + \frac{z^2}{R^2}\right) + \sin^{-1} F \right]$$

Superposition can be used to calculate the vertical normal stress induced at any depth by the uniform pressure on a rectangular area located any place on the surface. For an example, the stress at point A in Figure 3.2 caused by the stress applied over the area abcd, designated as σ_z is:

$$\sigma_z(abcd) = \sigma_z(ofcg) - \sigma_z(ofbh) - \sigma_z(oedg) + \sigma_z(oeah) \qquad [3.26]$$

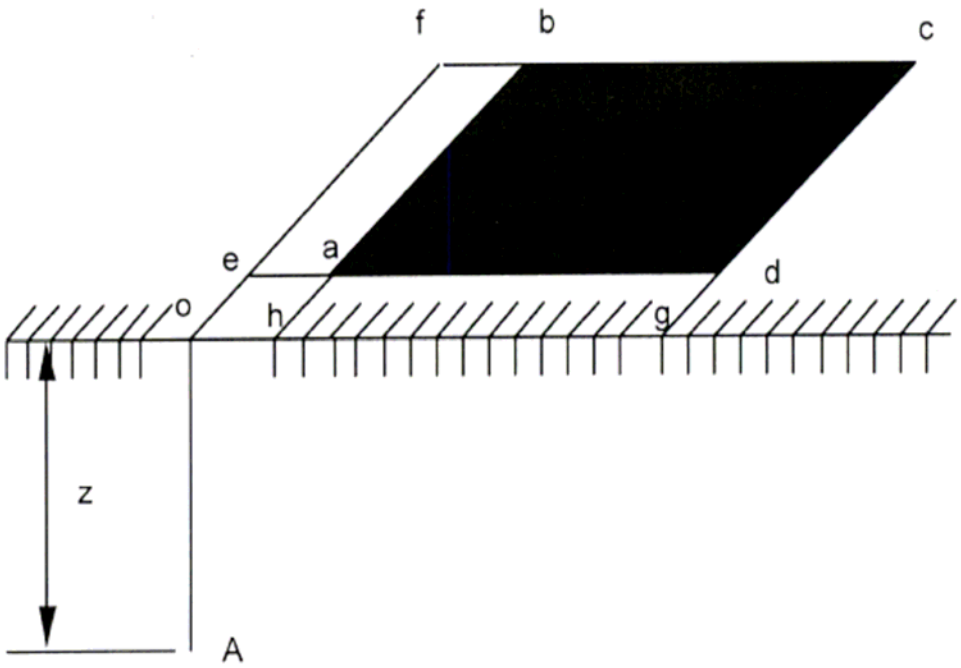

Figure 3.2: Schematic Diagram of Superposition (Olson, 1989)

Values of influence factors were calculated using Newmark (1940) for nodes in the groundwater flow model. Influence factors have been tabulated for a large number of different loading conditions because of their usefulness. They can be found in most classic foundation engineering texts; for example, Fadum (1948), Spangler (1951) and Taylor (1948).

4. PILE LOAD ANALYSIS

4.1 Introduction

The present chapter discusses the model construction procedure and the methodology used for the pile loading analysis. The pile layout for the present study and the construction of FEMWATER 3D model from the 2D grid stage to the 3D mesh stage using GMS interface are discussed. Two basic pile loading patterns are used in the study to independently investigate the influence of loading pattern (or pile construction practice) on pore pressure generation. A series of hydrostratigraphic scenarios with associated material properties is also investigated. Finally, the procedure to conduct a sensitivity analysis of the model material properties is discussed.

4.2 Pile Layout

The major components of a TMA are the tailings pile, the brine pond and the berm. In addition, a drainage ditch usually surrounds the entire pile and pond area. Figure 4.1 shows a cross sectional layout of the modelling domain.

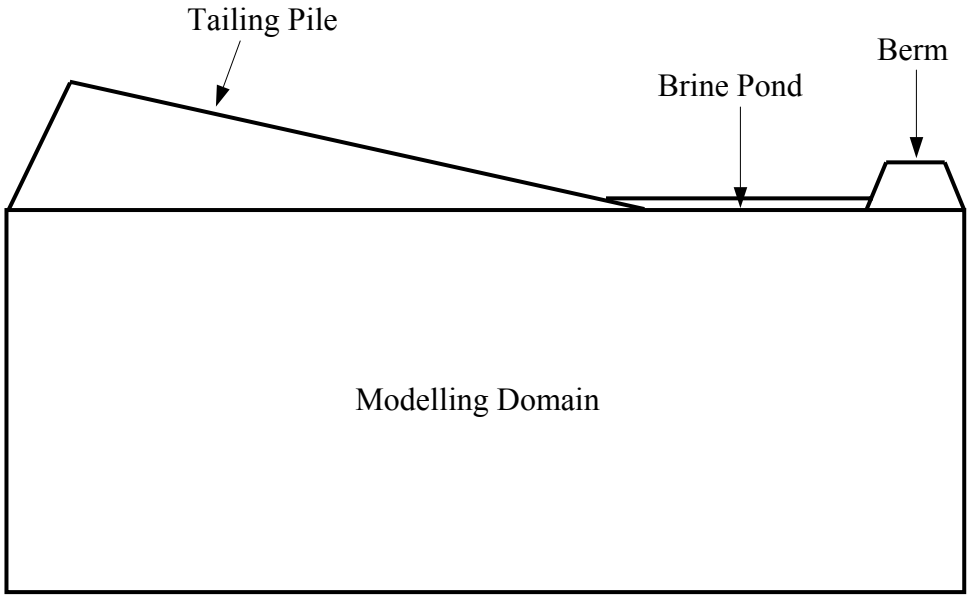

Figure 4.1: Pile Layout Diagram (Section)

Figure 4.1 is not drawn to a scale. The figure shows the part of the modelling domain for which elements are loaded during simulations. The entire modelling domain is shown and described in detail in section 4.3. The loaded elements cover a cross sectional area of 1600 m x 60 m.

Figure 4.2 illustrates the plan view of the pile area. Only a half of the symmetrical domain is shown in the figure.

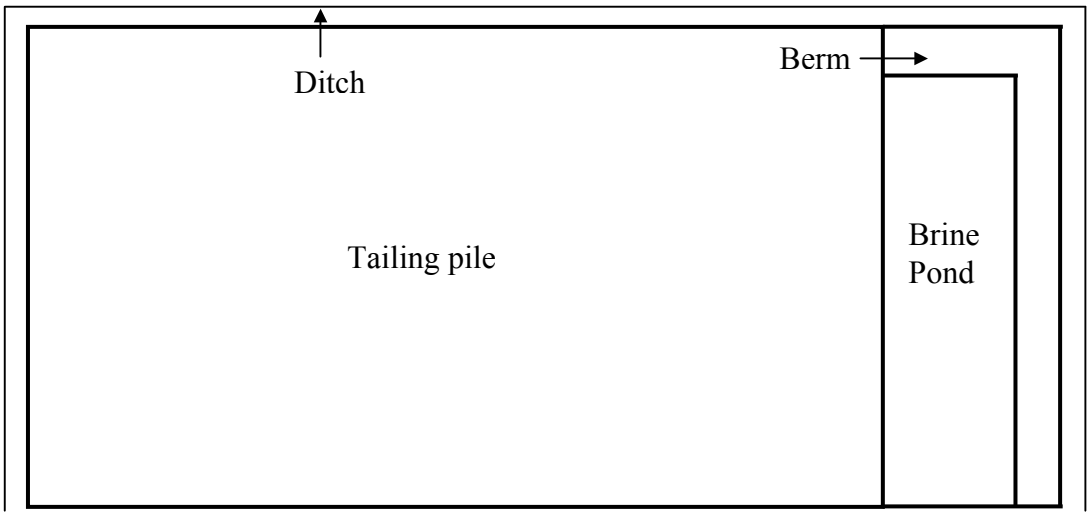

Figure 4.2: Pile Layout Diagram (Plan)

Table 4.1 describes the dimensions of the original mesh selected for 3D model study. Only a half space was modeled due to symmetry of the domain. Taking advantage of symmetry reduces the mesh size required and allows more rapid computation.

Table 4.1: Modelling Domain Dimensions

Parameter		Dimension (m)
Entire Domain	Length	7600
	Width	7600
	Depth	60
Pile	Length	1200
	Width	1600
	Maximum Height	60
Brine Pond	Length	320
	Width	1600
	Constant Height	2
Berm	Length	80
	Width	1600
	Constant Height	3

4.3 Finite Element Model

4.3.1 Model Construction

GMS-FEMWATER enables the creation of a 3D model in several steps. A 2D grid was first created using the 2D grid module of FEMWATER and then converted to a 2D mesh to represent the surface of the region of interest. The mesh construction uses the Triangulated Irregular Network (TIN) module of the FEMWATER interface. Identical TINs were created at the required elevations to represent different interfaces between materials in the model.

The mesh constructed after taking the advantage of symmetry covers a region of 7600 m x 3800 m x 60 m. The simulated pile covers a surface area of 1600 m x 800 m within the region. Grid block dimensions (i, j, k) of 40 m x 40 m x 2.857 m (21 layers) were constructed in the pile region. The 3D mesh of the half space consists of 47,190 nodes and 43,008 elements. The model was layered to facilitate the incorporation of different materials representing various hydrostratigraphic scenarios.

Figure 4.3 outlines the 3-D finite element mesh constructed in FEMWATER. The pile location with respect to the mesh is shown in the figure.

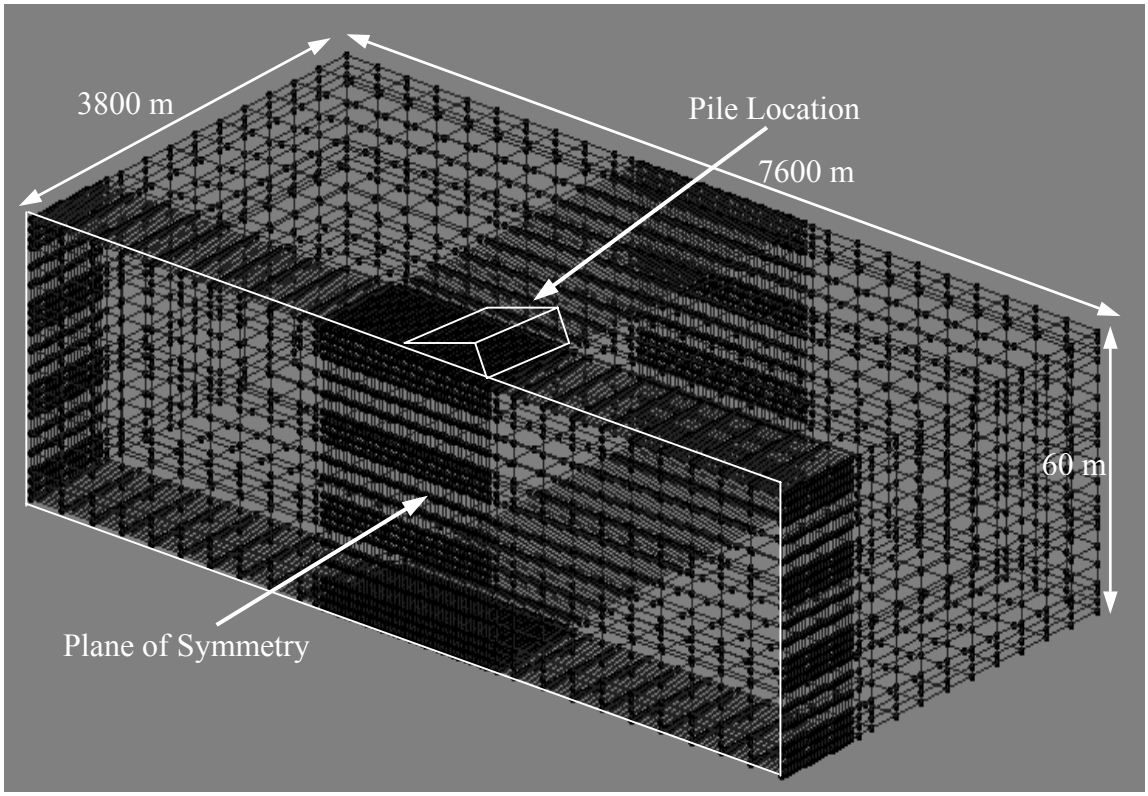

Figure 4.3: 3D Finite Element Model

Figure 4.4 shows the side elevation of the 3D model. The original mesh constructed with different materials layers can be seen in the figure. Thicknesses and material properties of these layers were altered for different hydrostratigraphic scenarios in the study. The location of the pile is also shown (not to vertical scale).

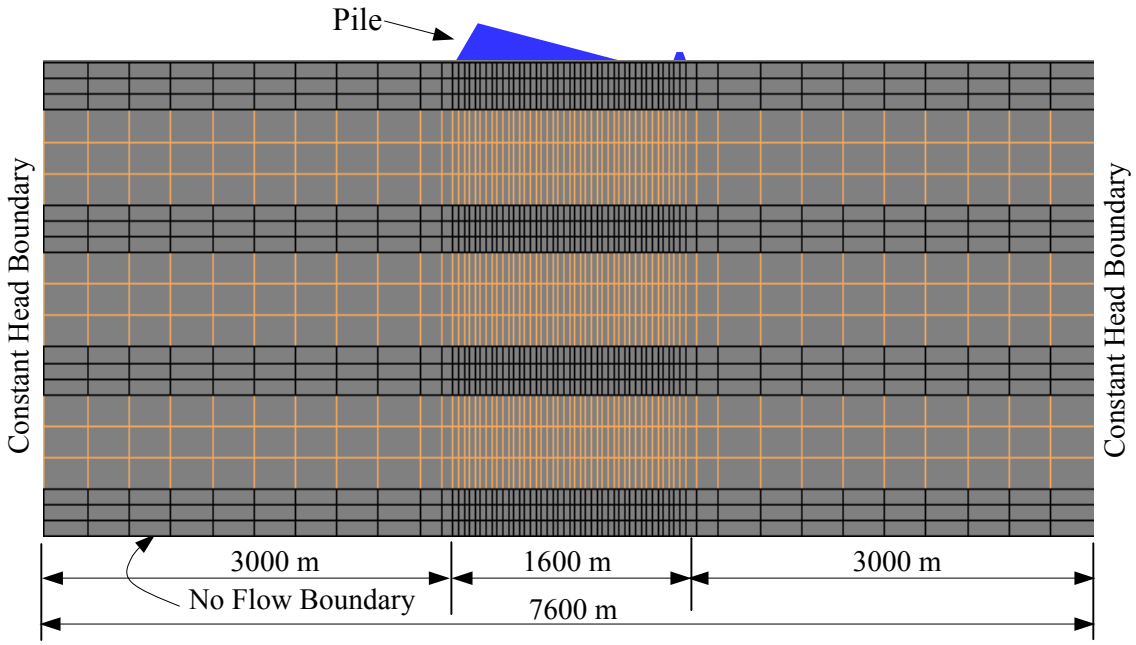

Figure 4.4: Side Elevation of 3D Model

No flow and constant head boundaries were assigned to the model as shown in Figure 4.4. The vertical dimension of the modelling domain is 60 m and it is assumed to extend from surface to the top of low-permeability bedrock that can be treated as a no flow boundary. The sides of the region are assumed to be constant head boundaries.

The value of constant head used in the study is +1 m. This ensures that the model domain remains fully saturated at all times. This may not be true for some TMAs but is considered a reasonable approximation in the vicinity of tailings ponds.

The 3D model plan view and the location of the pile are shown in Figure 4.5. The pile, berm, brine pond and the ditch are shown in details in Figure 4.6.

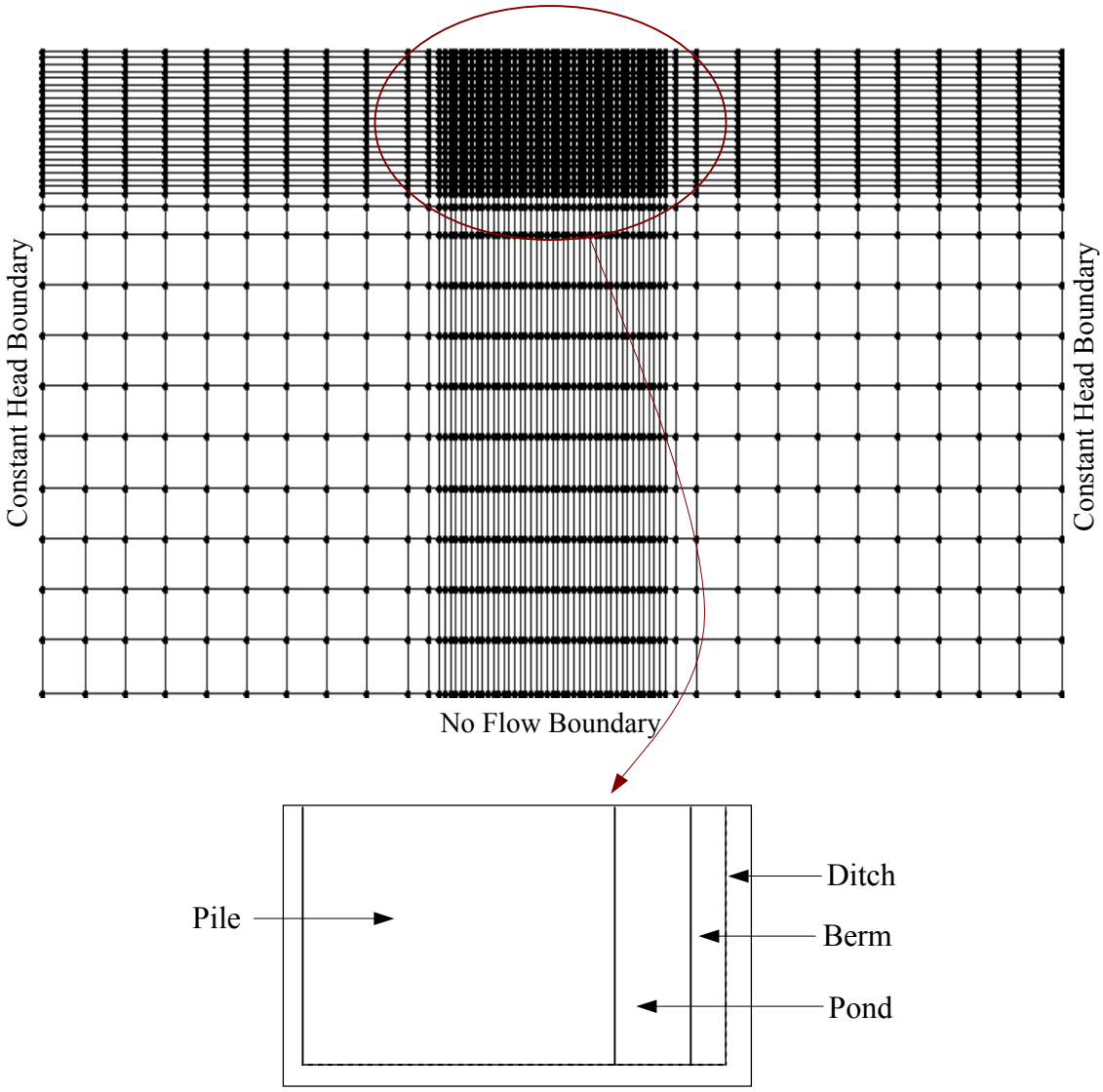

Figure 4.5: Top Elevation of 3D Model

4.3.2 Mesh Layout

Figure 4.6 shows the loaded element arrangement for the modelling domain. Elements in the ditch are not loaded. It is assumed that the brine pond has a constant elevation head of +2 m throughout the simulation period. The berm top has a constant elevation head of +3 m. These are assumed to represent typical dimensions for TMAs.

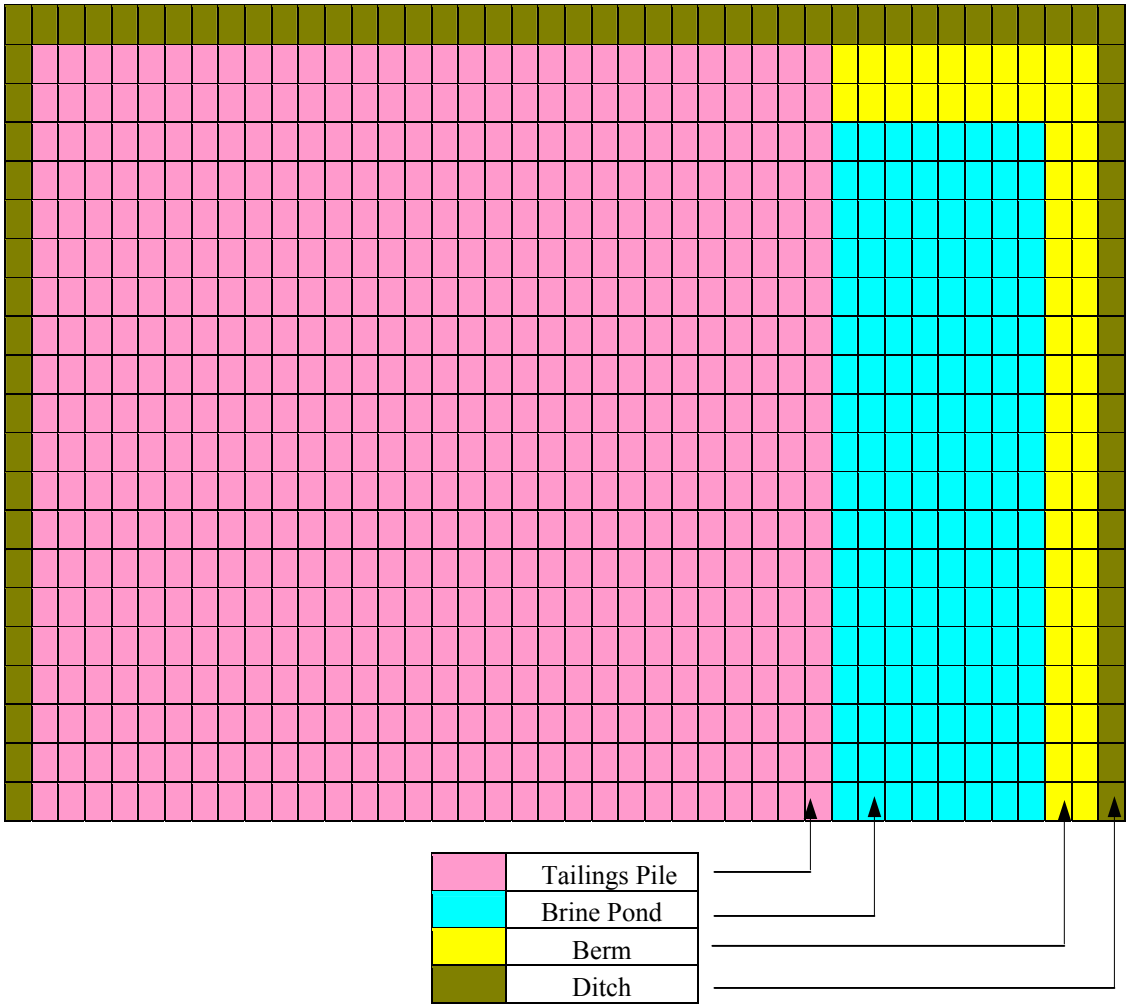

Figure 4.6: Element arrangement of the modeling domain

Details of the elements that are loaded are given in Table 4.2. There is a total of 21 model layers and the total number of loaded elements in the modelling domain is 16800 (800 x 21).

Table 4.2: Loaded elements details

Region	No of Elements/Layer
Tailings Pile	600
Brine Pond	144
Berm	56
Total number of loaded elements	800

4.4 Pile Loading Patterns

4.4.1 Loading Pattern 1

The load applied by the pile is simulated by two patterns for the study. The final height of the pile in both cases is 60 m. The purpose of investigating different loading patterns is to understand how the loading pattern affects pore pressure development.

Figure 4.7 illustrates the first loading pattern for pile construction. The simulated pile is constructed over a period of 30 years and there are 30 annual load increments labelled A_1 to A_{30}. Not all the increments are shown in Figure 4.7. The volume of the tailings added to the pile during each year is equal. Therefore the areas A_1, A_2, A_3…A_{30} are equal. This relationship is used for calculating the load applied for each time interval. The density of salt tailings material is assumed to be 1500 kg/m^3.

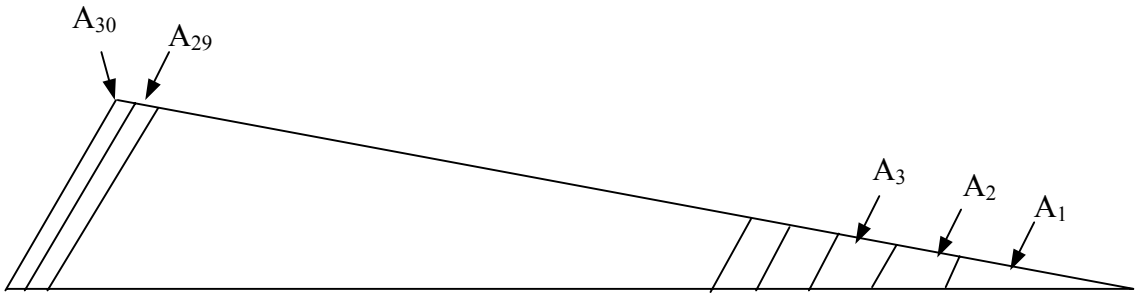

Figure 4.7: Side Elevation of Loading Pattern 1

4.4.2 Loading Pattern 2

The second pile construction loading sequence is shown in Figure 4.8. The final height of the pile remains 60 m. Unlike loading pattern 1, all the elements in the modelling domain are loaded for each time interval.

The area of tailings increment is the same for each time interval. There are again 30 area increments, and not all of the area increments are shown in the figure.

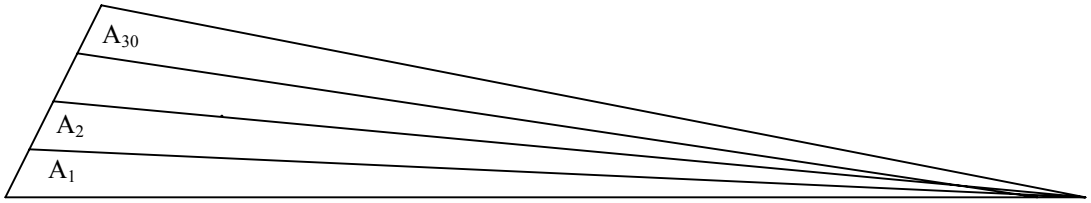

Figure 4.8: Side Elevation of Loading Pattern 2

The Newmark method (Newmark, 1940) is used to estimate stress intensity factors. Using the loads and the stress intensity factors, the stress distribution due to progressive pile loading was calculated for the various hydrostratigraphic cases. For loading case 1, some provisions are made for load transfer from the newly loaded area to adjacent areas. Detailed descriptions of the loading calculations and stress distributions using stress intensity factors are discussed in Appendix B.

4.5 Hydrostratigraphic Scenarios

Eleven different hydrostratigraphic scenarios are considered. Due to the variation in material properties, the pressure head development can vary significantly for different scenarios.

Table 4.3 describes the material properties used in the pile load analysis. The values listed are selected to represent the typical material properties found in the vicinity of Saskatchewan potash mines. Specific storage for each material is calculated using the relationship between porosity (n), soil compressibility (α), water compressibility (β) and water density (ρ). The equation that describes the above relationship is $S_s = (\alpha + n\beta)\rho g = (\alpha + n\beta)\gamma$: where γ is the specific weight of water.

Table 4.3: Material Properties

Parameter	Material	Value
Specific Weight	Water	9.8×10^{3} Pa.m^{-1}
Hydraulic Conductivity	Sand	1.0×10^{-4} m/s
	Till	1.0×10^{-8} m/s
	Clay	1.0×10^{-9} m/s
Compressibility	Water	4.8×10^{-10} Pa^{-1}
	Sand	2.0×10^{-8} Pa^{-1}
	Till	2.0×10^{-7} Pa^{-1}
	Clay	4.0×10^{-6} Pa^{-1}
Porosity	Sand	0.25
	Till	0.38
	Clay	0.40

4.5.1 Hydrostratigraphy: Single Drainage Scenario

For the four different single drainage scenarios, varying thickness ratios of sand and till are considered. The hydrostratigraphy shown in Figure 4.9 has a thin surface sand layer underlain by a thick till layer. Figures 4.10, 4.11 and 4.12 have similar hydrostratigraphies with increasing thickness of sand at the surface.

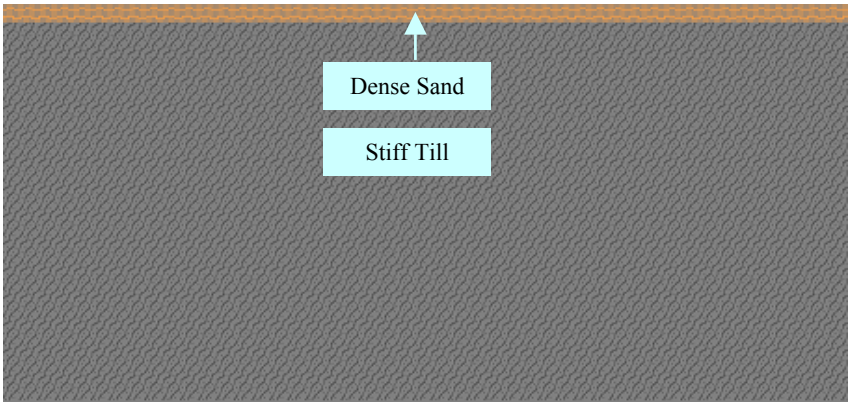

Figure 4.9: Single Drainage: Scenario 1

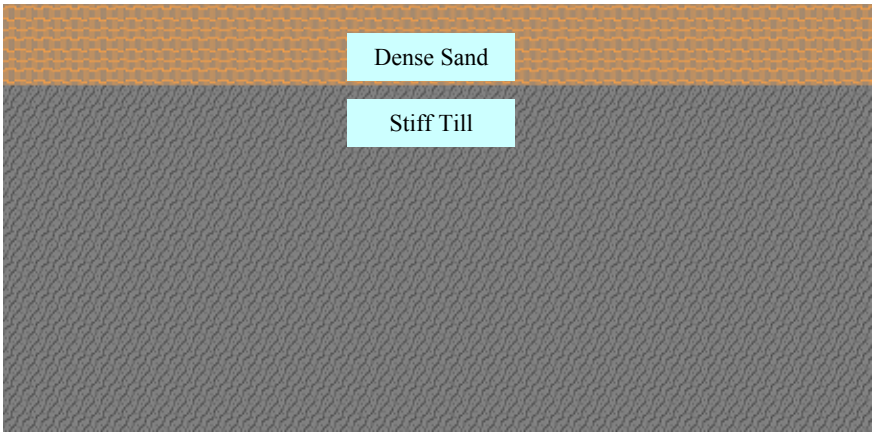

Figure 4.10: Single Drainage: Scenario 2

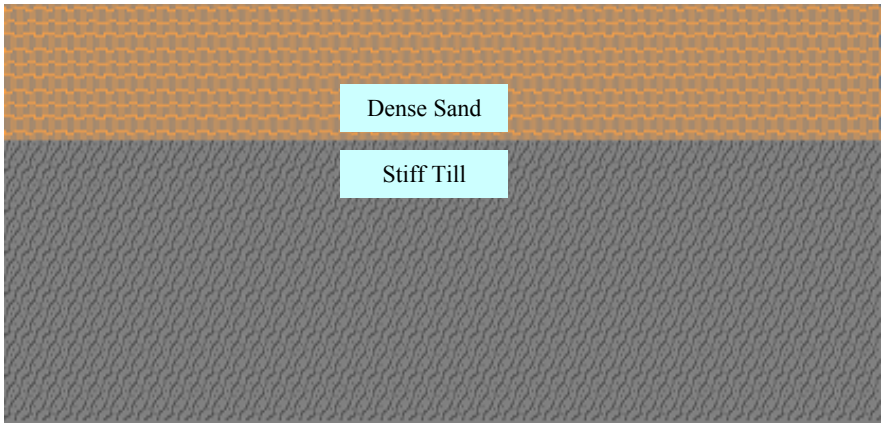

Figure 4.11: Single Drainage: Scenario 3

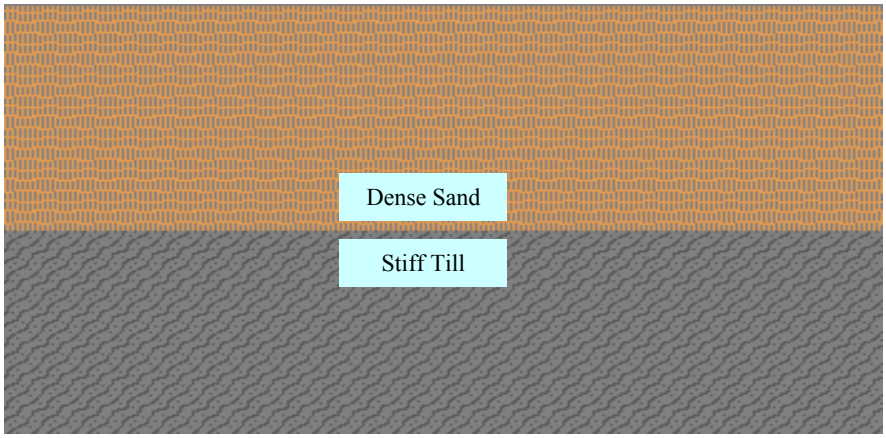

Figure 4.12: Single Drainage: Scenario 4

Table 4.4 details the thickness of each layer and the total thickness of material for the four single-drainage scenarios considered.

Table 4.4: Thicknesses of Layers in Single Drainage Problems

Scenario	Sand Thickness (m)		Till Thickness (m)	
	Each Layer	Total (t_S)	Each Layer	Total (t_T)
1	2.86	2.86	57.14	57.14
2	11.43	11.43	48.57	48.57
3	20.00	20.00	40.00	40.00
4	31.42	31.42	28.58	28.58

Table 4.5 gives the thickness ratio of sand: till for the four single drainage scenarios considered.

Table 4.5: Thickness Ratio for Single Drainage Problems

Scenario	Thickness Ratio (t_S/t_T)
1	0.05
2	0.23
3	0.50
4	1.10

4.5.2 Hydrostratigraphy: Double Drainage Scenarios

Figure 4.13 to 4.17 illustrate the hydrostratigraphies for the double drainage scenarios of the till units.

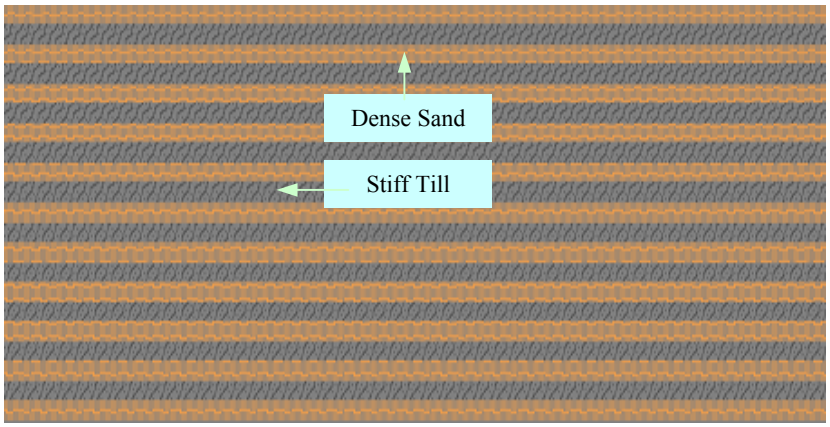

Figure 4.13: Double Drainage: Scenario 5

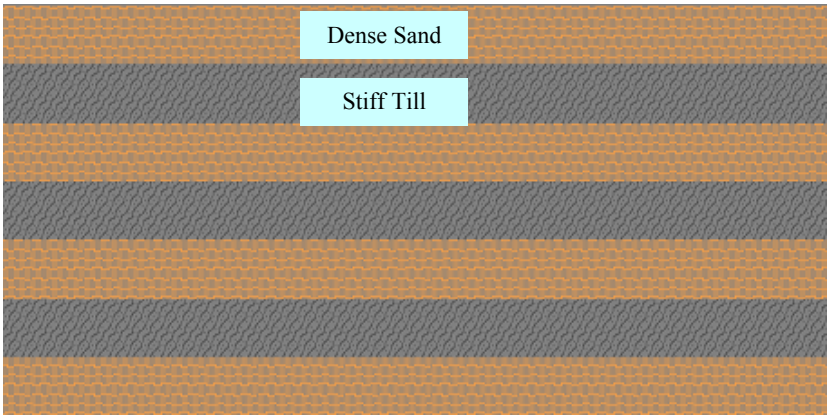

Figure 4.14: Double Drainage: Scenario 6

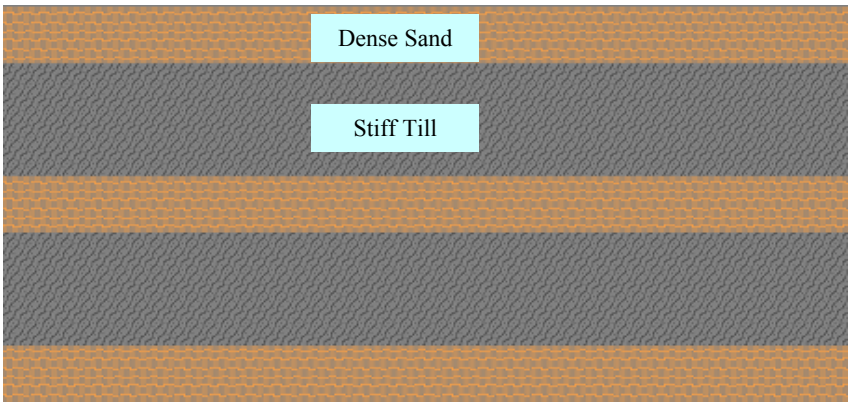

Fig 4.15: Double Drainage: Scenario 7

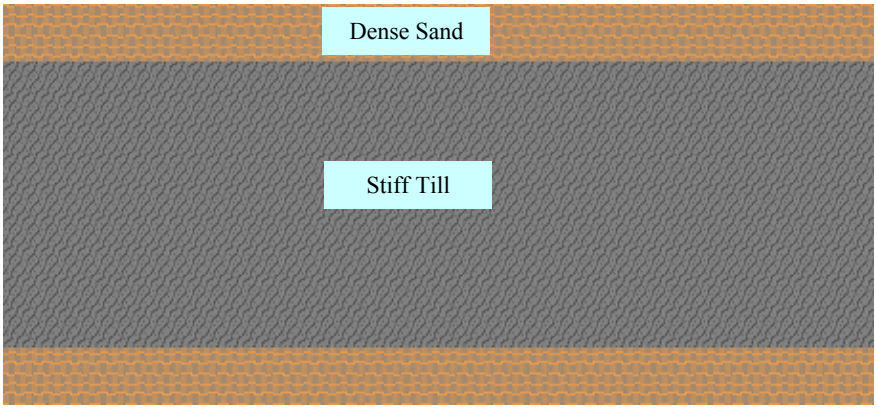

Figure 4.16: Double Drainage: Scenario 8

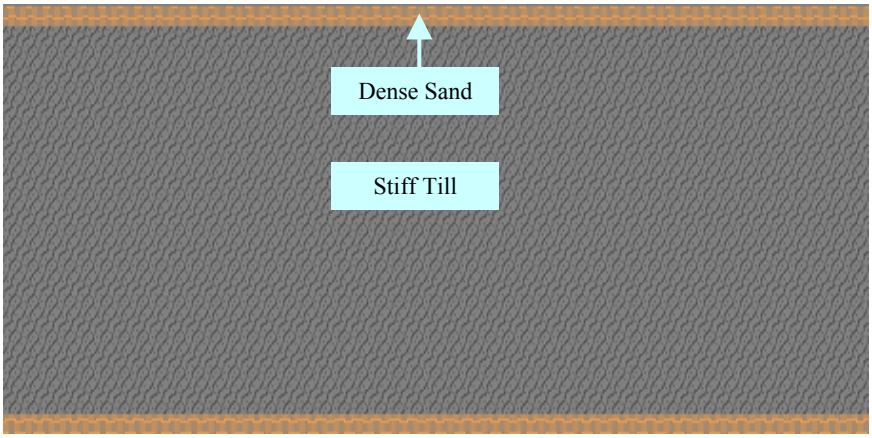

Figure 4.17: Double Drainage: Scenario 9

Table 4.6 details the thickness of materials in hydrostratigraphies for the five double-drainage scenarios.

Table 4.6: Thicknesses of Layers in Double Drainage Problems

Scenario	Sand Thickness (m)		Till Thickness (m)	
	Each Layer	Total (t_S)	Each Layer	Total (t_T)
5	2.86	31.46	2.86	28.60
6	8.57	34.28	8.57	25.71
7	8.57	25.71	17.14	34.28
8	8.57	17.14	42.86	42.86
9	2.86	5.72	54.28	54.28

Table 4.7 details the thickness ratios for the five double-drainage scenarios.

Table 4.7: Thicknesses Ratio for Double Drainage Problems

Scenario	Thickness Ratio (t_S/t_T)
5	1.10
6	1.33
7	0.75
8	0.40
9	0.10

4.5.3 Hydrostratigraphy: Plastic Clay Scenarios

Figures 4.18 and 4.19 shows two plastic clay scenarios considered. The plastic clay layer was added to represent sheared clay/till layers that can generate high pore pressure as a result of their storage/deformation characteristics.

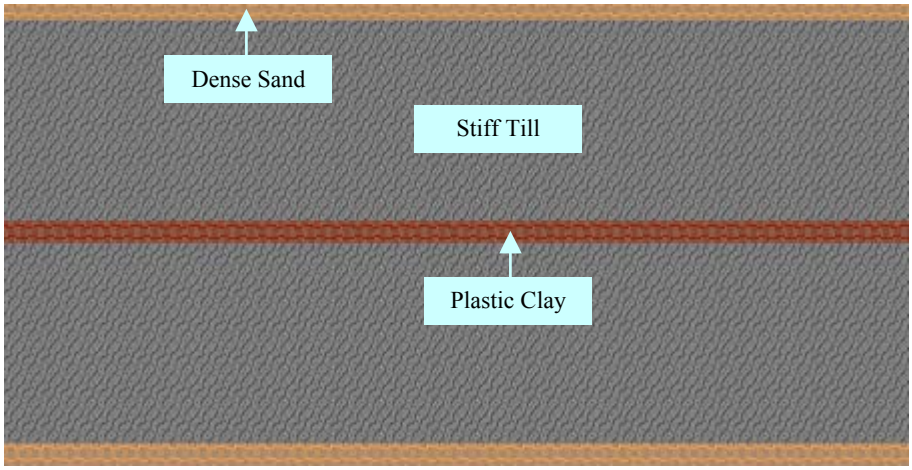

Figure 4.18: Plastic Clays: Scenario 10

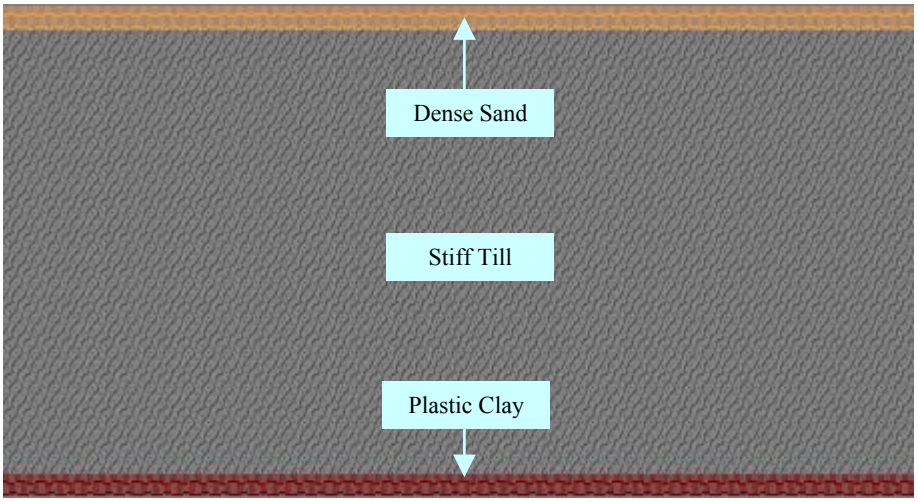

Figure 4.19: Plastic Clays: Scenario 11

Thicknesses of layers for the two hydrostratigraphies are described in Table 4.8.

Table 4.8: Thicknesses of Layers in Plastic Clay Problems

Scenario	Sand Thickness (m)		Clay Thickness (m)		Till Thickness (m)	
	Each Layer	Total (t_S)	Each Layer	Total (t_S)	Each Layer	Total (t_T)
10	2.86	5.72	2.86	2.86	25.71	51.42
11	2.86	2.86	2.86	2.86	54.28	54.28

Scenarios 9 and 10 have similar features. The thick till layer is divided by a thin plastic clay layer that has very low hydraulic conductivity and high specific storage. Scenario 11 has a plastic clay layer at the bedrock surface recognizing this surface as a potential paleo-shear-plane.

4.6 Sensitivity Analysis

A sensitivity analysis was conducted to investigate the influence of hydraulic conductivity of the till units on pore pressure development in such aquitards. Hydrostratigraphic scenario 11 shown in Figure 4.19 was selected for the sensitivity analysis. The hydraulic conductivity of the till layer was changed while keeping other parameters constants, and the model was run repeatedly to investigate the relative pore-pressure response. The model was run for a time period of 30 years for the sensitivity analysis.

Table 4.9 shows the till hydraulic conductivity parameters used in the sensitivity analysis. The range was chosen to cover typical values found in the vicinity of potash mines.

Table 4.9: Parameters for sensitivity analysis

Trial	Till Hydraulic conductivity (m/s)
1	3.16×10^{-8}
2	1.00×10^{-8}
3	3.16×10^{-9}
4	1.00×10^{-9}

5. RESULTS AND DISCUSSION

5.1 Introduction

This chapter discusses the results of the parametric model study. The groundwater flow model was run for two loading patterns with four different loading rates. The standard time period assumed for pile construction was 30 years. In addition, pile construction periods of 15, 25 and 35 years were also considered. Of the eleven hydrostratigraphic scenarios originally considered, four scenarios (8, 9, 1, and 11) were selected for detailed investigations of pore pressure development. The results predicted by the model for two loading patterns under different loading rates for these four cases are discussed. Finally, the results of the sensitivity analysis for till hydraulic conductivity on pore pressure development are discussed.

All the simulations were conducted for 40 years allowing pore pressure dissipation behaviour also to be investigated. The model was initially run for a pile construction period of 30 years for all eleven scenarios. The pile construction rate was changed in order to complete construction in 15, 25 and 35 years for the four cases analyzed in detail. The objective was to observe the impact of loading rate on pore pressure generation. The maximum total head occurs at the end of loading period for all

the runs, and the maximum head increases as the loading period is reduced (or as loading rate increases).

5.2 General Results

Table 5.1 details a summary of the results showing the variation of pore pressure head for the entire simulation period (40 years) for loading pattern 1. Results are shown only for selected time periods to discuss the general trend of the results. The pore pressure variation with time for pile construction period of 30 years for all eleven hydrostratigraphic scenarios are detailed in the table. For all the cases, maximum head was observed at 30 years.

For the four single drainage scenarios considered, the peak head at 30 years increases as the thickness of till layer is increased. The dissipation rate is increasing as the length of the drainage path is reducing. In Table 5.1, at the end of 40 years, except for scenario 1, the hydraulic head reduced to approximately about 2 m.

The five double drainage scenarios demonstrate similar behaviour to single drainage scenarios. In general, peak head at 30 years increases as the thickness of till layers is increased. However, the drainage path length is reduced by double drainage and hence dissipation rate is faster than that for the single drainage case. At the end of 40 years, for all the scenarios, pore pressures have dissipated to 2 m. The till layers have shorter drainage paths in double drainage case and hence pore pressure dissipates faster than

that for single drainage scenarios. Scenario 5 has very short drainage paths that there is no significant pore pressure increase throughout the simulation period.

Scenarios 10 and 11 are plastic clay scenarios that show very slow dissipation behaviour. Significant pore pressures are sustained at the end of 40 years. According to Table 5.1, plastic clay has very low hydraulic conductivity, which results in slow dissipation behaviour.

Table 5.1: Pore pressure heads observed for 11 scenarios for loading pattern 1 for a 30 years construction period

Time (yrs)		Head (m)										
		Scenario										
		Single Drainage				Double Drainage					Plastic Clays	
		1	2	3	4	5	6	7	8	9	10	11
Loading	1	7.5	7.3	7.0	6.6	2.0	2.0	4.5	7.3	7.5	7.4	7.5
	2	10.6	10.2	9.8	9.5	2.0	2.0	3.4	9.5	10.3	11.0	10.6
	5	16.5	16.1	15.3	13.6	2.0	2.9	7.3	13.6	15.3	17.4	16.1
	10	25.3	23.9	21.6	17.5	2.0	2.5	7.2	16.7	20.0	25.8	25.0
	20	37.8	33.7	29.2	23.6	2.0	2.0	7.1	21.1	26.9	36.7	39.3
	30	53.2	49.1	43.7	33.0	2.0	2.0	7.1	27.5	36.6	54.2	53.8
Dissipating	31	47.1	41.4	34.0	20.5	2.0	2.0	2.0	12.5	21.9	47.1	53.2
	32	40.6	33.5	25.2	12.0	2.0	2.0	2.0	5.6	12.8	40.3	52.8
	35	24.9	17.3	10.1	2.5	2.0	2.0	2.0	2.0	3.0	25.2	49.6
	40	11.8	6.1	2.4	2.0	2.0	2.0	2.0	2.0	2.0	11.9	41.7
		Case 3							Case 1	Case 2		Case 4

5.3 Influence of K/S_s Ratio (C_v)

The ratio of hydraulic conductivity (K) to specific storage (S_s) of a geological material is a critical factor in the present study. In soil mechanics this ratio is called the coefficient of consolidation (c_v). K/S_s (also known as hydraulic diffusivity) is a useful parameter to investigate the pore pressure behavior beneath a developing salt tailings pile. It describes how efficiently pore pressure dissipates through various materials.

Typical values of K/S_s ratio for dense sand, stiff till and plastic clay are listed in Table 5.2. The approximate values listed in the table are calculated based on the material properties listed in the Table 4.3 and neglecting the compressibility of water. Table 5.2 shows that the high value for dense sand indicates much more rapid pore pressure dissipation behaviour compared to that of plastic clays with much lower K/S_s values. The differences between the hydraulic diffusivities of sand, till and clay are about given orders of magnitude.

Table 5.2: K/S_s ratio for different materials

Material	**K/S_s (x 10^4 m^2/s)**
Dense sand	5.0×10^{3}
Stiff till	5.0×10^{-2}
Plastic clay	2.5×10^{-4}

5.4 Loading Pattern 1

The model results show that loading pattern 1 generates higher pore pressures beneath the pile compared to loading pattern 2. The four hydrostratigraphic scenarios selected for detail investigation were considered for four different loading rates.

The pile construction periods considered were 15, 25 and 35 years in addition to 30 years. Table 5.3 details the results for these cases for a 40 year simulation period. It can be clearly seen from the results that maximum peak head is observed at the end of pile construction period for each case. In general, the higher the pile construction rate, the greater the peak pore pressures.

Table 5.3: Pore Pressure Head vs. Time calculated for four pile construction periods for loading pattern 1

Time (yr)	Head (m)															
	Scenario															
	8				9				1				11			
	15	25	30	35	15	25	30	35	15	25	30	35	15	25	30	35
1	10.6	6.8	7.3	6.3	11.0	7.2	7.5	6.4	11.0	7.2	7.5	6.4	11.0	7.2	7.5	6.4
2	14.6	11.6	9.5	9.3	15.9	12.4	10.3	9.8	16.1	12.5	10.6	9.8	16.0	12.5	10.6	9.8
5	20.4	18.3	13.6	14.4	24.6	20.5	15.3	16.2	26.7	21.1	16.5	16.9	26.4	21.0	16.1	16.8
10	28.4	19.2	16.7	12.3	33.6	25.2	20.0	17.4	41.3	30.5	25.3	23.7	40.0	29.6	25.0	23.3
15	41.6	18.1	15.8	21.5	51.0	26.3	21.5	26.6	57.5	38.2	33.3	32.6	56.3	37.7	33.2	31.5
16	19.1	23.6	20.7	15.6	31.4	31.6	27.6	19.6	51.8	41.2	36.5	30.3	53.1	40.0	35.6	30.9
17	8.5	27.5	22.3	17.6	18.6	34.5	28.0	24.1	45.5	41.7	34.4	33.9	52.8	40.3	34.9	33.5
20	2.0	29.3	21.1	22.0	4.5	37.2	26.9	28.0	29.7	46.9	37.8	36.6	50.3	45.2	39.3	35.2
25	2.0	31.2	20.4	17.7	2.0	40.6	26.3	23.0	15.1	54.7	44.0	38.8	42.8	54.0	46.3	41.7
26	2.0	14.2	27.2	24.1	2.0	24.5	35.7	31.5	13.2	48.9	49.7	44.6	41.2	53.2	49.4	44.4
27	2.0	6.3	21.7	18.0	2.0	14.4	28.1	23.4	11.5	42.3	45.3	40.5	39.6	52.8	48.7	43.9
30	2.0	2.0	27.5	23.0	2.0	3.4	36.6	30.5	7.8	26.1	53.2	44.4	35.1	49.9	53.8	46.1
31	2.0	2.0	12.5	16.9	2.0	2.3	21.9	23.7	6.8	22.3	47.1	45.2	33.6	48.5	53.2	48.7
32	2.0	2.0	5.6	22.1	2.0	2.0	12.8	29.3	6.1	19.2	40.6	42.9	32.3	47.0	52.8	48.5
35	2.0	2.0	2.0	24.5	2.0	2.0	3.0	33.1	4.3	12.8	24.9	51.6	28.5	42.1	49.6	53.4
36	2.0	2.0	2.0	11.1	2.0	2.0	2.1	19.8	3.8	11.2	21.2	45.3	27.3	40.5	48.2	53.2
37	2.0	2.0	2.0	5.0	2.0	2.0	2.0	11.5	3.4	9.8	18.1	38.9	26.2	38.9	46.6	52.6
40	2.0	2.0	2.0	2.0	2.0	2.0	2.0	2.7	2.4	6.6	11.8	23.7	23.1	34.4	41.7	49.3
	Case 1				**Case 2**				**Case 3**				**Case 4**			

5.4.1 Case 1 (Scenario 8)

A schematic diagram for the hydrostratigraphic scenario 8, Case 1, which is a double drainage scenario with till between sand layers, is shown in Figure 5.1. The thickness of the sand layers is 8.57 m each and that for till is 42.86 m.

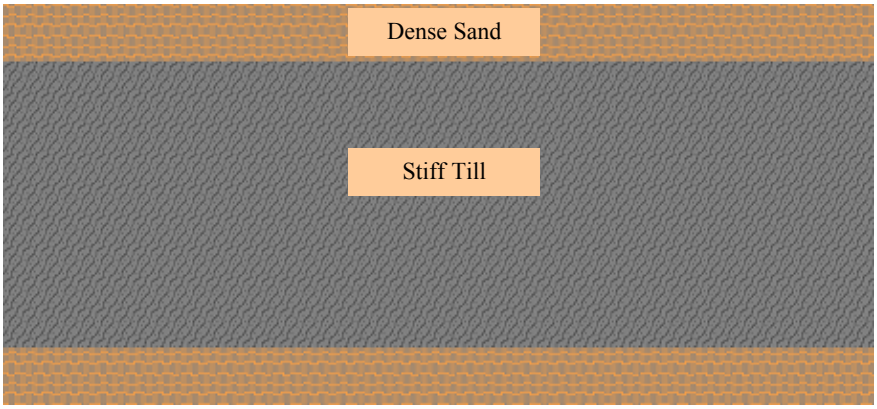

Figure 5.1: Hydrostratigraphic Case 1

Figure 5.2 illustrates the pore pressure head generation sequence beneath the pile for loading of Case 1 for a 30 year of pile construction period with loading pattern 1 (t= 1, 2, 5, 10, 20 and 30 years). Pore pressure propagation with the pile construction can be observed in the figure. The contour specified values are in meters. Pore pressure dissipation is shown in Figure 5.3 for t= 31, 32, 35 and 40 years.

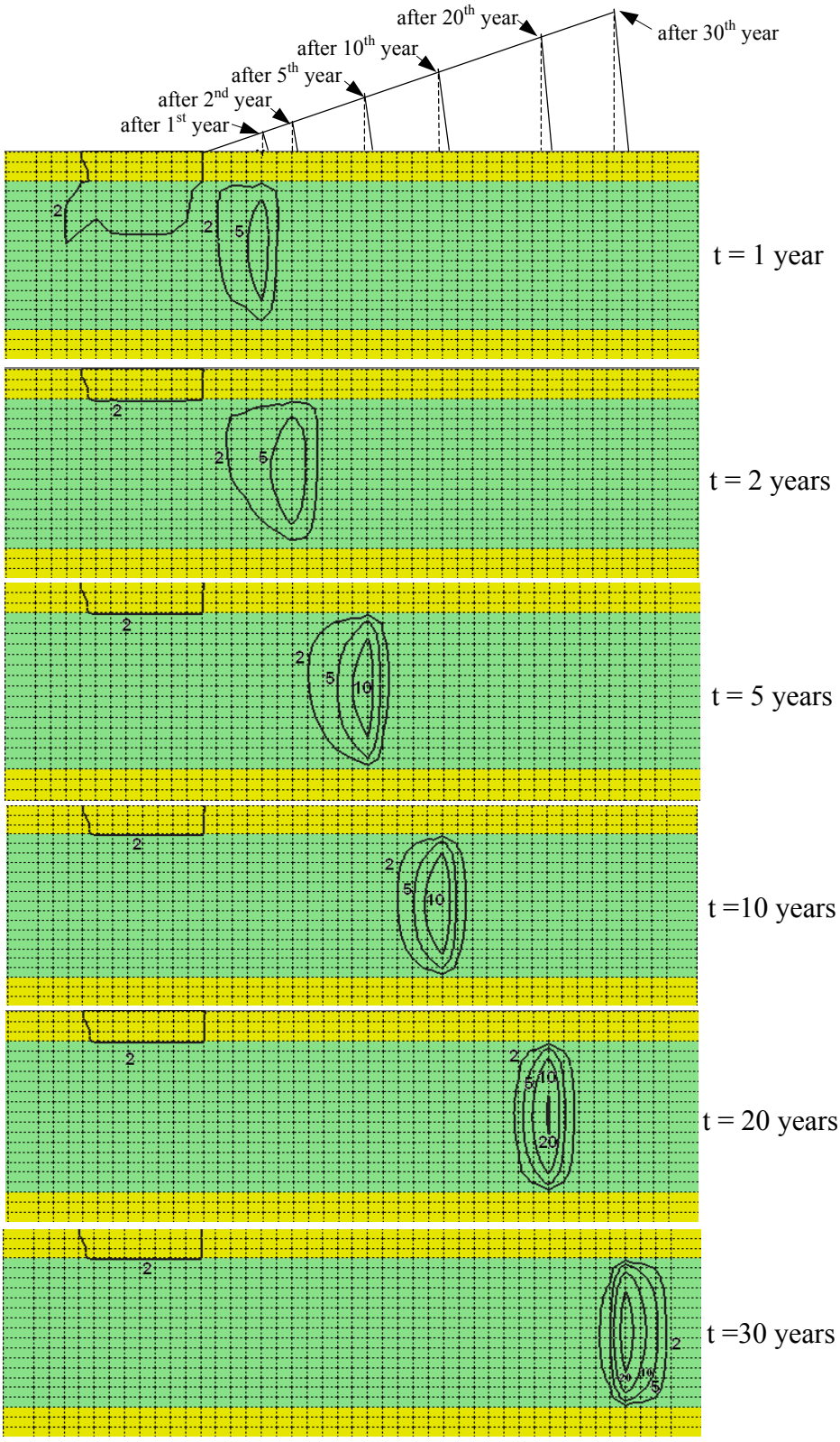

Figure 5.2: Pore pressure development patterns for loading for Case 1

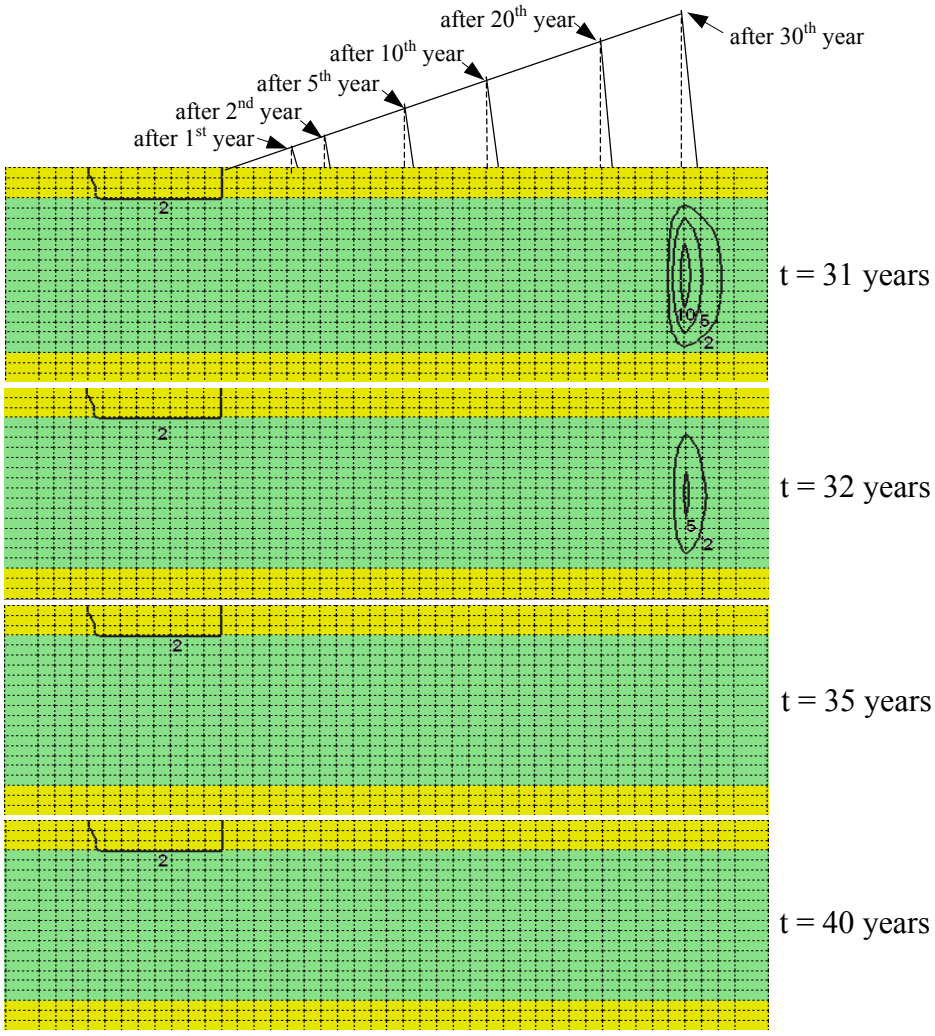

Figure 5.3: Pore pressure dissipation patterns for Case 1

Figure 5.4 and 5.5 respectively demonstrate the pore pressure generation for t = 1, 2, 5 years and t = 10, 20, 30 years in 3-D for Case 1. Figure 5.6 and 5.7 respectively demonstrate the pore pressure dissipation patterns for t= 31, 32, 35 years and t = 40 years. The pore pressure propagation with the pile construction can be seen as a three dimensional view.

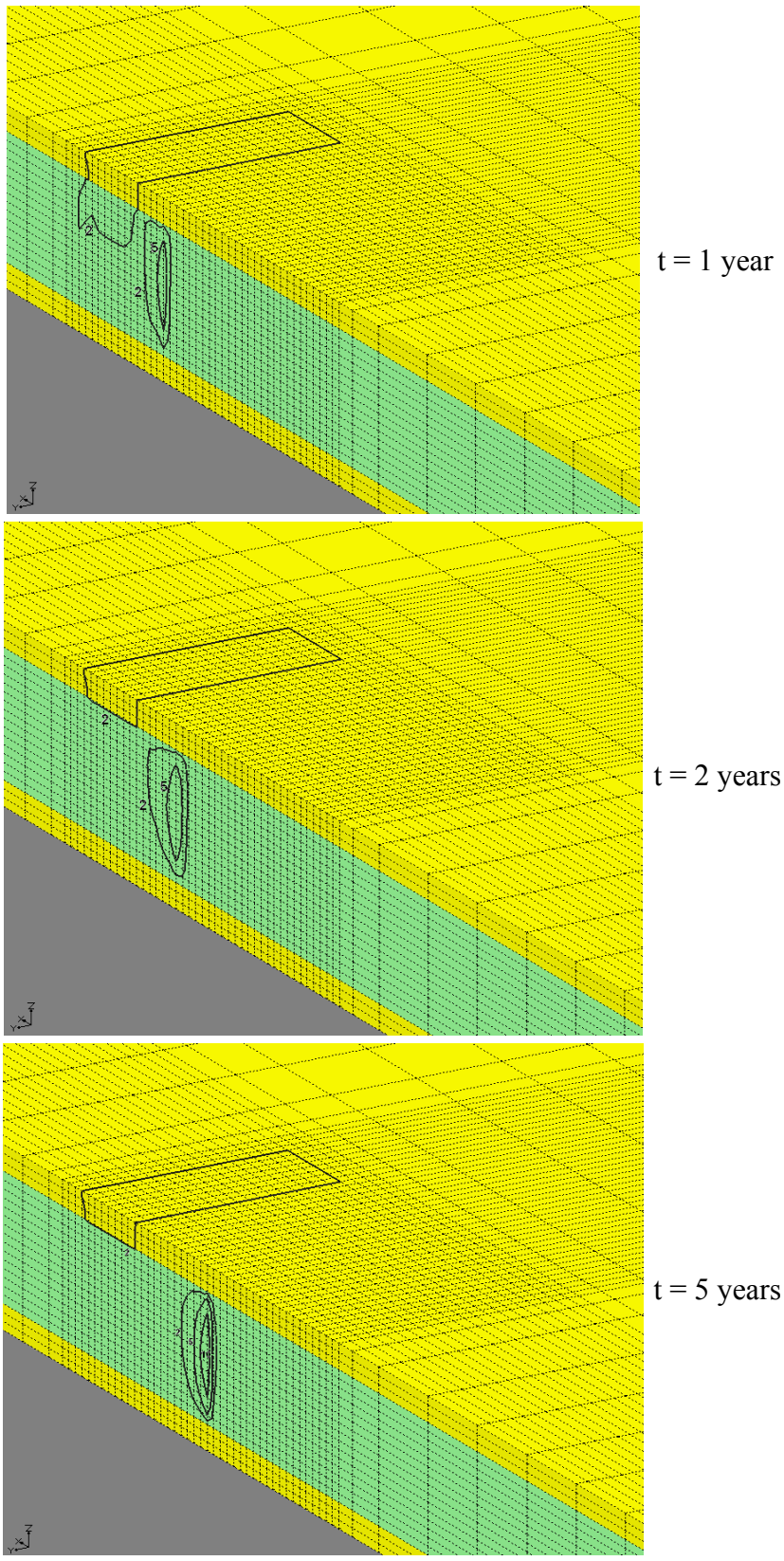

Figure 5.4: 3-D view of the pile during pore pressure development for loading for Case 1 (t = 1, 2, 5 years)

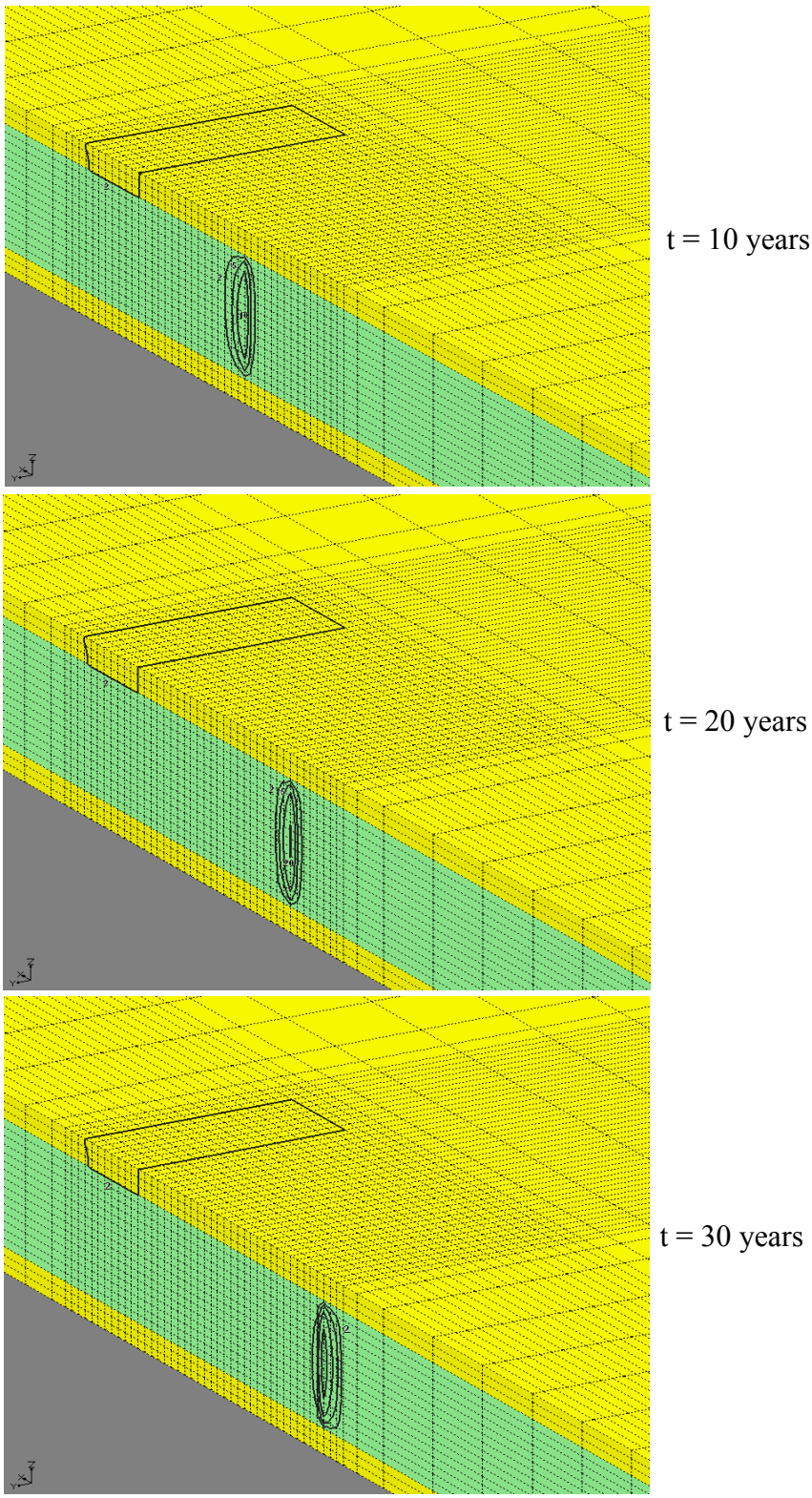

Figure 5.5: 3-D view of the pile during pore pressure development for loading for Case 1 (t = 10, 20, 30 years)

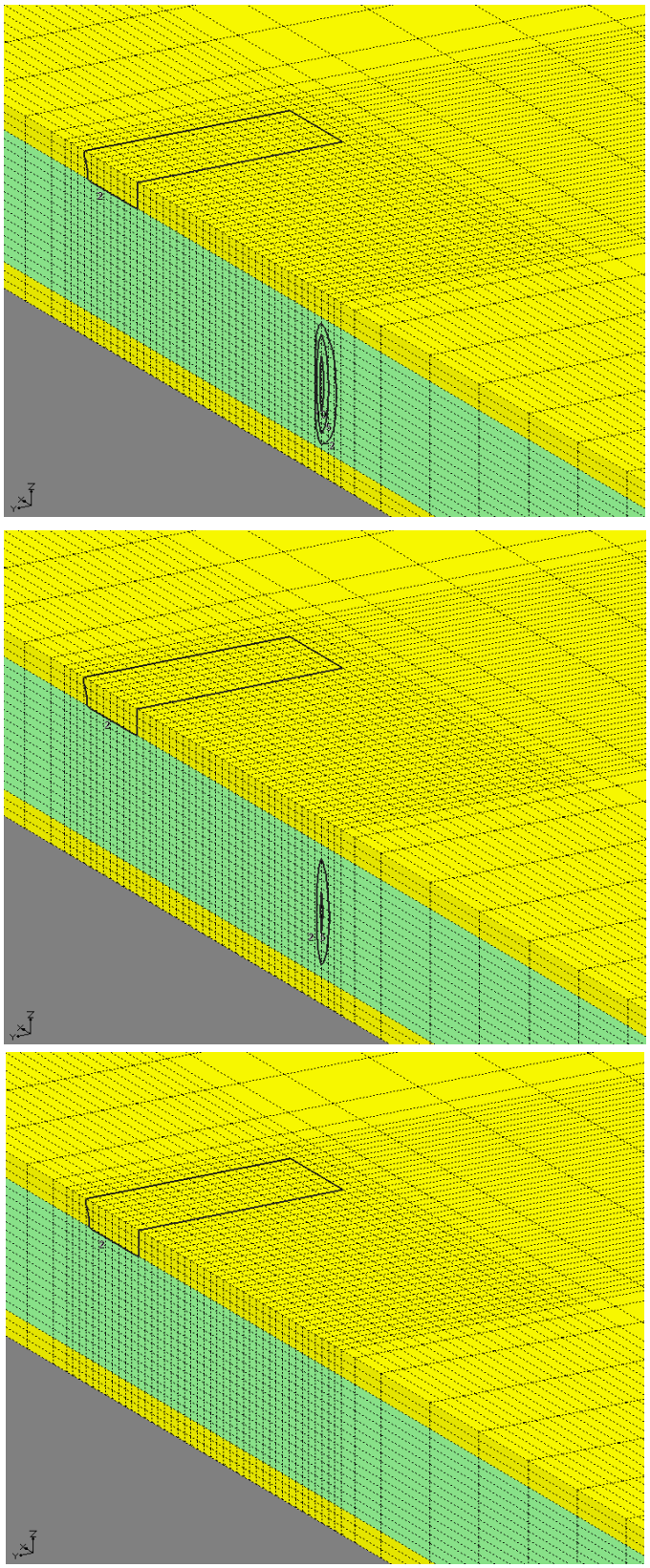

Figure 5.6: 3-D view of the pile during pore pressure dissipation for Case 1 (t =31, 32, 35 years)

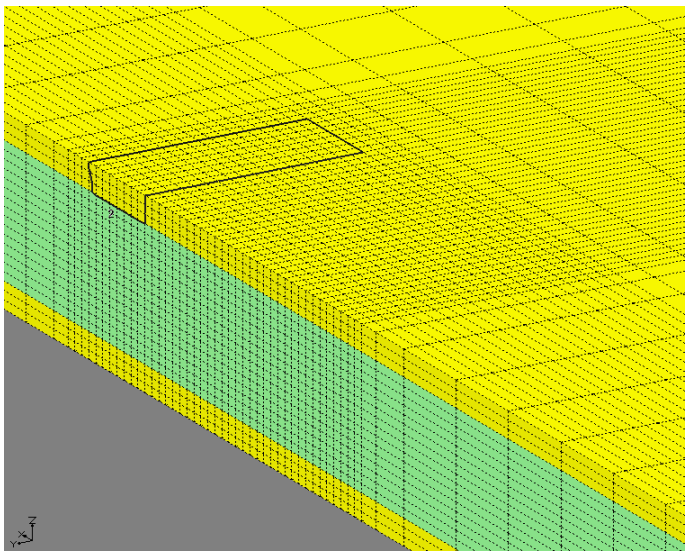

Figure 5.7: 3-D view of the pile during pore pressure dissipation for Case 1 (t = 40 years)

According to Figure 5.7, after 40 years, pore pressure completely dissipated from the system for Case 1.

Figure 5.8 shows the model-predicted pore-pressure responses for 40 years (14600 days) with pile construction periods of 15 years (5475 days), 25 years (9125 days), 30 years (10950 days) and 35 years (12775 days). Pore pressure generation depends significantly on pile construction rate according to Figure 5.8. The oscillation of the graphs is caused by the treatment of the applied load as a series of discrete annual time steps rather than a continuous uniform loading rate. The model results were smoothened to damp the effect of this fluctuation.

Table 5.4 details the maximum pore pressure head observed for four loading rates for Case 1.

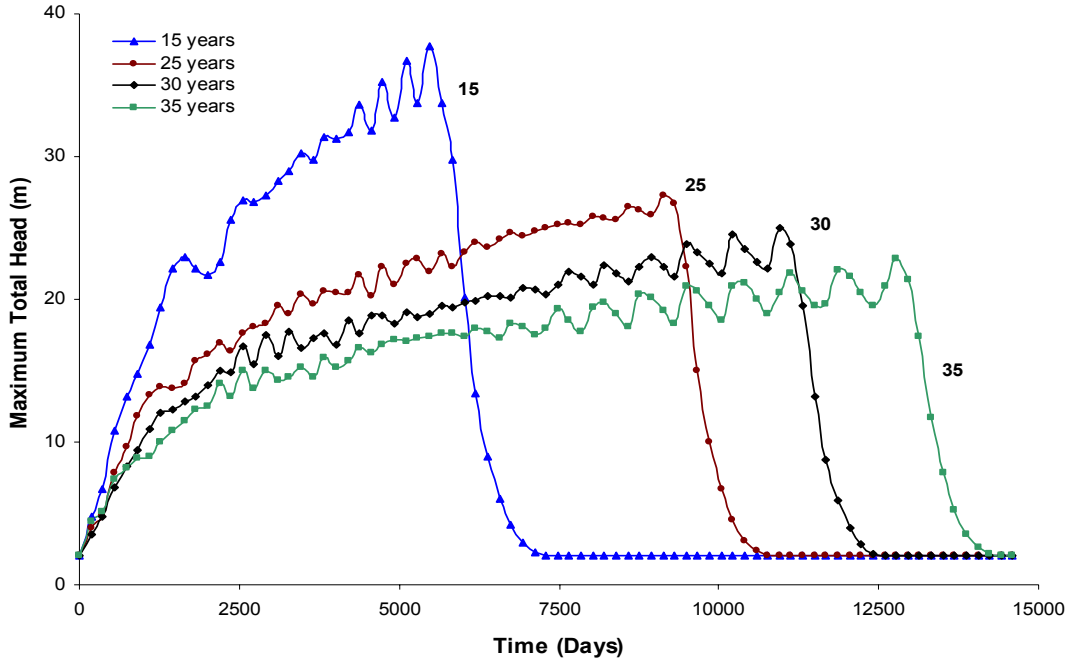

Figure 5.8: Maximum Total Head vs Time for Case 1

Table 5.4: Maximum total head values for Case 1

Pile construction period (Years)	Maximum total head observed (m)
15	42
25	31
30	27
35	24

The simulation was continued after the loading period to investigate the pore pressure dissipation. For all cases, the maximum simulation time was 40 years. In Figure 5.8, similar dissipation patterns can be observed for all four cases. For the 15 year construction period, pore pressure head dissipates from 42 m to 2 m within 5 years (8.0 m/yr). Similar to the 15 year construction period, pore pressure drops from the corresponding maximum value to 2 m head within 5 years for all the other loading rates. It appears that the dissipation rate is insensitive to loading rate than the peak pressure.

5.4.2 Case 2 (Scenario 9)

Figure 5.9 describes the hydrostratigraphic scenario 9, Case 2. The thickness of each sand layer is 2.86 m and that for till is 54.28 m. Compared to Case 1, the thickness of the sand layer is smaller and that for till is greater. High pore pressure generation and slower dissipation rate was observed for this Case when compared to Case 1.This Case is similar to Case 1 hydrostratigraphically but with thicker, high K/S_s till and thinner, low K/S_s dense sand layers present.

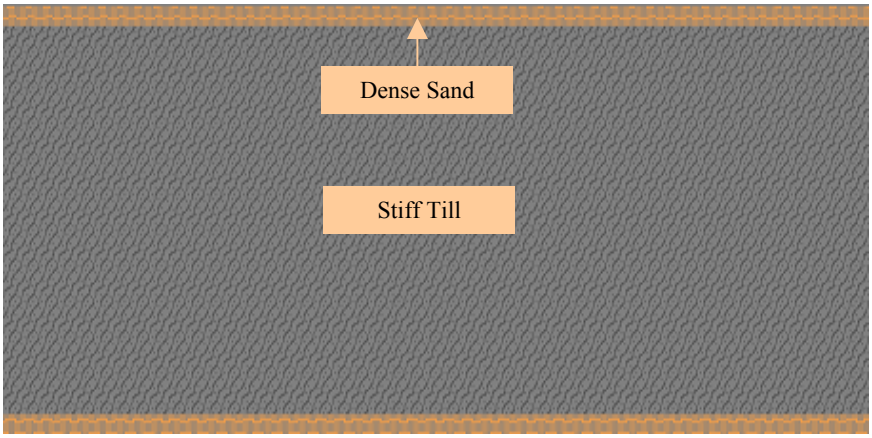

Figure 5.9: Hydrostratigraphic Case 2

Figure 5.10 shows the pore pressure generation behaviour for hydrostratigraphic scenario 9, Case 2. A similar pore pressure generation pattern is observed for this hydrostratigraphic scenario with thicker till but the pressures are higher (by 9-10 m).

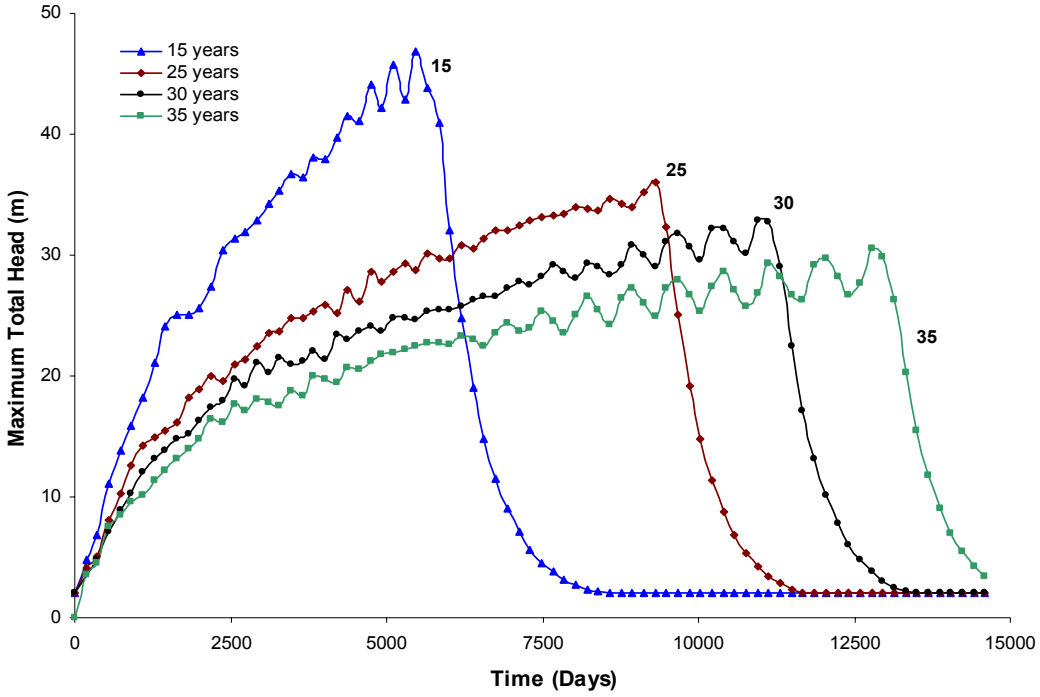

Figure 5.10: Maximum Total Head vs Time for Case 2

Table 5.5 shows the maximum total head observed for four loading rates for Case 2. The maximum pore pressure head was again observed at the end of the pile construction period.

Table 5.5: Maximum total head values for Case 2

Pile construction period (Years)	Maximum total head observed (m)
15	51
25	41
30	37
35	33

Pore pressure dissipation rates with the thicker till are lower compared to Case 1. The thicker till layers extend the drainage path and are responsible for the lower dissipation rate. The total head drops from 51 m to 2 m in 9 years for 15 year pile construction period. For 25 years pile construction, maximum head drops from 41 m to 2 m in about 7 years. For 30 years pile construction, maximum pressure head drops from 37 m to 2 m in about 7 years. For 35 years pile construction, pore water head drops to only 3 m from 33 m at the end of the simulation period. It appears that increasing the till thickness leads to some measurable differences in pore-pressure dissipation rates compared to Case 1.

5.4.3 Case 3 (Scenario 1)

Hydrostratigraphic scenario 1, Case 3, shown in Figure 5.11 is a single drainage scenario. The sand and till layers have thickness of 2.86 m and 57.14 m respectively. Excessive pore pressure generation and slow dissipation rates were observed for this Case, compared to Case 1 and 2.

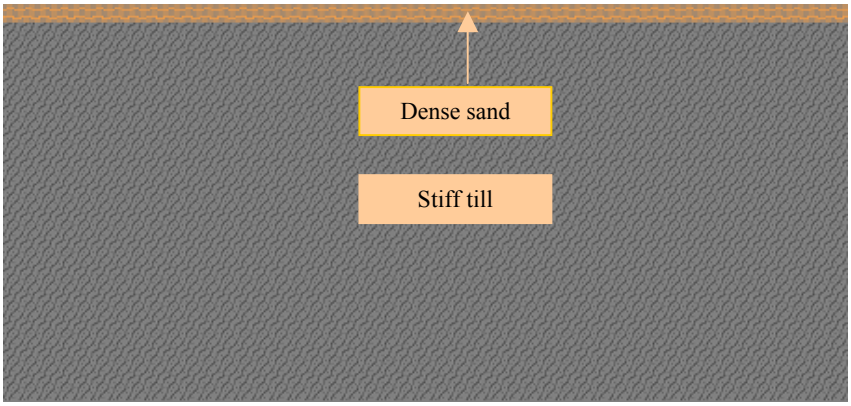

Figure 5.11: Hydrostratigraphic Case 3

Figure 5.12 illustrates the pore pressure development for Case 3. Figure 5.13 shows the pore pressure dissipation with time. Contour specified values are in meters. In general single drainage scenarios have slower dissipation rate compared to double drainage scenarios. For this single drainage Case, dissipation is slow compared to the double drainage Case 1 previously discussed. Therefore, significant pore pressures are sustained at the end of 40 years.

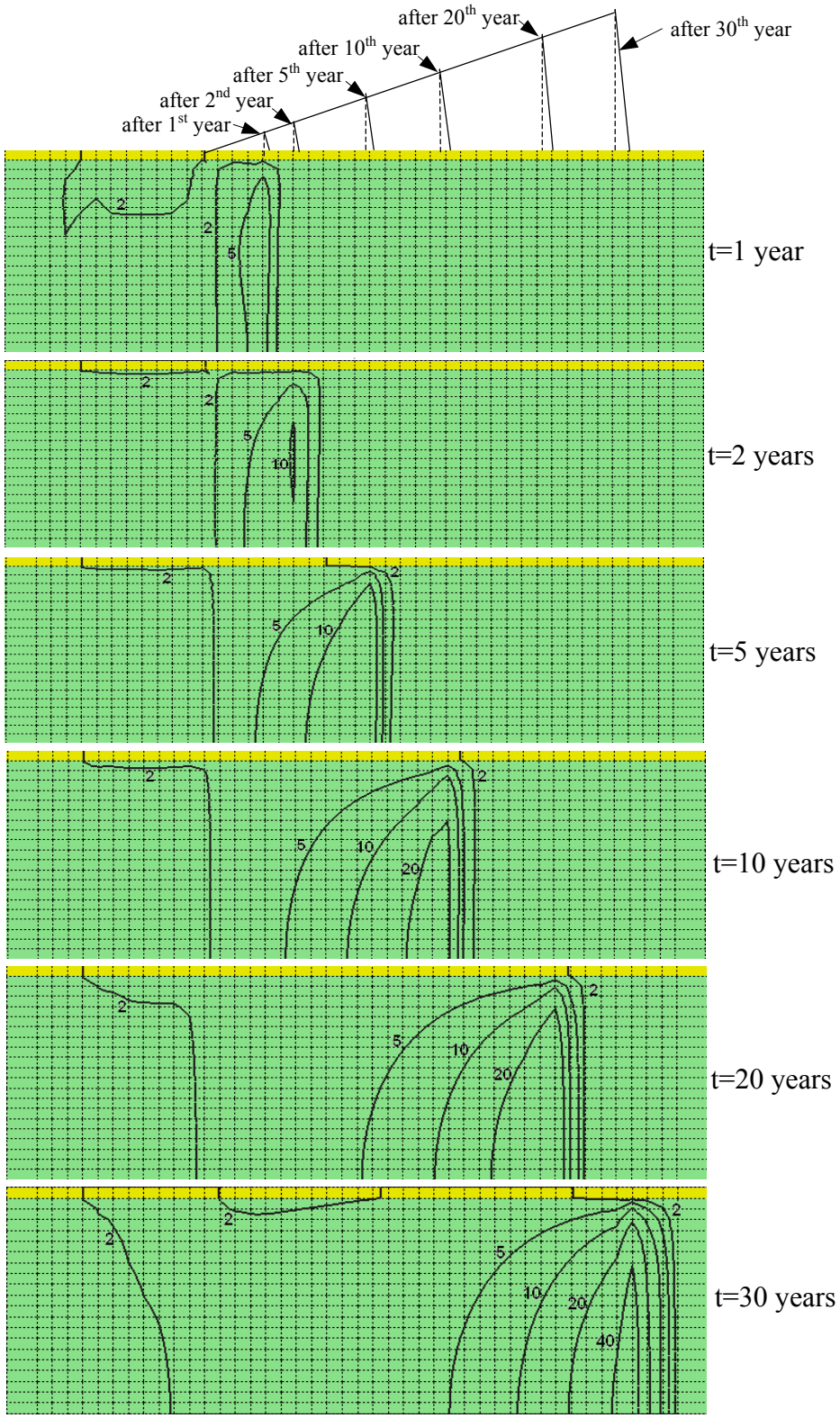

Figure 5.12: Pore pressure development patterns for loading for Case 3

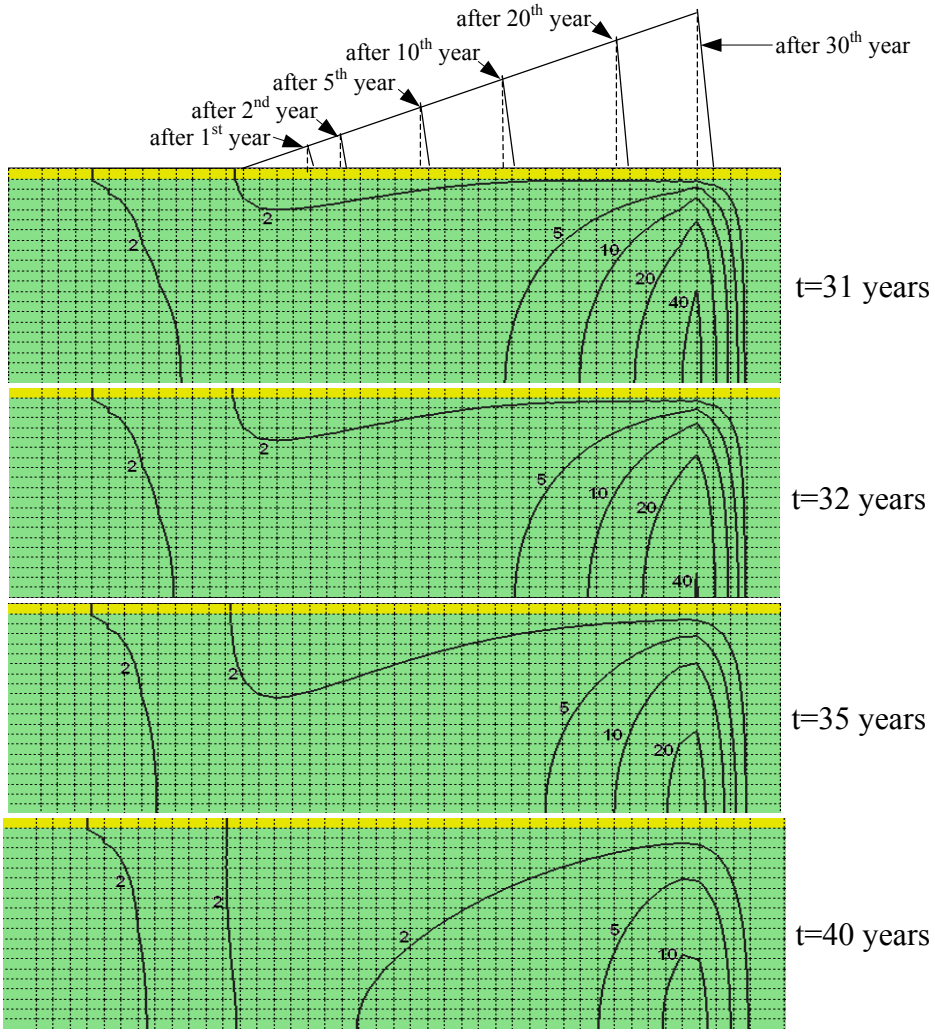

Figure 5.13: Pore pressure dissipation patterns for Case 3

Figure 5.14 and 5.15 respectively demonstrate the 3-D views of pore pressure development patterns for t = 1, 2, 5 years and t = 10, 20, 30 years. Figure 5.16 and 5.17 respectively demonstrate the pore pressure dissipation patterns for t = 31, 32, 35 years and t = 40 years.

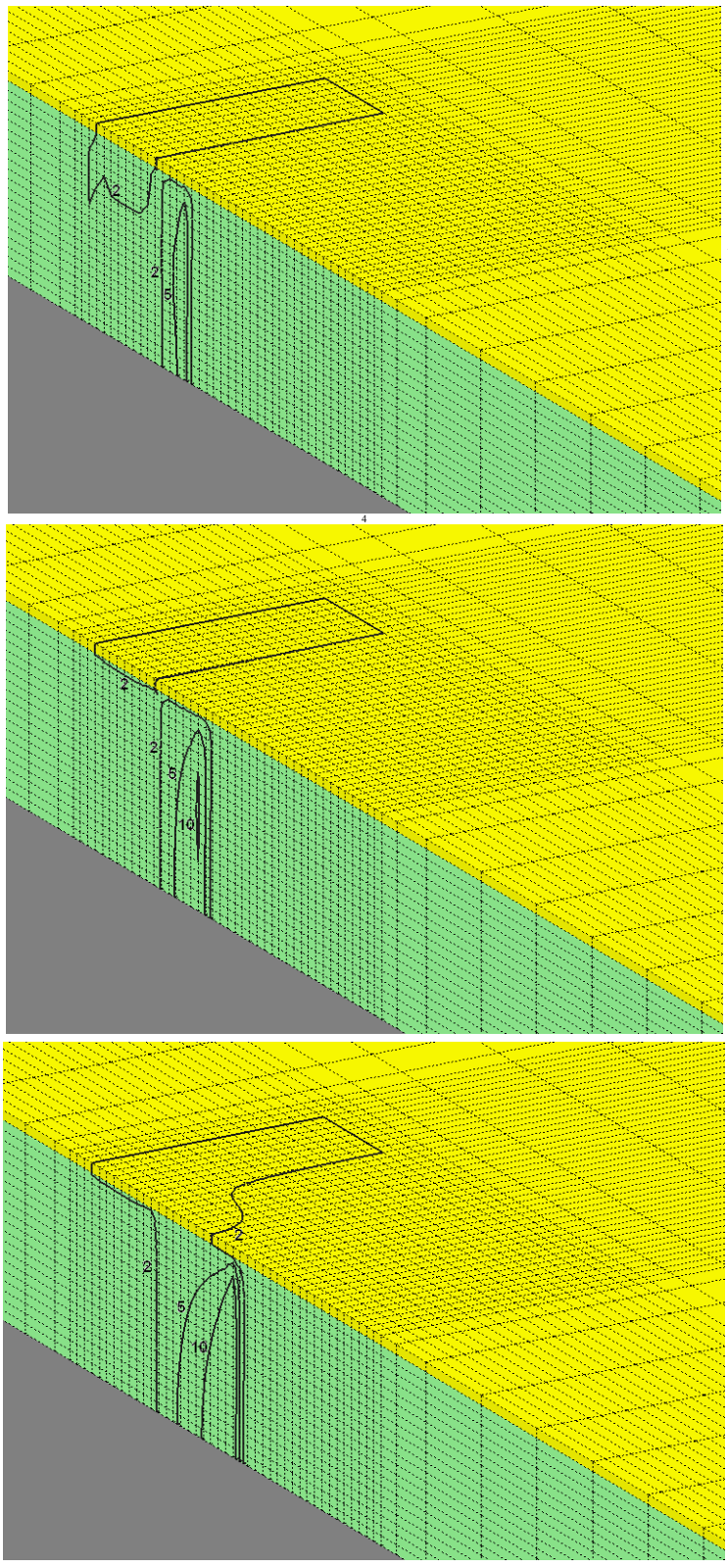

Figure 5.14: 3-D view of the pile during pore pressure development for loading for Case 3 (t = 1, 2, 5 years)

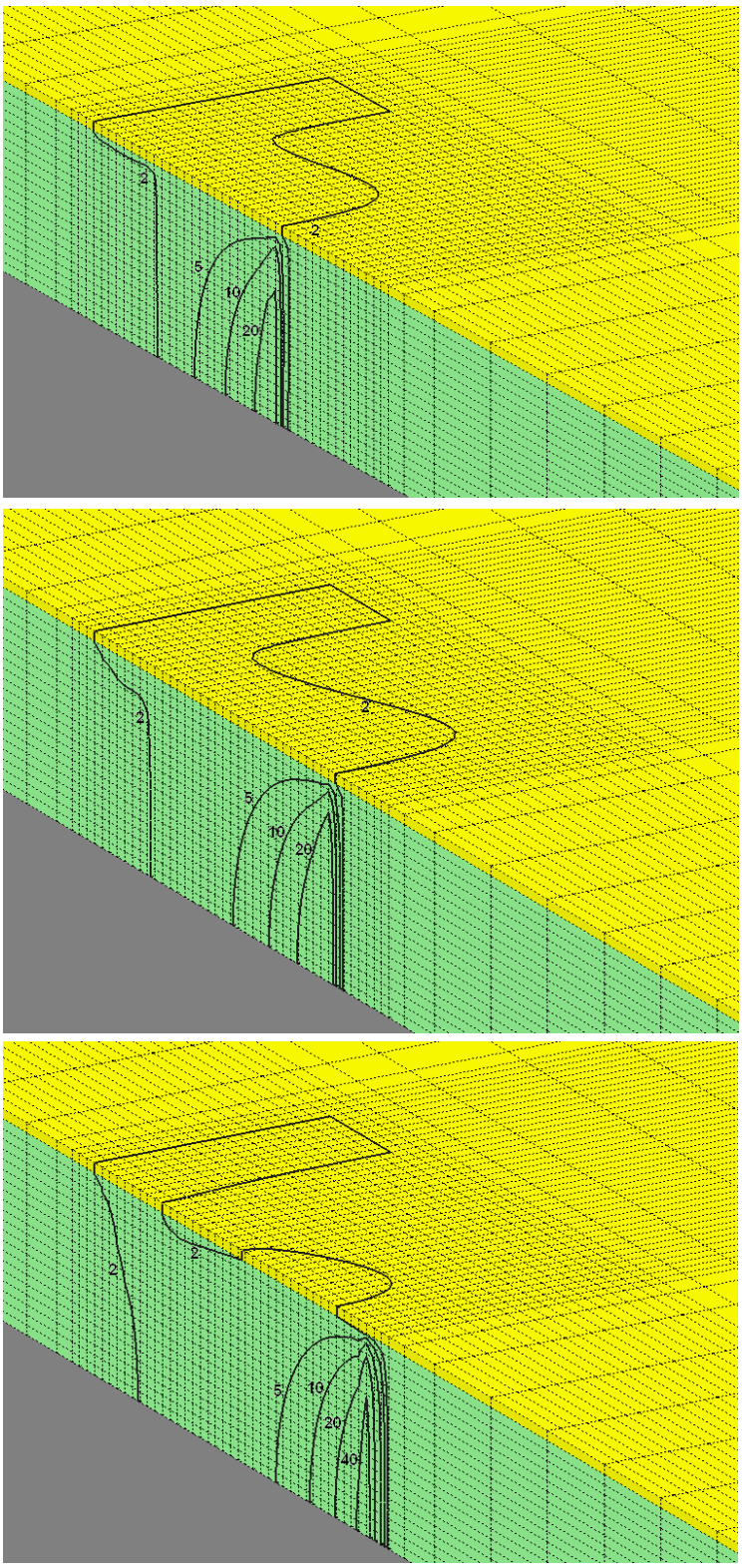

Figure 5.15: 3-D view of the pile during pore pressure development for loading for Case 3 (t = 10, 20, 30 years)

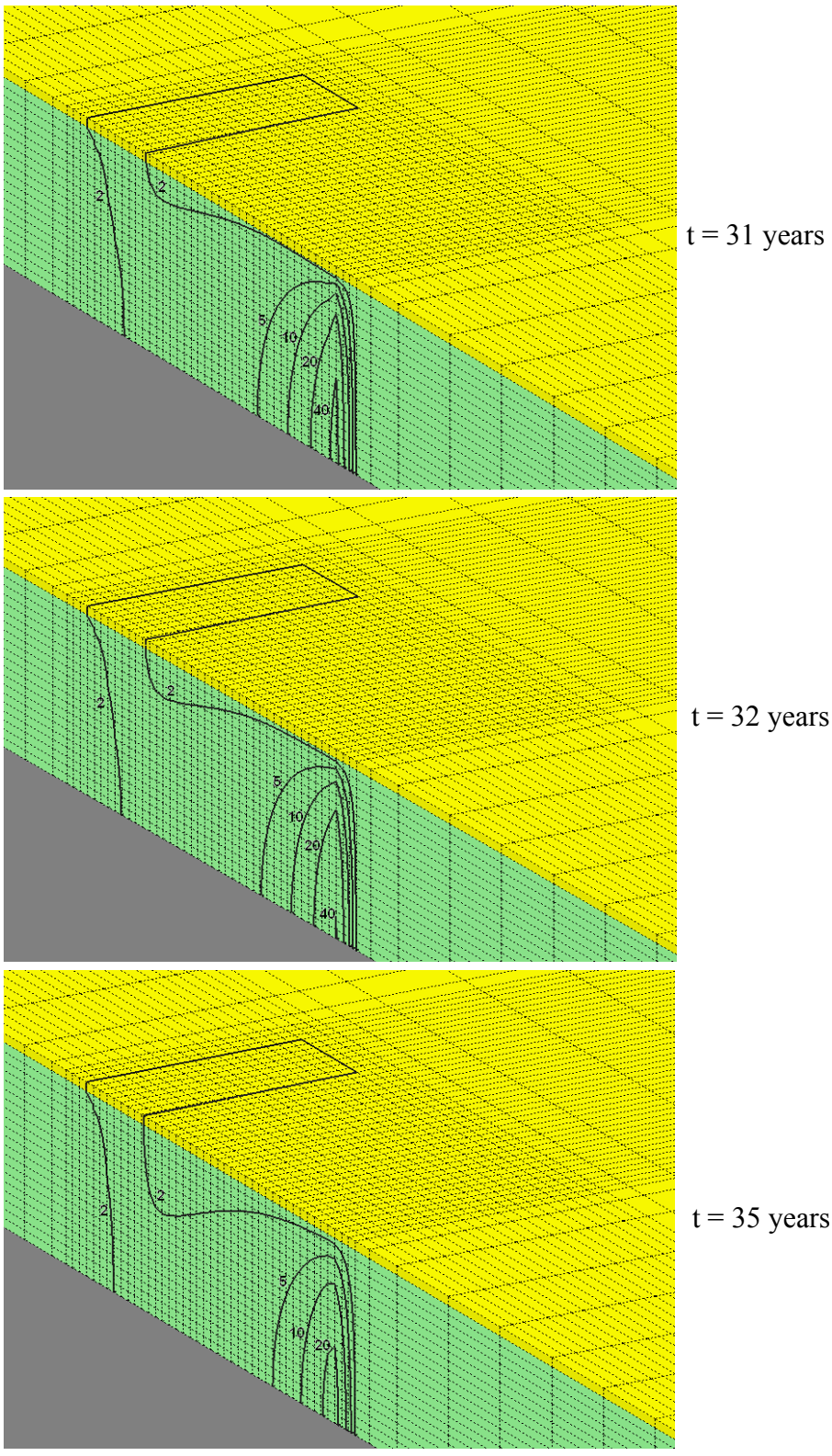

Figure 5.16: 3-D view of the pile during pore pressure dissipation for Case 3 (t= 31, 32, 35 years)

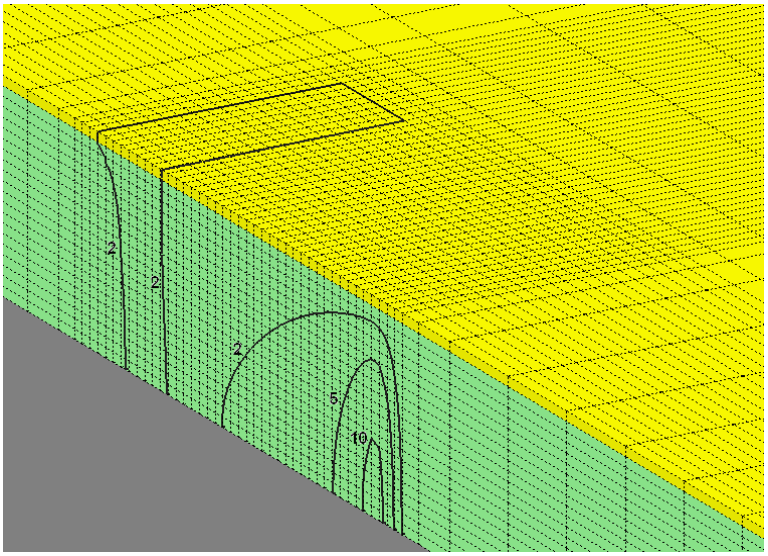

t = 40 years

Figure 5.17: 3-D view of the pile during pore pressure dissipation for Case 3 (t= 40 years)

According to Figure 5.17, significant pore pressures are sustained in the system at the end of 40 years.

In Figure 5.18, for all construction rates, the maximum total head varies between 52-58 m. Slow dissipation rates are observed because of the thicker till material and the longer drainage path associated with the single drainage boundary. For the 15 year construction period, it takes about 25 years for the head to fall from 58 m to 2 m. In all the other cases, a similar rate of dissipation is observed for relatively similar maximum head values.

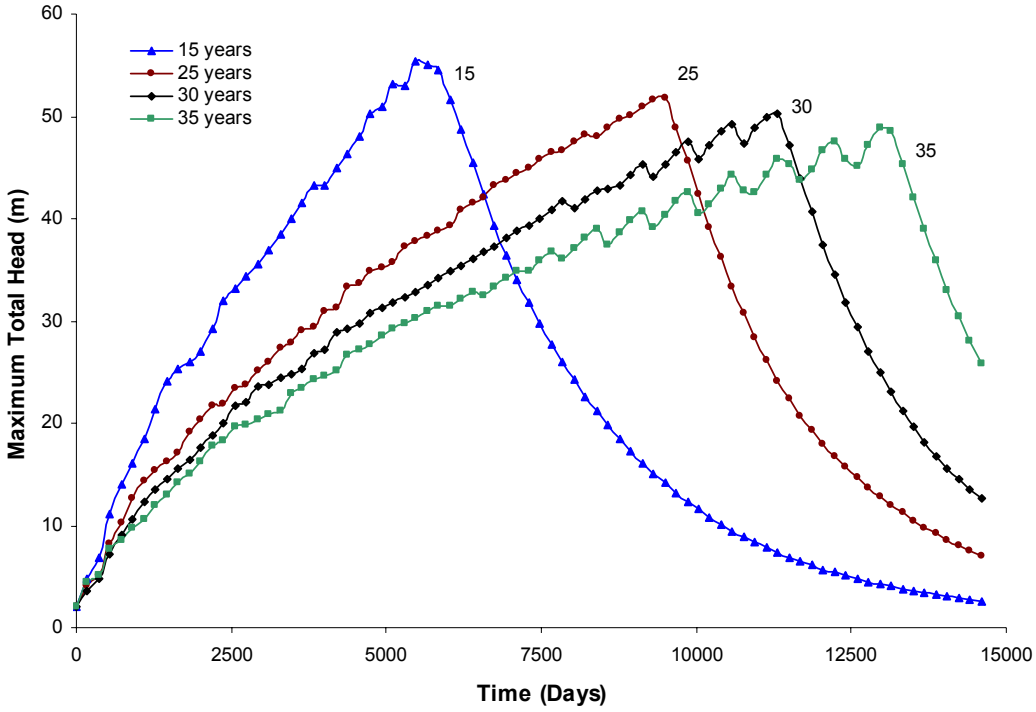

Figure 5.18: Maximum Total Head vs Time for Case 3

Table 5.6 details the maximum total head observed for the four construction periods under hydrostratigraphic scenario 1, Case 3. Unlike the previous two Cases, the maximum heads observed for the different construction periods do not vary significantly. For all loading rates, maximum head was observed at the end of pile construction period.

Table 5.6: Maximum total head values for Case 3

Pile construction period (Years)	Maximum total head observed (m)
15	58
25	55
30	53
35	52

5.4.4 Case 4 (Scenario 11)

Figure 5.19 is hydrostratigraphic scenario 11 with a plastic clay layer present. Plastic clay has a lower K/S_s (c_v) ratio compared to till and very much lower compared to sand. A very low pore pressure dissipation rate is observed because of the low K/S_s ratio. The sand and plastic clay layers are 2.86 m thick and the till layer is 54.28 m in thickness. This case simulates a thick till over bedrock shale with a shear surface at the bedrock contact.

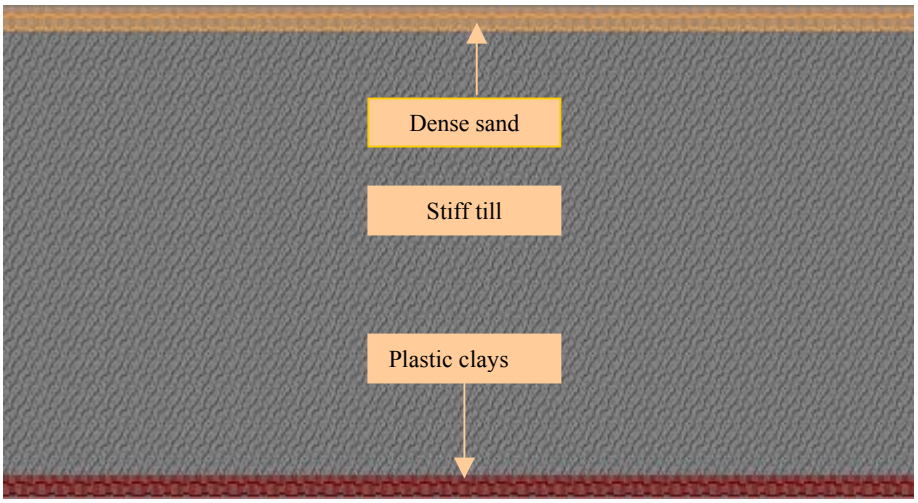

Figure 5.19: Hydrostratigraphic Case 4

Regardless of the pile construction period, approximately the same excess head (55 m) is developed as shown in Figure 5.20. For the 15 year pile construction period, the head drops by only about 24 m in 25 years. The plastic clay has a very low K/S_s value and does not allow the excess head to dissipate. High excess pore-pressures can be sustained for extended periods (decades) in this Case.

Table 5.7 details the maximum total head values observed for four loading rates for case 4.

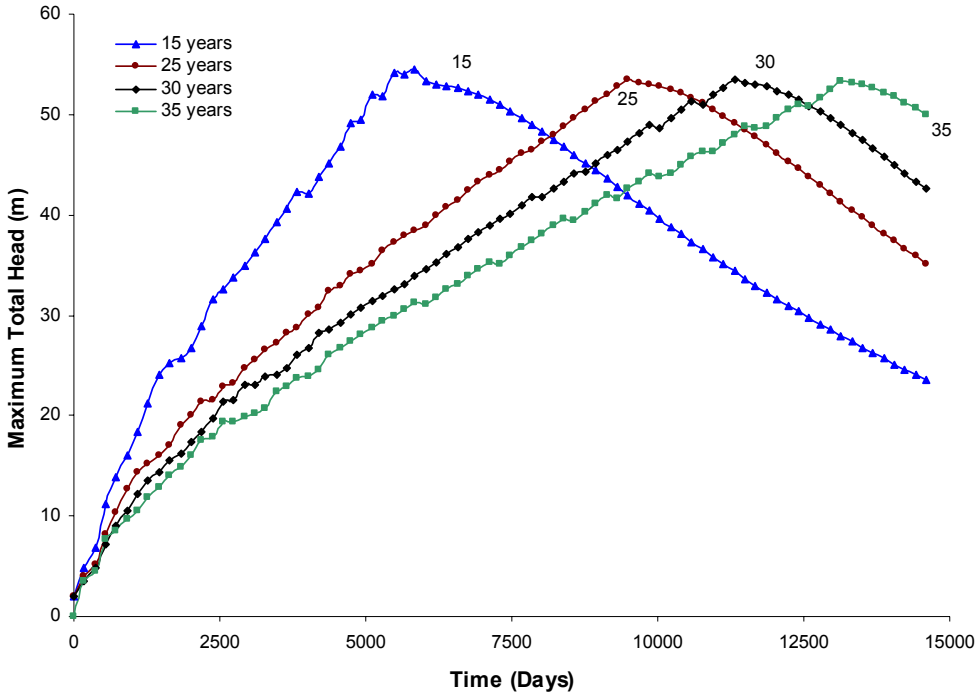

Figure 5.20: Maximum Total Head vs Time for Case 4

Table 5.7: Maximum total head values for Case 4

Pile construction period (Years)	Maximum total head observed (m)
15	56
25	54
30	54
35	54

5.5 Loading Pattern 2

A relatively smaller excess head development was observed for the second loading pattern, where the load increments were applied over the entire footprint of the pile. For this reason, head generation was significantly lower compared to loading pattern 1. Only the 30 years construction period was considered for the uniform loading pattern 2. The same hydrostratigraphic scenarios (8, 9, 1, and 11) that were investigated in details for loading pattern 1 were used.

Table 5.8 details the general results for loading pattern 2 for pore pressure variation with time at selected time intervals. Compared to loading pattern 1, relatively lower pore-pressure head development was observed throughout the simulation period. For scenario 11, the peak head and head development is similar to loading pattern 1. The presence of plastic clay is the reason for this.

Table 5.8: Pore pressure head observed for four scenarios for loading pattern 2 for 30 years construction period

Time (yrs)		Head (m)			
		Scenario			
		8	9	1	11
Loading	1	2.2	2.3	2.3	2.3
	2	2.7	3.3	3.7	3.7
	5	3.8	5.7	9.8	10.3
	10	3.9	6.4	16.3	20.9
	20	4.0	6.6	21.4	37.2
	30	4.1	6.7	23.0	47.9
Dissipating	31	2.0	4.4	20.8	46.5
	32	2.0	3.0	18.6	45.0
	35	2.0	2.6	13.0	40.5
	40	2.0	2.5	7.3	33.8
		Case 5	Case 6	Case 7	Case 8

5.5.1 Case 5 (Scenario 8)

Figure 5.21 shows a comparison of the pore pressure development for loading patterns 1 and 2 for a 30 years construction period for scenario 8. A very significant difference in head generation can be observed. For loading pattern 1, the maximum head observed was about 27 m at 30 years. For loading pattern 2, the maximum head was 4 m. It should be emphasized that loading pattern 1 more representative of pile construction at the potash mine sites.

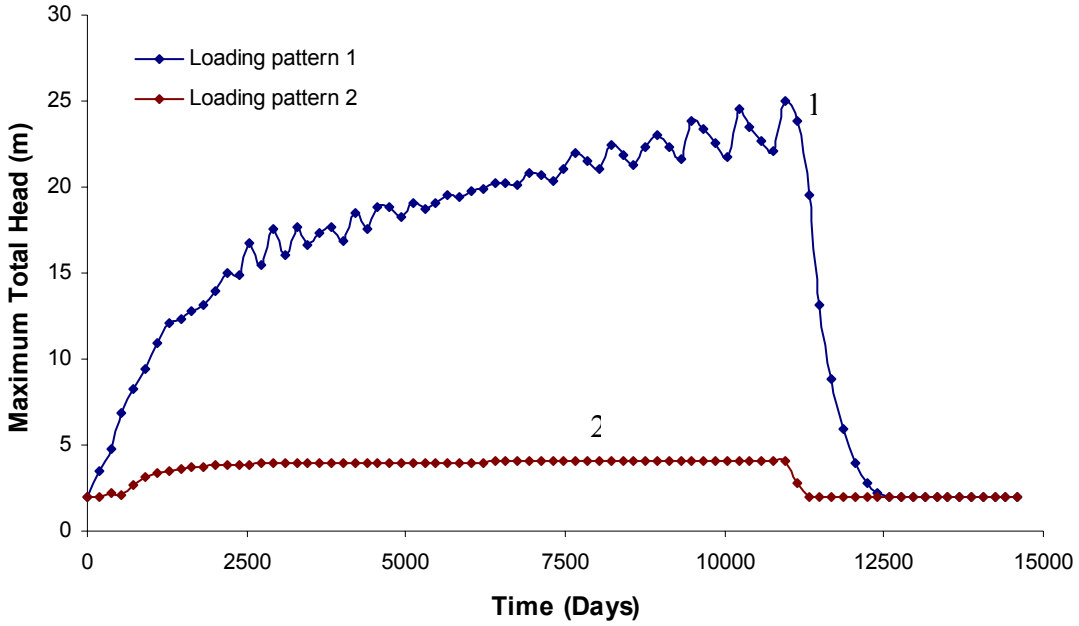

Figure 5.21: Maximum Total Head vs. Time for 30 years for Case 5

5.5.2 Case 6 (Scenario 9)

Figure 5.22 shows a comparison between loading pattern 1 and 2 for hydrostratigraphic scenario 9. The pore pressure generation and dissipation follow similar patterns for case 5 and case 6. In case 6, the maximum head observed for pattern 1 was 37 m and that for loading pattern 2 was 7 m. The greater till thickness results in higher excess heads and slower dissipation.

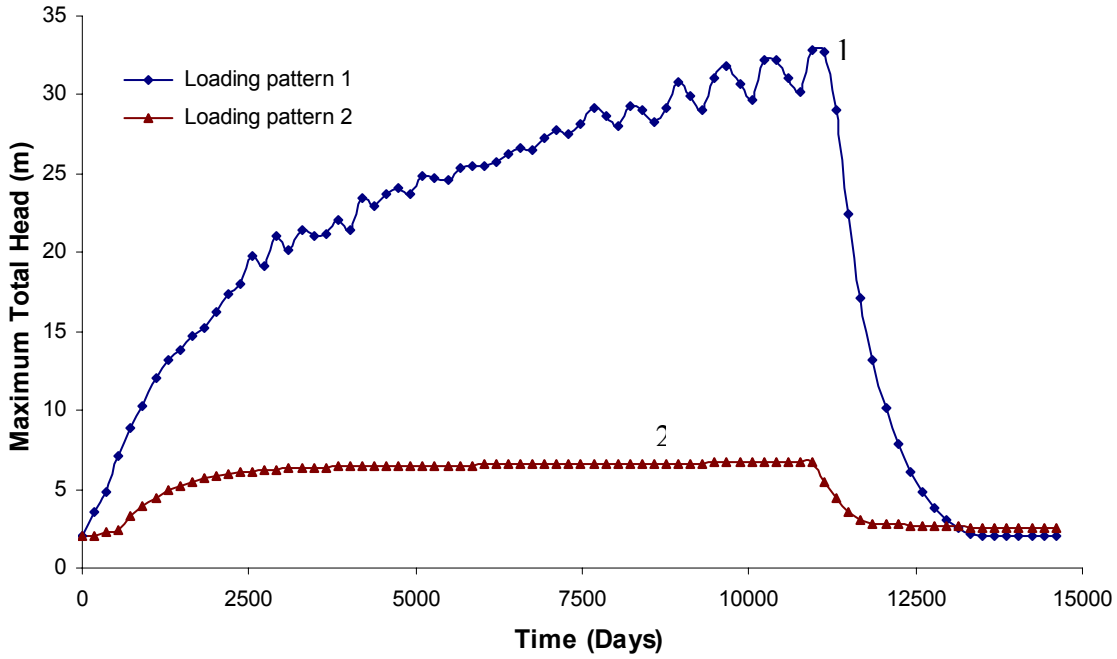

Figure 5.22: Maximum Total head vs. Time for 30 years for Case 6

5.5.3 Case 7 (Scenario 1)

Figure 5.23 shows the comparison of the two loading patterns for hydrostratigraphic scenario 1. The maximum head observed for loading pattern 1 was 53 m and that for loading pattern 2 was 23 m. The difference in head for the two loading patterns remains significant for the single-drainage scenario but is not an extreme as for the double-drainage scenarios (cases 5 and 6).

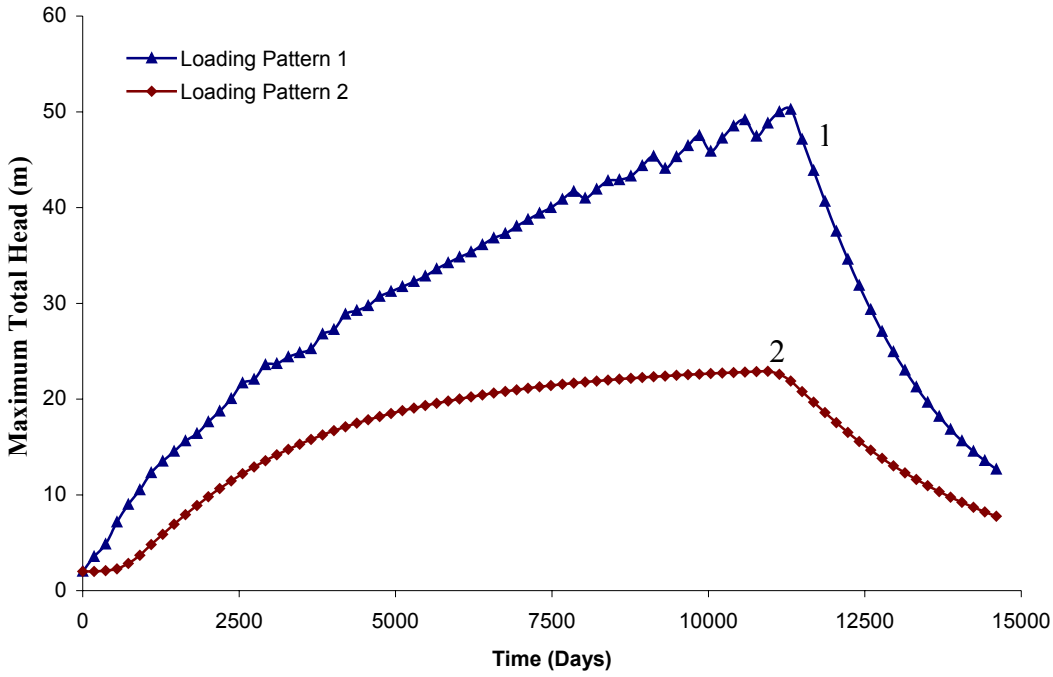

Figure 5.23: Maximum Total head vs. Time for 30 years for Case 7

5.5.4 Case 8 (Scenario 11)

Figure 5.24 illustrates the comparison for the hydrostratigraphic scenario 11 with a plastic clay layer. The very low K/S_s of plastic clay layer results in significantly higher heads for both cases loading patterns. The maximum head for pattern 1 was 54 m and that for pattern 2 was 48 m. Unlike in the previous cases, difference between the maximum head for two loading patterns is small. The plastic clay layer combined with the long drainage path prevents the rapid dissipation of the excess head. It appears that in circumstances where large excess pore-pressures can be expected, the influence of loading pattern is not large.

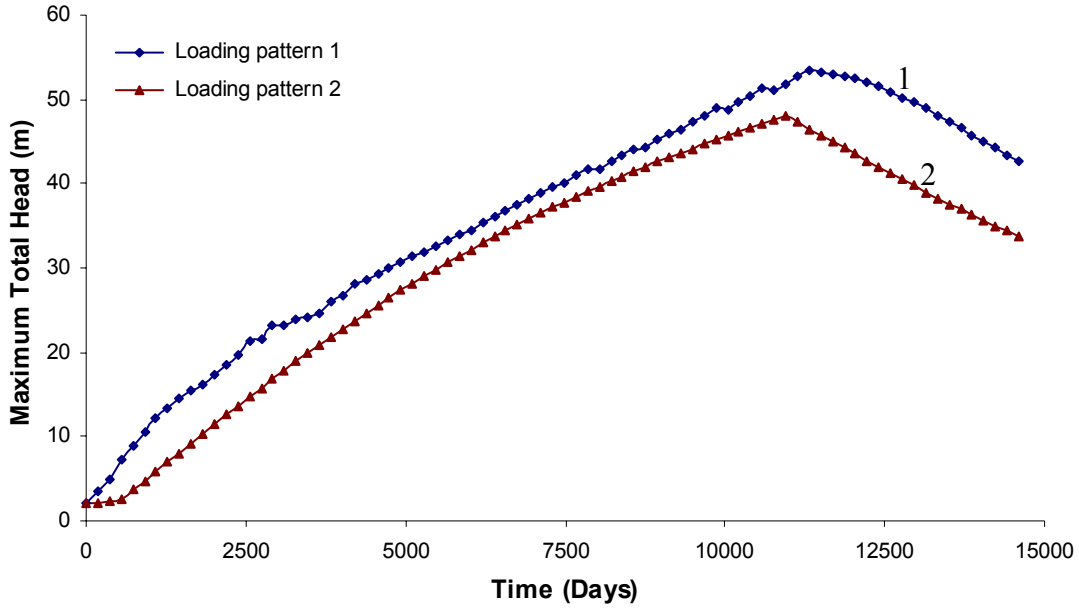

Figure 5.24: Maximum Total head vs. Time for 30 years for Case 8

5.6 Sensitivity Analysis

A sensitivity analysis was conducted to evaluate the impact of material properties on pore pressure generation. The sensitivity analysis was conducted by changing the hydraulic conductivity of the till layer (the thickest component). Four different hydraulic conductivity cases were considered for till layer by keeping the hydraulic conductivities of sand and plastic clay layers constant. The hydrostratigraphic scenario 11 with the plastic clay layer was selected for the sensitivity analysis. Table 5.9 shows the material properties used for sensitivity analysis.

Table 5.9: Material properties used for sensitivity analysis

Trial	Hydraulic conductivity of sand (m/s)	Hydraulic conductivity of plastic clay (m/s)	Hydraulic conductivity of till (m/s)
1	1.00×10^{-4}	1.00×10^{-9}	3.16×10^{-8}
2	1.00×10^{-4}	1.00×10^{-9}	1.00×10^{-8}
3	1.00×10^{-4}	1.00×10^{-9}	3.16×10^{-9}
4	1.00×10^{-4}	1.00×10^{-9}	1.00×10^{-9}

The results of the sensitivity analysis are shown in Figure 5.25. The hydraulic conductivity of till influences excess pore pressure generation. The smaller the hydraulic conductivity, the greater the head but the differences are relatively small over a range of two and a half orders of magnitude.

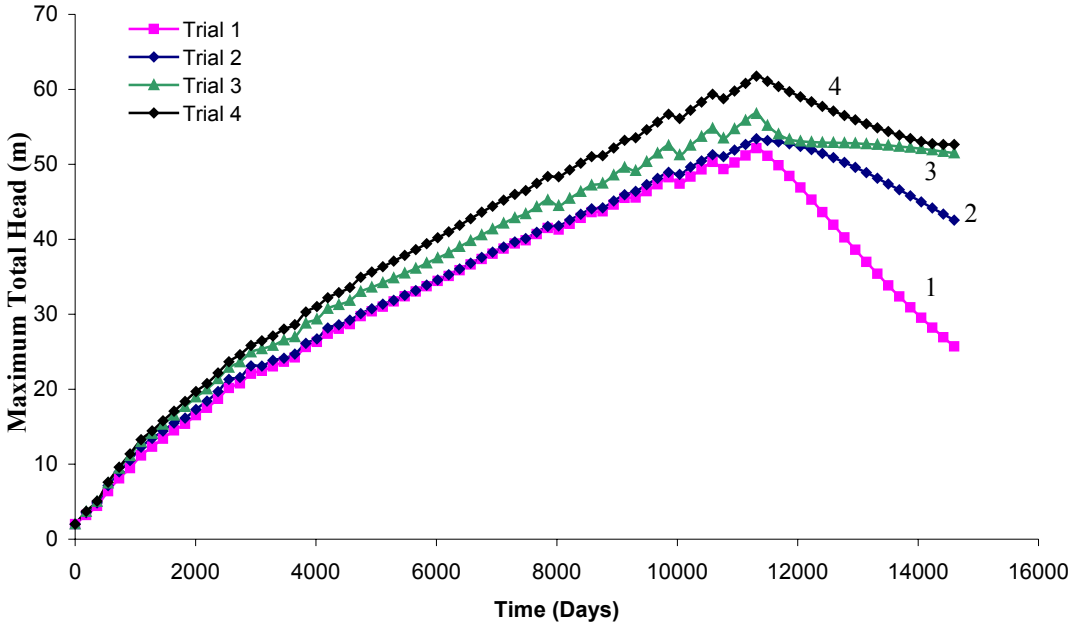

Figure 5.25: Maximum Head vs. Time for Sensitivity Analysis

6. CONCLUSIONS AND RECOMMENDATIONS

6.1 General Conclusions

The study investigated eleven hydrostratigraphy scenarios for two loading patterns to simulate the effect of salt tailings pile construction on pore pressures in the vicinity of TMAs. The hydrostratigraphic scenarios were chosen to represent a range of materials and stratigraphies typical of conditions found at potash mine sites in Saskatchewan. The loading patterns were chosen to represent pile construction methods (end-tipping and uniform vertical growth) that can be regarded as "end members" producing respectively the greatest (end-tipping) and smallest (uniform vertical growth) local concentrations of load.

The Terzaghi 1-D consolidation equation is used extensively in geotechnical practice to predict both pore-pressures and settlements. The model study produced the expected results relating to material properties and lengths of drainage paths. The eleven model scenarios cover a wide range of sand-till sequences with varying aquitard thickness. The results are consistent with expected values estimated from the 1-D consolidation equation.

6.2 Pile Construction Conclusions

The most interesting conclusions are those relating to loading pattern and loading rates, reflecting pile construction methods. For both double and single drainage cases, pile construction has a strong influence on the magnitude of predicted peak excess pore-pressures. Such pore-pressures can potentially be transmitted to critical locations beneath the toe of scarp-slope of piles by discontinuous lenticular sand bodies.

Incremental loading, applied over the certain footprint of the zone of the TMA allocated to the pile (Loading pattern 2), generates the smallest peak excess pore pressures. Growth of the scarp-edge of the pile by end-tipping produces locally concentrated high loads (Loading pattern 1) and generates the greatest peak excess pore pressures. The magnitudes of the peak head can exceed the height of the pile when adverse materials (plastic clays) are present. These findings are consistent with observations made at several mining sites where such conditions are found. Where such conditions exist, with single drainage, predicted peak pore-pressures are relatively very sensitive to the loading pattern and loading rate (although loads predicted for loading pattern 1 always exceed those for loading pattern 2 and rapid loading always generates greater heads than slower loading). It appears that extensive continuous aquifer layers are effective at rapidly dissipating pore pressures. Where such natural drains do not exist, excess heads of 50-60 m may be sustained for extended periods.

6.3 Sensitivity Analysis Conclusions

The sensitivity analysis reveals that the excess pore pressure generation behaviour is sensitive to the hydraulic conductivity of the materials. The smaller the hydraulic conductivity, the higher the pore pressures generated and the more slowly they dissipate. However the sensitivity analysis shows that increasing the K-value by two and a half orders of magnitude reduces the predicted maximum excess head from 60 m to 50 m for the case where predicted heads are greatest.

6.4 Recommendations for Future Work

Time and available funding limited the research study but it can be further extended in a few directions to enhance the results.

- Pile loading analysis was investigated for four basic geological scenarios with sand, till and plastic clays. The research can be further extended to examine some other geological features such as lenticular units with different material properties.
- Fluctuations of the modelled pore pressure generation can be minimized in a future investigation. The time step selected for the study was 1.825 days. This discrete time step is the reason for this. Discrete time steps can't be avoided but can be further reduced. If the time step is minimized, the running time would be

greater and the cost will be higher. However, much more stable results can be generated if a small time step is used in a future study.

- More accurate results can be obtained by reducing the mesh spacing for the model. The spacing for the existing mesh is 40 m x 40 m. This was selected by considering the dimensions of the region to be modelled. If the mesh spacing is reduced, the time and the cost for the model running will be greater.
- Sensitivity analysis was conducted only for hydraulic conductivity of the till lithology. From this study, a general conclusion can be made about the impact of hydraulic conductivity on pore pressure generation and dissipation behaviour. It is recommended in a future study that a more comprehensive sensitivity analysis might be conducted for hydraulic conductivity (K) and specific storage (S_s). Hydraulic conductivity was chosen because it is subject to the greatest variation under field conditions, although K/S_s would be a better choice if all materials were to be investigated. For an individual material, S_s shows relatively little variation compared with K. Therefore K also varies in a similar manner to K/S_s.

REFERENCES

Boussinesq, M.J. 1885. *Application des potentiels a l'etude de l'equilibre et du movement des solides elastiques, principalement au calcul des deformations exerces sur une petite partie de leur surface ou de leur interieur: memoire suivi de notes etendues sur divers points de physique mathematique et d'analyse*, GauthierVillars, Paris, pp. 722.

Bredehoeft, J.D., and B.B.Hanshaw. 1968. *On the maintenance of anomalous fluid pressures: I. Thick sedimentary sequences*. Geological Society of America Bulletin 79, no 9. pp: 1097-1106.

Eigenbrod, K.D., and T. Issigonis. 1996. Pore-water Pressures in Soft to Firm Clay during Driving of Piles into Underlying Dense Sand. Canadian Geotechnical Journal. 33, pp: 209-218.

Eisenstein, Z., and S.T.C. Law. 1977. Analysis Behavior of Mica Dam. American Society of Civil Engineers, Journal of the Geotechnical Engineering Division, Vol 108, no: 8, pp: 879-895.

Fadum, R.E. 1948. Influence Values for Estimating Stresses in Elastic Foundations. Proceedings of Sec. Intern. Conf. on Soil Mech. And Found. Engr., Vol. 2, pp: 77-84.

Gibson, R.E.1958. *The progress of consolidation in a clay layer increasing in thickness with time*. Geotechnique, Vol.8, No. 4, pp: 171-182.

Hemond, H.F., and J.L. Fifield. 1982. *Subsurface Flow in a Salt Marsh Peat: A Model and Field Study*. Limnology and Oceanography 27, no 1. pp:126-136.

Hemond, H.F., W.K. Nuttle, R.W. Burke, and K.D. Stolzenbach. 1984. Subsurface Infiltration in Salt Marshes: Theory, measurements, and biogeological implications. Water Resources Research 20, no. 5, pp: 591-600.

Landine, P. G., 1993. *Weathering and Diagenesis of Saskatchewan Potash Tailings*. PhD Thesis, University of Saskatchewan, Saskatoon, Canada.

Lin, H.C., Richards, D.R., Talbot C. A., Yeh, G.T., Cheng, G.R., Cheng, H.P. and Jones, N.L. 2001 *FEMWATER: Three-Dimensional Finite Element Computer Model for Simulating Density-dependent Flow and Transport in Variably Saturated Media.* Version 3.0 Reference Manual, 587p.

Loi, J.I., 1988. *Engineering Properties of Potash Tailings*. M.Sc Thesis, University of Saskatchewan, Saskatoon, Canada.

Neuzil, C.E. 1993. *Low fluid pressure within the Pierre Shale: A transient response to erosion*. Water Resources Research 29, no 7. pp: 2007-2020.

Neuzil, C.E. 1995. *Abnormal pressures as hydrodynamic phenomena*. American Journal of Science 295, no.6. pp: 742-786.

Newmark, N.M. 1940. *Stress Distribution in Soils*. Proceedings of the Purdue conference on Soil Mechanics and Its Applications, pp: 295-303.

Olson, R.E. 1989 (spring) and J. Lai. 2003 (fall, modified). Unit 8: Stress Distribution. A series of lecture notes prepared for the course "Advanced Soil Mechanics". Department of Construction Engineering, Chaoyang University of Technology, Taichung County 41349, Taiwan

Provost, A.M., C.I. Voss, and C. E. Nuezil. 1998. Site 94: Glaciation and Regional Ground-Water Flow in the Fennoscanian Shield. Tech. report Ski 96.11. Stockholm: Swedish Nuclear Power Inspectorate (SKi).

Reeves, H.W., Thibodeau, P.M., Underwood, R.G. and Gardner, L.R. 2000. *Incorporation of Total Stress Changes into the Groundwater Model SUTRA.* Groundwater. Vol.38 (1), pp: 89-98.

Reeves, M. 2005. *Proposal to the Saskatchewan Potash Producers Association for a Grant-in-Aid of Research*. University of Saskatchewan, Saskatoon, Canada.

Reeves, M. and Dissanayake, N. 2006. *Verification of a Modified Version of the FEMWATER Code for Variable Density Flow and Transport in Variably Saturated Porous Media*. Report submitted to Saskatchewan Potash Producers Association. University of Saskatchewan, Saskatoon, Canada.

Spangler, M.G. 1951. Soil Engineering, International Textbook Company, Scranton, USA.

Taylor, D.W. 1948. Fundamentals of Soil Mechanics, John Wiley and Sons, New York City.

Thibodeau, P.M., L.R. Gardner, and H.W. Reeves. 1998. *The role of groundwater flow in controlling spatial distribution of soil salinity and rooted macrophytes in a southeastern sea marsh, USA.* Mangroves and Salt Marshes 2, no. 1:1-13.

Voss, C.I. 1984. SUTRA, A Finite Element Simulation Model for saturated-Unsaturated Fluid Density Dependent Ground-Water Flow with Energy Transport or Chemically Reactive Single-Species Solute Transport. Water Resources Investigations Report 84-4369. Reston, Virginia: U.S. Geological Survey.

APPENDIX A

A1 Verification of the FEMWATER Model

A detailed verification study was conducted for FEMWATER model before it was applied to investigate the total stress problems in the vicinity of potash tailings. In this study, simulation results for standard benchmark problems using FEMWATER model are compared with available analytical solutions and with published groundwater modeling codes results. The numerical codes used to compare the performance of FEMWATER included FEFLOW, NAMMU, SEAWAT, SEEPW, SUTRA and TOUGH2.

The range of benchmark problems used to test the code included:

- Transient and steady-state saturated flow
- Transient and steady-state unsaturated flow
- Advective transport
- Diffusive and dispersive transport
- Pore-pressure response to total stress loading

The FEMWATER code has been successfully verified for the following benchmark problems. Standard results that were used to compare the FEMWATER results are also listed below.

- Theis's Problem (Theis, 1935)- Results compare reasonably well with Theis's analytical solution, Pinder and Frind (1972)'s Finite Difference Method (FDM) and FEFLOW code results.
- Elder's Problem (Elder, 1967) - Results compares reasonably well with Elder's FDM, SEWAT, SUTRA ands FEFLOW code results.
- Henry's Problem (Henry, 1964) - Results compares reasonably well with Henry's approximate analytical solution (1964), FEFLOW and SUTRA code results.
- Layers Problem (Thiele and Diersch, 1986) - Results compare reasonably well with the analytical solutions of Thiele and Diersch (1986) and with FEFLOW code results.
- HYDROCOIN/ Salt Dome Problem (Konikow et. al., 1997) - Results compare reasonably well with FEFLOW, TOUGH2 and NAMMU code results.
- Patch Problem (Cleary and Ungs, 1978) - Results compare reasonably well the analytical solution provided by Cleary and Ungs (1978), Cell-Analytical method (CAN), and Alternating Direction Galerkin (ADG) method.
- Matrix Diffusion Problem (Tang et. al., 1981) - Results approximately compare with the analytical solution provided by Tang et. al. (1981) and slightly inferior with FEFLOW results and the analytical solution provided by Grisak and Pickens (1980).
- Webb's Capillary Barrier Problem (Ross, 1990) - Results compare well with FEFLOW and SEEP/W results.

- Terzaghi's problem (Terzaghi, 1925, 1943) - Results compare well with the analytical solution provided by Terzaghi and Aboshi et.al. (1970) and with SUTRA code results.

The detailed verification study report (Reeves and Dissanayake, 2006) that includes all the above problems was submitted to Saskatchewan Potash Producers Association (SPPA). Out of the problems list above, Terzaghi's Problem is discussed as it describes the total stress changing groundwater flow rates.

A2 TERZAGHI'S PROBLEM

A2.1 Introduction

Most numerical models used to simulate groundwater flow are derived with the assumption that the total stress imposed on the aquifer remains constant with time (Reeves et al., 2000). If an aquifer is subjected to time dependent total stress, these models fail to properly simulate this time varying pore pressure conditions. Loading of aquifers by mine waste piles is an example of a situation where total stress changes can have a significant impact on ground water flow.

A block of a porous medium 1 m x 1 m was subjected to a changing water level on the surface and no water is allowed to flow out of the sides of the block. The pore water pressure should change in response to changes in the total stress imposed by the weight of the water on the surface of the block and the change in effective stress should be zero for a saturated system with an incompressible water phase (Reeves et al., 2000).

Figure A1 illustrates the finite element mesh and boundary conditions employed by Reeves et al. (2000) for a simple total stress problem using the USGS code SUTRA (Voss, 1984).

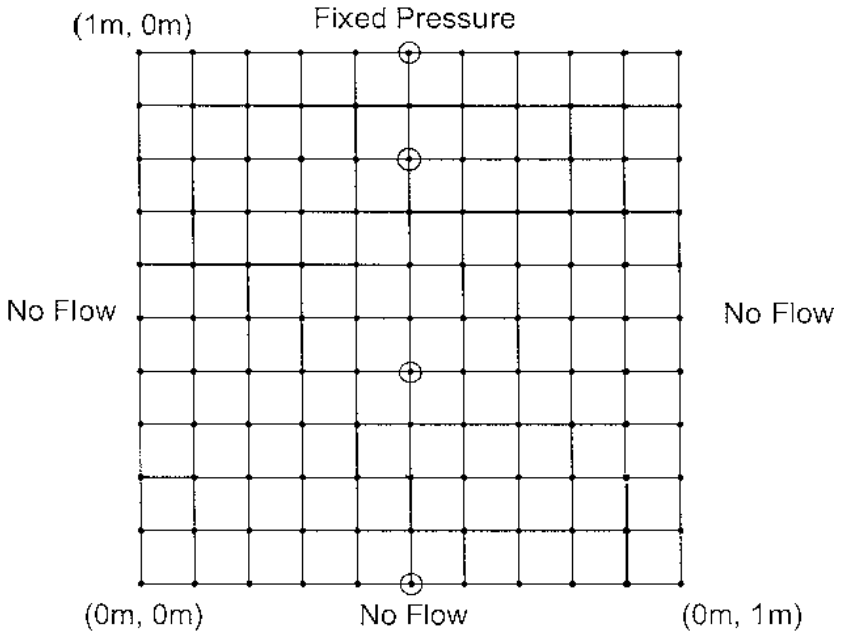

Figure A1: Model domain for example problem (Adapted from Reeves et al., 2000)

In the present study, results from a modified version of the FEMWATER code are compared with the published results using modified version of the SUTRA code. Both models are also compared with available analytical solution. The ability of the modified codes to simulate the excess pore pressure dissipation was investigated by comparing the numerical solution with the analytical solution of the 1-D consolidation equation (Terzaghi, 1925). The FEMWATER code was further tested by simulating 1-D consolidation with total stress loading applied at a constant rate for a finite period (Aboshi et al., 1970).

A2.2 Governing Equations

The governing partial differential equation for consolidation is:

$$\frac{\partial u_e}{\partial t} = c_V \frac{\partial^2 u_e}{\partial z^2} \qquad [A1]$$

where

c_V = Coefficient of consolidation, [L^2T^{-1}];

u_e = Excess pore water pressure, [MLT^{-2}];

z = Depth below the top of the clay layer, [L];

t = Time measure from the start of the consolidation, [T].

The governing partial differential equation describing application of an external total stress applied at a constant rate causing consolidation can be written as:

$$C_V \frac{\partial^2 u}{\partial z^2} = \frac{\partial u}{\partial t} - \frac{\partial \sigma}{\partial t} \qquad [A2]$$

where

$\frac{\partial \sigma}{\partial t}$ = Applied stress rate, [$ML^{-1}T$].

A2.3 Analytical Solution

Terzaghi (1925, 1943) obtained the following analytical solution to equation A1 in terms of excess pore water pressure:

$$u_e = \sum_{N=0}^{\infty}\left(\frac{2\Delta\sigma_z}{M} \sin\frac{Mz_{dr}}{H_{dr}} \exp\left\{-M^2 T_v\right\}\right) \qquad [A3]$$

where

$\Delta\sigma_z$ = Change in vertical total stress, [MLT^{-2}];

z_{dr} = Distance from computational point to closest drainage boundary, [L];

H_{dr} = Length of longest drainage path, [L];

M = (2N+1) π/2, a constant, [ ];

T_v = Dimensionless time factor, $T_v = \dfrac{c_v t}{H^2{}_{dr}}$.

The coefficient of consolidation (c_v) is defined as:

$$c_v = \frac{K}{S_s} \qquad [A4]$$

where

K = Hydraulic conductivity, [LT^{-1}];

S_s = Specific storage, [L^{-1}].

Specific storage is defined as:

$$S_s = \gamma(\alpha + n\beta) \qquad [A5]$$

where

α = Compressibility of the porous medium skeleton, [$M^{-1}LT^2$];

β = Compressibility of the pore fluid, [$M^{-1}LT^2$];

n = Porosity, [ ];

γ = Specific weight of the pore fluid, [$ML^{-1}T^{-2}$].

Aboshi et al. (1970) extended Terzaghi's solution for an instantaneous total stress to the case of an increasing total stress applied at a constant rate.

For a layer of thickness H, with a permeable top and an impermeable base, subjected to an external pressure on the surface, the analytical solution (Aboshi et al., 1970) derived, for pore pressure at time t is:

$$u = \sum_{N=1,3,5..}^{n=\infty} \frac{2\Delta\sigma}{M_a^3 T_v} \sin\frac{M_a z}{H} \left\{1 - \exp\left(-M_a^2 T_v\right)\right\} \qquad [A6]$$

where

$\Delta\sigma_2$ = External total stress at time t, [MLT^{-2}];

M_a = $N\pi/2$, a constant, [ ].

A2.4 Numerical Analysis

Reeves et al. (2000) carried out a numerical simulation including incorporation of total stress change using a modified version of the USGS numerical code SUTRA. In order to check the validity of the modified code, the numerical results were compared with available analytical solutions.

Table A1 details the model parameters used for simulations using both the FEMWATER and SUTRA codes.

Table A1: Simulation Parameters

Parameter	SUTRA	FEMWATER	Dimensions	Units
Number of nodes	121	242		
Number of elements	100	100		
Density of water	999	999	ML^{-3}	kgm^{-3}
Intrinsic permeability	$1x10^{-14}$	$1x10^{-14}$	L^2T^{-1}	m^2
Compressibility of porous medium	$7.7x10^{-8}$	$7.7x10^{-8}$	LT^2M^{-1}	ms^2kg^{-1}
Compressibility of water	0	$4.4x10^{-10}$	LT^2M^{-1}	ms^2kg^{-1}
Simulation period	21600	21600	T	s

Figure A2 describes the head variation for sample problem applying a sinusoidal pore pressure variation using the original SUTRA code. Results for the analytical solution are shown as the solid line. The total hydraulic head applied at the model surface is varied according to:

$$H = 1 + 1.2\left[1 + \sin(\omega t)\right] \qquad [A7]$$

where

$\varpi = \frac{2\pi}{21600} \sec onds^{-1}$ is the period.

Reeves (2000) has an error in this equation, which appeared as $H = 2.2[1 + \sin(\omega t)]$.

The pore pressure response varies with depth and is both attenuated and delayed. The greatest delay and attenuation occur at the lower impermeable boundary of the model domain (z=0.0 m). The effective stress changes as a result of the varying pore pressure with constant total stress.

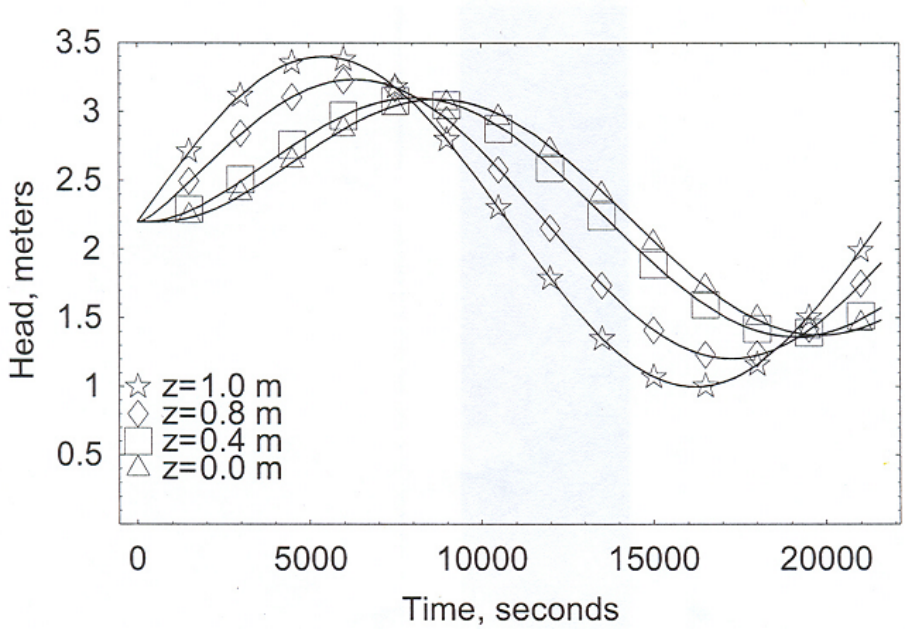

Figure A2: Variation of head for original SUTRA code (Adapted from Reeves et al., 2000)

Figure A3 shows the results for the modified code to incorporate the total stress term. The parameter H represents the water level that is varied to apply a varying total stress

representing the weight of the simulated water column applied at the surface. The solid line shows the analytical solution to the problem.

In this case the effective stress should remain unchanged as a result of the change in total stress and no attenuation or delay is expected if the pore fluid is incompressible (or relatively incompressible in comparison to the porous medium skeleton). The additional total stress is transferred instantaneously to the pore fluid.

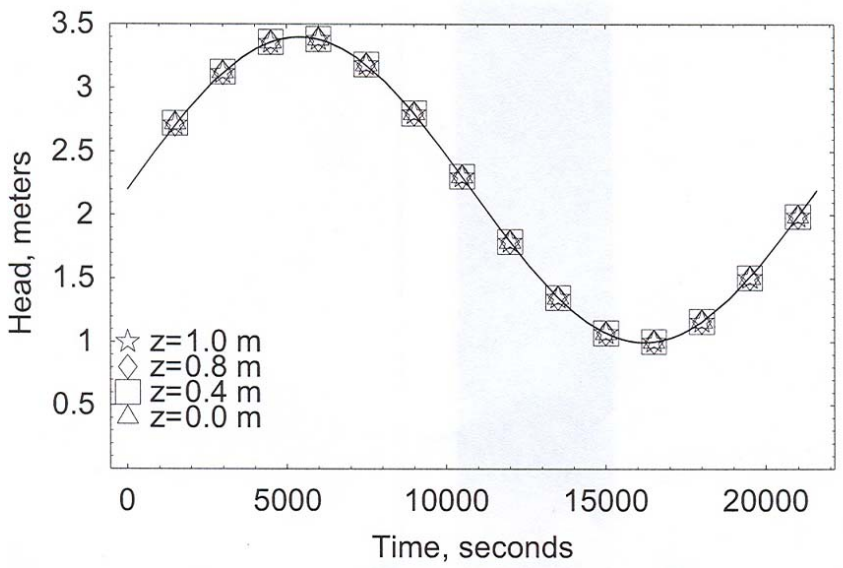

Figure A3: Variation of head for modified SUTRA code (Adapted from Reeves et al., 2000)

Figure A4 tests the ability of the modified SUTRA code to simulate the excess pore water pressure dissipation and the same problem domain. The results are compared with Terzaghi's analytical solution for consolidation equation.

A rapid change in total stress was applied over one simulation time-step (36 seconds) by adding 1 m of total head. The total stress was held constant for the remainder of the

simulation. The drainage boundary at the surface of the model domain was maintained at a total hydraulic head of 2 m and the 1 m excess pore pressure dissipates as time passes. Thee solid line shows the analytical solution.

Figures A2, A3 and A4 illustrate that the modified SUTRA code shows excellent agreement with the analytic solutions for these simple test problems.

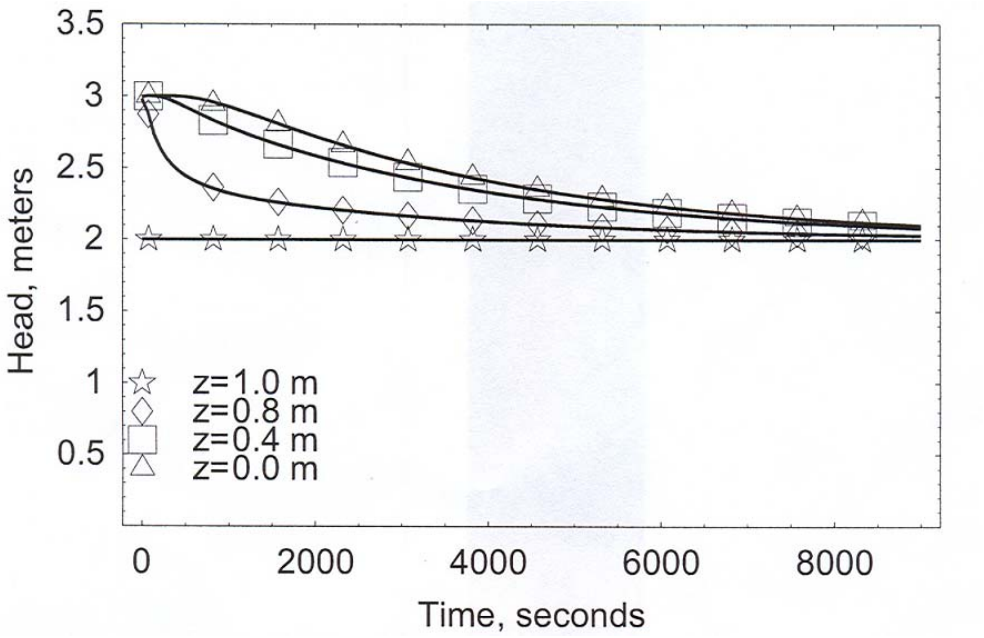

Figure A4: Consolidation problem results for the modified SUTRA code (Adapted from Reeves et al. 2000)

A2.5 FEMWATER Results

The mesh used for the FEMWATER simulation consisted of one hundred 3D blocks elements (242 nodes) with mesh dimensions of 10 x 10. The simulation ran for a period

of 6 hours (21600 seconds). This is almost identical to the SUTRA model domain (Reeves et al., 2000) with one hundred 2D elements (121 nodes).

The mesh and boundary conditions were described in Figure A1 and the material parameter values were given in Table A1. The FEMWATER parameters are identical to those used in the SUTRA simulations.

Figure A5 shows the numerical results for head variation obtained using the modified FEMWATER code. The analytical solution is shown as a solid line. The results compare with the analytical solution and the corresponding SUTRA results (Figure A2). Results are plotted for z elevations of 0.0, 0.4, 0.8 and 1.0 m corresponding to drainage path lengths of 1.0, 0.6, 0.2 and 0.0 m respectively.

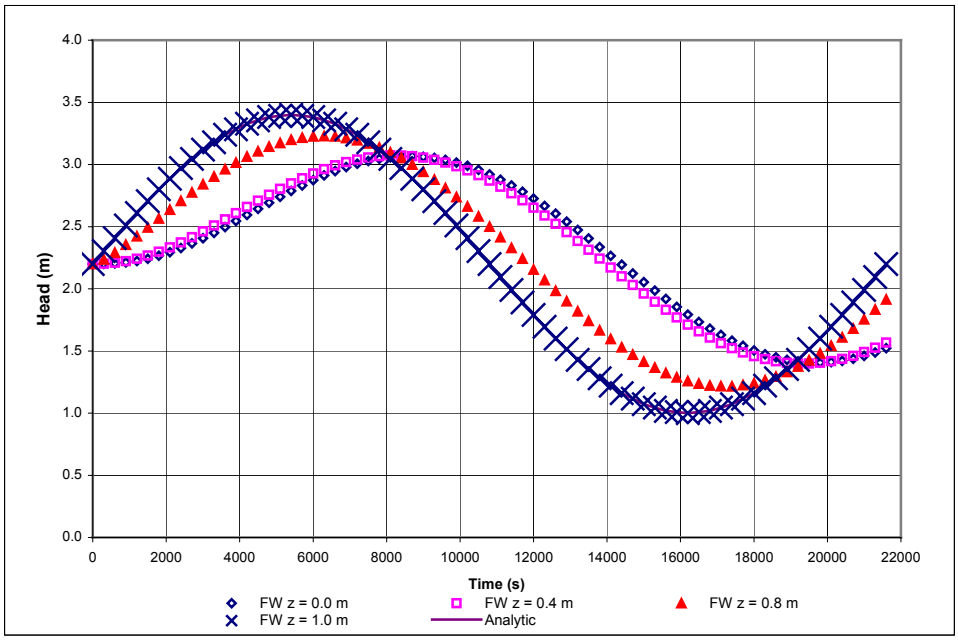

Figure A5: Comparison of simulated heads and analytic solution for constant total stress using the modified FEMWATER code

Figure A6 compares the results obtained for total stress loading with the modified FEMWATER code. The results match both the SUTRA results (Figure A3) and the analytic solutions.

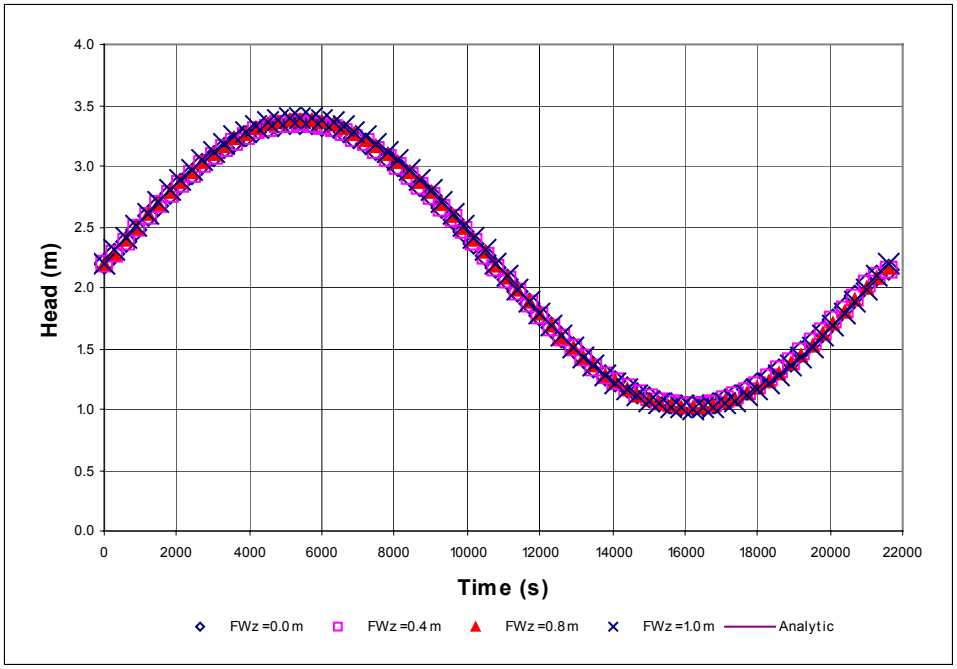

Figure A6: Comparison of simulated heads and analytic solutions for changing total stress using modified FEMWATER code

A comparison of simulation results for the consolidation problem and Terzaghi's analytical solution is shown in Figure A7 for the modified FEMWATER code. The results are plotted up to 9000 seconds. The total stress was increased from 2 m to 3 m rapidly within one time step (36 seconds) and then held constant for the rest of simulation period. This is exactly similar to the loading conditions of SUTRA model. Solid lines show the analytical solution. The numerical results agree very closely with the analytical solution. There is an excellent agreement between the similarly modified FEMWATER and SUTRA code results (Figure A4).

The FEMWATER results show a slight tendency towards delay and attenuation of the pore pressure response because the compressibility of water was assumed to be finite ($\alpha >> \beta$) rather than zero (with $\beta/\alpha = 4.4 \times 10^{-10} / 7.7 \times 10^{-8} = 0.0057$).

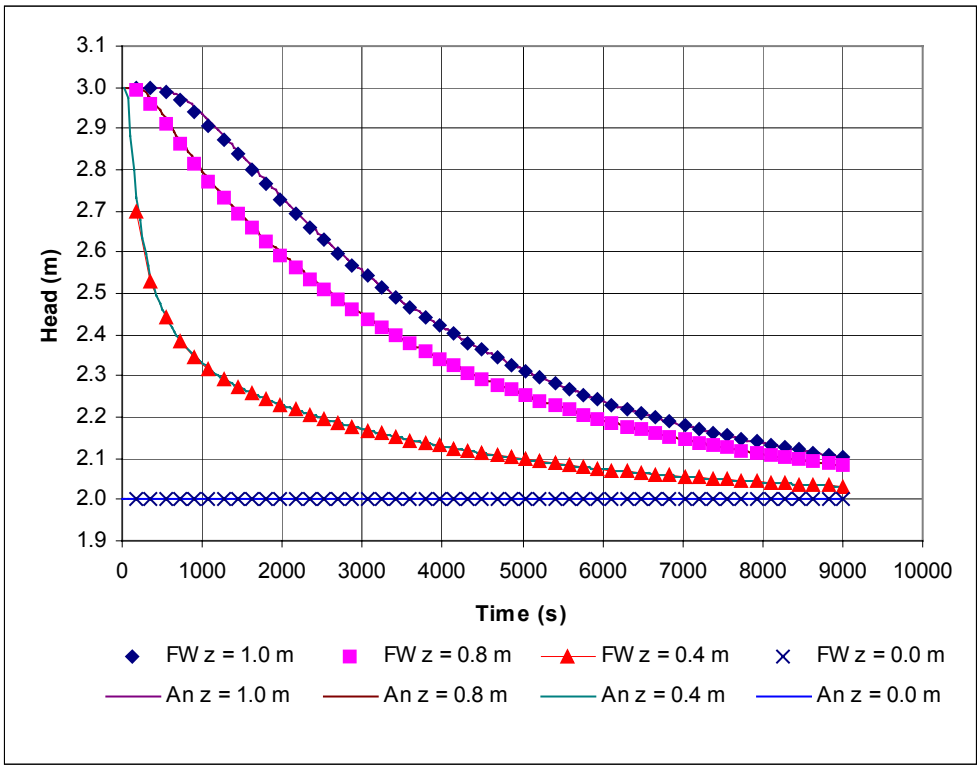

Figure A7: Comparison of FEMWATER results with Terzaghi's analytical solution

A second check of modified FEMWATER code was carried out by comparing the numerical solution with the Aboshi analytical solution for a constant loading rate. In this case, the total stress was increased from 2 m to 3 m over 30 time steps (1080 seconds) and kept constant for the rest of the 9000 seconds simulation period.

Figure A8 compares the FEMWATER results with Aboshi's analytical solution for pore pressure response. Excellent agreement can be observed between the numerical and analytical solutions.

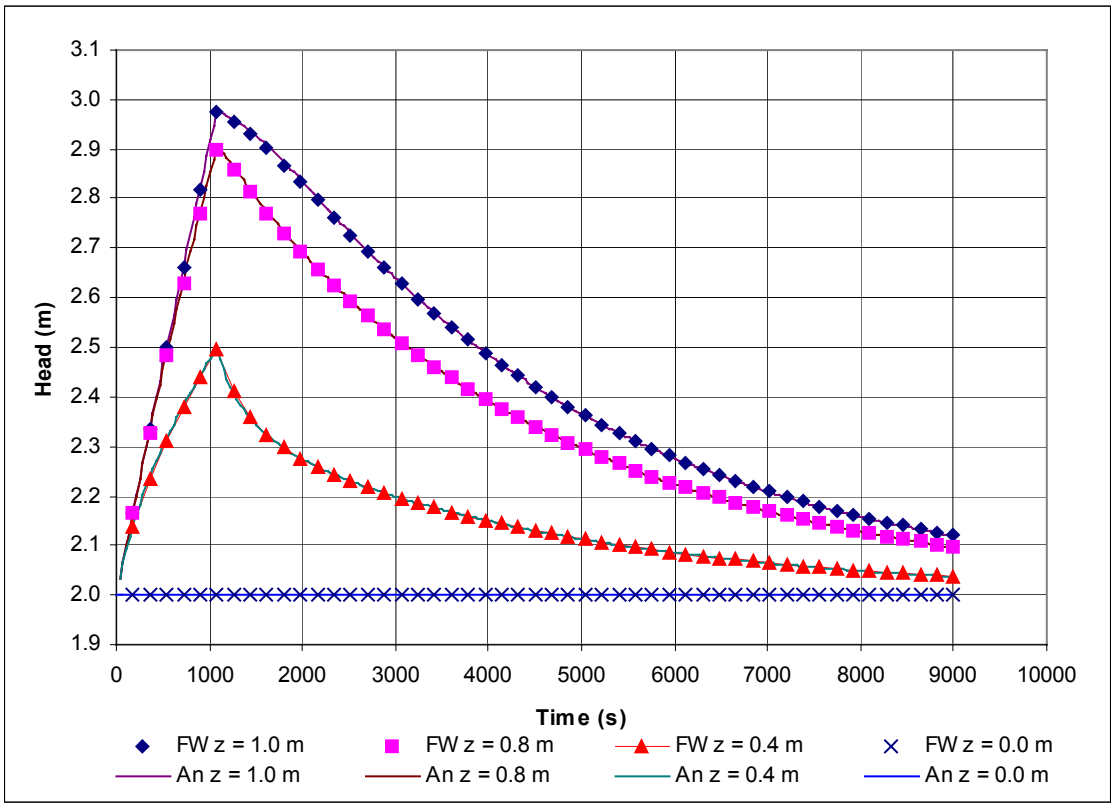

Figure A8: Comparison of FEMWATER results with Aboshi's analytical solution

The results demonstrate the ability of the modified FEMWATER code to reproduce one-dimensional total stress loading effects under saturated conditions.

The code has not been specifically adapted to correctly model total stress effects in the unsaturated zone. The assumptions for the FEMWATER code adaptations will remain reasonable for the unsaturated zone if soil deformation is negligible. This is likely the

case for overconsolidated tills but may not be valid for some lightly consolidated lacustrine clay.

Allowance for density dependence must be included in the calculation of total stress increments that must be input as equivalent freshwater heads corresponding to estimated fluid composition at the time of application. It is recommended that the Boussinesq distribution be used to estimate total stress variation with depth. For large areas of loading, such as waste rock piles, the radius of the pile may be many times greater than the depth under consideration for groundwater flows and applying a uniform stress beneath the footprint of the loaded area will be a reasonable approximation.

A2.6 References

Aboshi, H., Yoshikuni, H. and Maruyama, S. 1970. Constant Loading Rate Consolidation Test. Soil and Foundations. Vol. 10(1), pp: 44-56.

Lin, H.C., Richards, D.R., Talbot C. A., Yeh, G.T., Cheng, G.R., Cheng, H.P. and Jones, N.L. 2001. *FEMWATER: Three-Dimensional Finite Element Computer Model for Simulating Density-dependent Flow and Transport in Variably Saturated Media.* Version 3.0 Reference Manual, 587p

Reeves, H.W., Thibodeau, P.M., Underwood, R.G. and Gardner, L.R. 2000. *Incorporation of Total Stress Changes into the Groundwater Model SUTRA.* Groundwater. Vol.38 (1), pp: 89-98.

Terzaghi, K. 1925. Erdbaumechanik auf Bodenphysikalischer Grundlage. Leipzig und Wien: Franz Dueticke.

Terzaghi, K.1943. Theoretical Soil Mechanics, John Wiley, New York, 502p.

Voss, C.I. 1984. SUTRA, *A Finite Element Simulation Model for Saturated-Unsaturated Fluid-Density-Dependent Ground-water Flow with Energy Transport or Chemically Reactive Single-Species Solute Transport*. Water Resources Investigations Report 84-4369, U.S.Geological Survey, Reston Va.

APPENDIX B

B1 Loading Calculations: Pattern 1

Figure B1 outlines the cross sectional diagram of the pile. The 3D finite element mesh domain that represents the aquifer beneath the pile is also shown below the diagram. The entire mesh is not shown in the figure and is not drawn to the same vertical scale. The mesh dimension below the pile is 1200 m x 60 m. The width of an element is 40 m and the depth is 2.857 m (60 /21 layers).

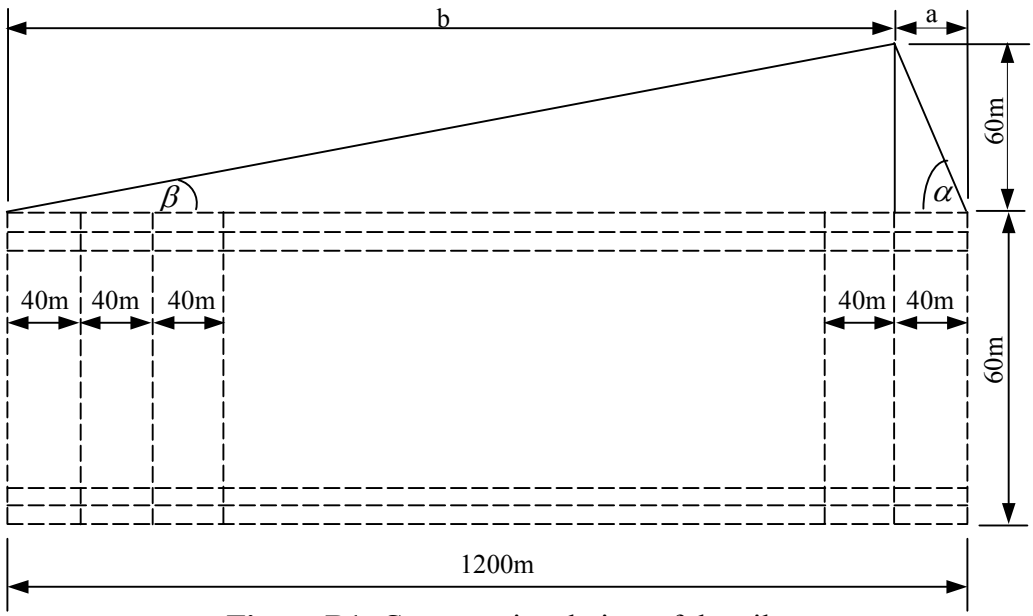

Figure B1: Cross sectional view of the pile

A cross sectional view of the pile constructed after the first three years is shown in Figure B2. For modelling purposes, as described in section 4.4.1, the pile was initially constructed in 30 years and therefore 30 loading increments are needed. Subsequently the loading rate was changed to finish construction of pile in 15, 25 and 35 years. The pile is constructed in such a way that the volume of the tailings added to the pile after each year is equal. Therefore the areas A_1 (abdc), A_2 (cdgf), $A_3 \ldots A_{30}$ are equal. It is assumed that the location of peak pile height after each year coincides with a mesh node (points *c* and *f* etc.). This assumption is used to simplify complex loading calculations.

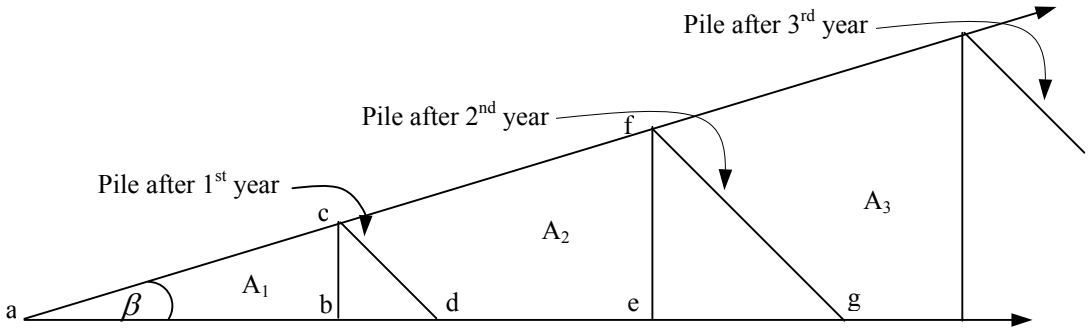

Figure B2: Pile cross section after first 3 years

Figure B3 describes the procedure used to distribute the load over the mesh elements. All the loads are calculated per meter length of the pile.

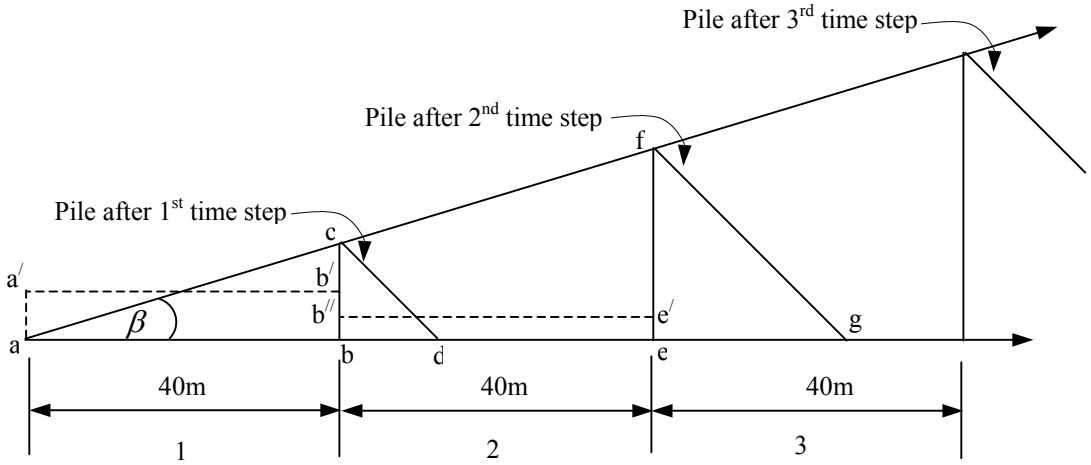

Figure B3: Load distribution over the mesh

From the geometry of Figure B3:

After 1st time step, the load on triangular area *abc* per meter length = Uniform load of rectangular area $abb^{/}a^{/}$ per meter length.

Load on triangular area *bcd* per meter length = Uniform load of rectangular area $bee^{/}b^{//}$ per meter length.

By equating the areas, the average height at the middle of each element is calculated. This height is proportional to the pressure head applied on the element at the corresponding time period to represent the total stress increment. This methodology is followed for the entire pile to calculate the loads on each element after each time interval.

The parameters used for loading pattern 1 calculations are given in the Table B1 below.

Table B1: Pile load calculation parameters

Parameter	Value
Mesh size (dx)	40 m
Time period of pile construction (t)	30 years
Maximum pile base width (a+b)	1200 m
Maximum pile height (h)	60 m
Pile cross sectional area after 30 yrs (A)	36000 m^2
Rate of change of pile area (dA/dt)	1200 m^2/yr
Scarp slope angle (α)	56.31°
Dip slope angle (β)	2.96°
Specific gravity of pile material	1.5
Specific gravity of brine	1.2
Specific gravity of berm material	2.0

Figure B4 is an illustration of the dimensions of the pile cross section required for estimating loading in pattern 1. Based on the information given in the Table B1, pile height (h), base dimensions (a and b) and cross sectional area (A) after each time interval are estimated. Area increment at the edges of each mesh is calculated based on the dimensions found. Time period required to fill out each area increment is then calculated using the rate of change of area (dA/dt) and the area calculated (A).

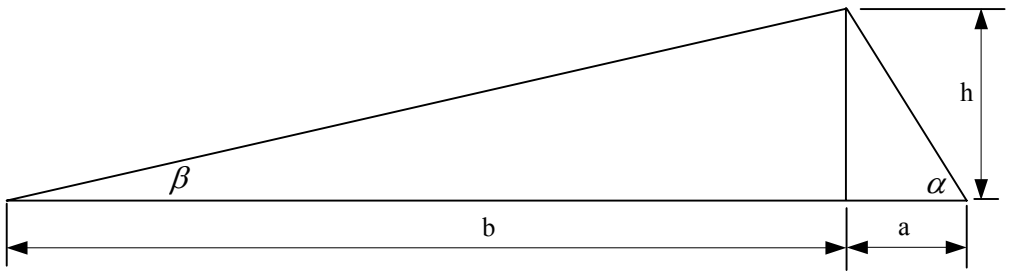

Figure B4: Pile dimensions for loading pattern 1

Calculated time periods were rounded off so that they are exact multiple of 365 days. This ensures that the loads are calculated exactly corresponding to the model time steps.

Table B2 details the pile dimensions estimated for loading pattern 1.

Table B2: Pile dimensions for loading pattern 1

Dip Slope Base b (m)	Scarp Slope Base a (m)	Pile Base a+b (m)	Peak Pile Height h (m)	Pile Cross Sectional Area A (m^2)
40	1.38	41.38	2.07	42.81
80	2.76	82.76	4.14	171.22
120	4.14	124.14	6.21	385.26
160	5.52	165.52	8.28	684.90
200	6.90	206.90	10.34	1070.15
240	8.28	248.28	12.41	1541.02
280	9.66	289.66	14.48	2097.50
320	11.03	331.03	16.55	2739.60
360	12.41	372.41	18.62	3467.30
400	13.79	413.79	20.69	4280.62
440	15.17	455.17	22.76	5179.55
480	16.55	496.55	24.83	6164.09
520	17.93	537.93	26.90	7234.24
560	19.31	579.31	28.97	8390.01
600	20.69	620.69	31.03	9631.39
640	22.07	662.07	33.10	10958.38
680	23.45	703.45	35.17	12370.99
720	24.83	744.83	37.24	13869.20
760	26.21	786.21	39.31	15453.03
800	27.59	827.59	41.38	17122.47
840	28.97	868.97	43.45	18877.53
880	30.34	910.34	45.52	20718.19
920	31.72	951.72	47.59	22644.47
960	33.10	993.10	49.66	24656.36
1000	34.48	1034.48	51.72	26753.86
1040	35.86	1075.86	53.79	28936.98
1080	37.24	1117.24	55.86	31205.71
1120	38.62	1158.62	57.93	33560.05
1160	40.00	1200.00	60.00	36000.00

Figure B5 describes the calculation of equivalent heights after each time interval.

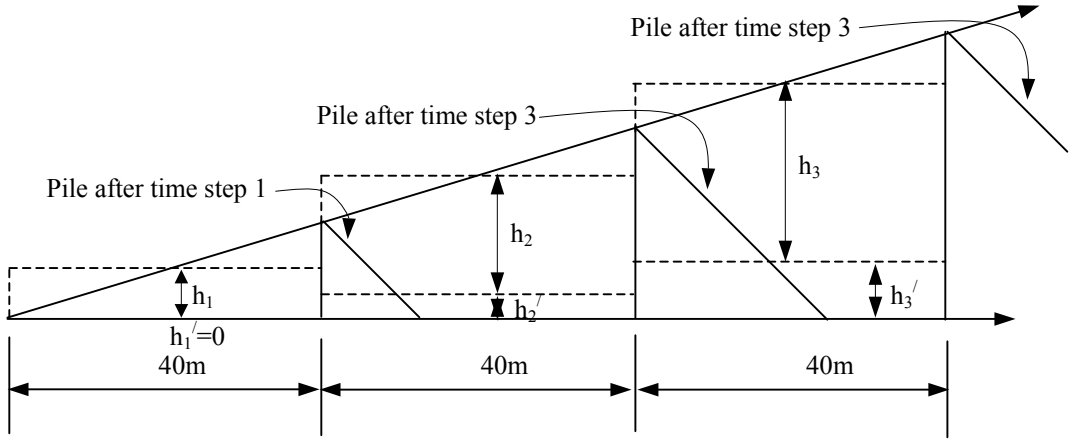

Figure B5: Pile uniform heights calculation diagram

From Figure B5:

Equivalent pile height on mesh element 1 after time step 1 = h_1

Equivalent pile height on mesh element 2 after time step 1 = $h_2^{/}$

Equivalent pile height on mesh element 2 after time step 2 = h_2

Equivalent pile height on mesh element 3 after time step 2 = $h_3^{/}$

where

h_i = Equivalent pile height on i th element at time interval t, [L];

$h_i^{/}$ = Equivalent pile height on i th element due to previous load step at time interval t, [L].

Using this method, the uniform equivalent pile heights on each element after each time interval are calculated. Table B3 describes rounded off time intervals and the equivalent pile heights used for loading calculations.

Table B3: Tabulation of equivalent pile heights for time steps

Time Step Number	Time Step (days)	Dip Node Height h_i(m)	Scarp Node Height $h_i^{/}$(m)	h_i (m)+ $h_i^{/}$(m)
1	14.60	1.05	0.00	1.05
2	51.10	3.11	0.04	3.15
3	116.80	5.10	0.14	5.24
4	208.05	7.02	0.32	7.34
5	324.85	8.86	0.57	9.43
6	467.20	10.64	0.89	11.53
7	638.75	12.34	1.28	13.62
8	832.20	13.97	1.75	15.72
9	1054.85	15.54	2.28	17.82
10	1303.05	17.03	2.89	19.92
11	1576.80	18.44	3.57	22.01
12	1876.10	19.79	4.32	24.11
13	2200.95	21.07	5.14	26.21
14	2551.35	22.27	6.03	28.30
15	2930.95	23.40	6.99	30.39
16	3332.45	24.47	8.03	32.50
17	3763.15	25.46	9.13	34.59
18	4219.40	26.38	10.31	36.69
19	4701.20	27.22	11.56	38.78
20	5208.55	28.00	12.88	40.88
21	5741.45	28.71	14.27	42.98
22	6303.55	29.34	15.73	45.07
23	6887.55	29.90	17.27	47.17
24	7500.75	30.39	18.87	49.26
25	8135.85	30.81	20.55	51.36
26	8800.15	31.16	22.29	53.45
27	9490.00	31.44	24.11	55.55
28	10209.05	31.64	26.00	57.64
29	10950.00	31.78	27.97	59.75

A specimen calculation for pile load is given below:

Consider the load after 14.60 days:

Time increment for this step = 14.60-0.00

= 14.60 days

Specific gravity of pile material = 1.5

Equivalent height of pile for element 1 = 1.05 m

Loading rate for element 1 for 1st time step = (1.5 x 1.05)/14.60

= 0.1077m/d (m of freshwater equivalent)

Equivalent height of pile for element 2 = 0.04 m

Loading rate for element 1 for 1st time step = (1.5 x 0.04)/14.60

= 0.0037m/d (m of freshwater equivalent)

Consider the load after 51.10 days:

Time increment for this step = 51.10-14.60

= 36.50 days

Specific gravity of pile material = 1.5

Equivalent height of pile for element 2 = 3.11 m

Loading rate for element 2 for 2nd time step = (1.5 x 3.11)/36.50

= 0.1278m/d (m of freshwater equivalent)

Equivalent height of pile for element 3 = 0.14 m

Loading rate for element 3 for 2nd time step = (1.5 x 0.14)/36.50

= 0.0059m/d (m of freshwater equivalent)

And so on …..

The calculated loads for each time interval are tabulated in Table B4 below.

Table B4: Tabulated loads for each time interval

Time Step Number	Cumulative Time (days)	Time Interval (days)	Incremental Load Rate (for h_i, m/d)	Incremental Load Rate (for $h_i^{/}$, m/d)
1	14.60	14.60	0.1077	0.0037
2	51.10	36.50	0.1278	0.0059
3	116.80	65.70	0.1164	0.0073
4	208.05	91.25	0.1153	0.0094
5	324.85	116.80	0.1138	0.0115
6	467.20	142.35	0.1121	0.0135
7	638.75	171.55	0.1079	0.0153
8	832.20	193.45	0.1084	0.0177
9	1054.85	222.65	0.1047	0.0195
10	1303.05	248.20	0.1029	0.0216
11	1576.80	273.75	0.1011	0.0237
12	1876.10	299.30	0.0992	0.0257
13	2200.95	324.85	0.0973	0.0278
14	2551.35	350.40	0.0953	0.0299
15	2930.95	379.60	0.0925	0.0317
16	3332.45	401.50	0.0914	0.0341
17	3763.15	430.70	0.0887	0.0359
18	4219.40	456.25	0.0867	0.0380
19	4701.20	481.80	0.0848	0.0401
20	5208.55	507.35	0.0828	0.0422
21	5741.45	532.90	0.0808	0.0443
22	6303.55	562.10	0.0783	0.0461
23	6887.55	584.00	0.0768	0.0485
24	7500.75	613.20	0.0743	0.0503
25	8135.85	635.10	0.0728	0.0527
26	8800.15	664.30	0.0704	0.0545
27	9490.00	689.85	0.0684	0.0565
28	10209.05	719.05	0.0660	0.0583
29	10950.00	740.95	0.0643	0.0607

B2 Loading calculation for brine pond

Average height of the brine pond was assumed to remain constant throughout the period of construction. Load is applied over the first year only.

Height of brine pond for construction period = 2 m

Therefore, the average loading rate = (2 x 1.2)/365

= 0.00657m/d (m of freshwater equivalent)

B3 Loading calculation for berm

Average height of the berm was assumed to remain constant throughout the period of construction. Load is applied over the first year only

Height of Berm for construction period = 3 m

The pile load = (3 x 2)/365

= 0.01644m/d (m of freshwater equivalent)

Loads for berm and brine pond remain same throughout the construction period.

B4 Loading calculations: Pattern 2

Unlike the loading pattern 1, all the elements in the modelling domain are loaded after each time interval. Pile geometry and dimensions are same as loading pattern 1. Final height of the pile remains 60 m.

Figure B6 shows the loading sequence for loading pattern 2. The pile is loaded in equal volume increments of tailings for each time interval ($A_1=A_2=A_3$……..$A_{29}=A_{30}$). Figure B6 is not drawn to scale.

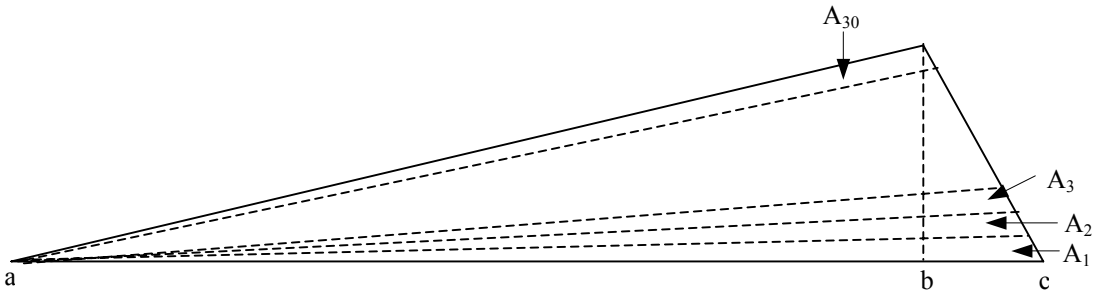

Figure B6: Loading pattern 2

Figure B7 illustrates the calculation of height of pile after each time interval. Unlike pattern 1, the procedure is very straight forward and loads applied after each year can be directly calculated. After each time interval, loads are applied to all elements over the footprint of the pile. The average pile height increment for every time interval (from 1-30 years) will be the same. After the average heights were calculated, the pile loads are calculated using the similar methodology used for loading pattern 1 to account for material densities.

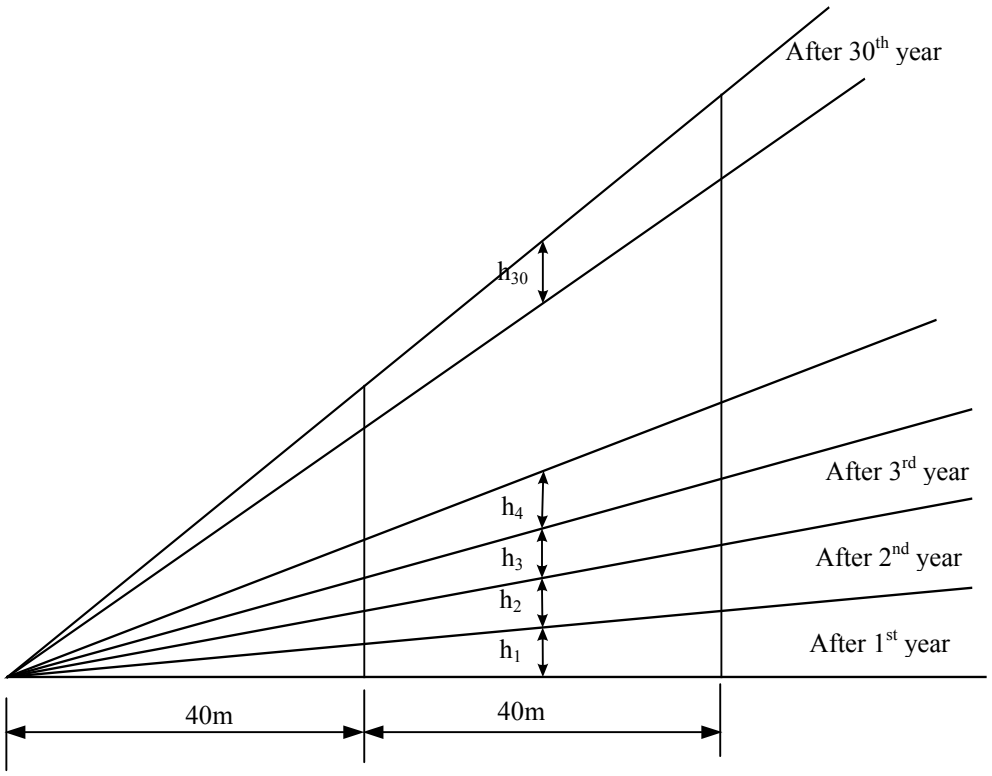

Figure B7: Expanded view for first two elements for loading pattern 2

As illustrated in Figure B7, for elements load 2, $h_1 = h_2 = h_3 ..... = h_{29} = h_{30}$. This is same for a to b in Figure B6.

For last element layer (from **b** to **c** in Figure B6), the above procedure cannot be used because of the geometry. For this element, the uniform heights are based on rectangular area method (refer Figure B5 for method).

Table B5 lists the pile loads for first 29 elements in loading pattern 2 (**a** to **b** in Figure B6).

Table B5: Average pile height for all time steps up to end of construction (**a** to **b** in Figure B6)

Element Number	Average pile height (m)	Pile load (m/d)
1	0.034	0.00014
2	0.103	0.00043
3	0.172	0.00071
4	0.241	0.00099
5	0.310	0.00128
6	0.379	0.00156
7	0.448	0.00184
8	0.517	0.00213
9	0.586	0.00241
10	0.655	0.00269
11	0.724	0.00298
12	0.793	0.00326
13	0.862	0.00354
14	0.931	0.00383
15	1.000	0.00411
16	1.069	0.00439
17	1.138	0.00468
18	1.207	0.00496
19	1.276	0.00524
20	1.345	0.00553
21	1.414	0.00581
22	1.483	0.00609
23	1.552	0.00638
24	1.621	0.00666
25	1.690	0.00694
26	1.759	0.00723
27	1.828	0.00751
28	1.897	0.00779
29	1.966	0.00808

For 30th element layer (**b** to **c** in Figure B6) the average pile height varies for each time interval and the corresponding pile heights and loads are given in Table B6.

Table: B6: Pile height increments and loading rates for 30th element

Time (Days)	Equivalent Pile Height (m)	Pile Loading Rate (m/d)
365	1.935	0.00795
730	1.873	0.00770
1095	1.810	0.00744
1460	1.747	0.00718
1825	1.684	0.00692
2190	1.621	0.00666
2555	1.557	0.00640
2920	1.494	0.00614
3285	1.430	0.00587
3650	1.365	0.00561
4015	1.301	0.00535
4380	1.236	0.00508
4745	1.171	0.00481
5110	1.106	0.00455
5475	1.041	0.00428
5840	0.976	0.00401
6205	0.910	0.00374
6570	0.844	0.00347
6935	0.778	0.00320
7300	0.711	0.00292
7665	0.645	0.00265
8030	0.578	0.00237
8395	0.511	0.00210
8760	0.443	0.00182
9125	0.376	0.00154
9490	0.308	0.00127
9855	0.240	0.00099
10220	0.172	0.00071
10585	0.103	0.00042
10950	0.034	0.00014

B5 Stress Distribution Calculation

Unlike the loading, the stress for each element is different due to non-uniformity of vertical stress distribution throughout the modelling domain with sequential pile construction. By calculating stress intensity factors, stress due to pile load on each node can be calculated. The Newmark method (Newmark, 1940) is used to calculate the stress intensity factors for each element in the model. The Newmark method is described in details in section 3.3.3. This section describes the technical details of calculating Stress Intensity Factors.

The element size for the model is 40 m x 40 m x 2.857 m. There are 800 elements (40 x 20) in a layer and the total number of layers is 21. Nodal stress intensity factors depend on the xyz location of the element within the mesh. A program was written in Excel to calculate the intensity factors at each node.

Average stress intensity factors for each element are then determined by considering the average of intensity factors for eight nodes for each rectangular element. Since the loading rate for each element is already determined, the incremental stress can be calculated by direct multiplication of loading rate and intensity factor.

The Visual Basic function used for determining stress intensity factors using Newmark method is given below:

```
Function Newmark (i As Integer, j As Integer, dx As Single, dy As Single, z As Single)
As Single
Pi = 4 * Atn(1)
x = i * dx
y = j * dy
R = Sqr(x ^ 2 + y ^ 2 + z ^ 2)
a = 2 * x * y * z * R / (x ^ 2 * y ^ 2 + z ^ 2 * R ^ 2)
F = a / Sqr(1 - a ^ 2)
If (x * y / z < R) Then
b = Atn(F)
Else
b = Pi - Atn(F)
End If
Newmark = (a * (1 + (z / R) ^ 2) + b) / (4 * Pi)
End Function
```

Using the above function, intensity factors for nodes for each element are calculated. The average stress intensity factor for each element is then calculated.

APPENDIX C

C1 FEMWATER code input modification for total stress

As previously discussed FEMWATER source code was modified to facilitate the inclusion total stress changes as a result of pile loading. In assigning boundary conditions, an additional term (PS3 card) is used for assigning an incremental total stress term for each element.

XY1 series are used to specify the stresses and the corresponding time period. The series are then related to corresponding elements by PS3 cards. Material properties and boundary conditions are supplied to the FEMWATER model through the 3bc file. An example for a 3bc file is given below.

C2 Example 3bc File for 15 years of pile loading run

The following file is given below to understand the sequence of assigning boundary conditions to the FEMWATER model.

```
3DFEMWBC
T1  Total stress variation below a salt pile berm/pond modified
T2  Stress distribution for a period of 15 years step 1.825 days
T3
OP1  10
OP2  1   1   1   0   1  22
OP3  1.00000000e+000 1.00000000e+000 1.00000000e+000 1.00000000e-002
1.50000000e+000 5.00000000e-003 6.66700000e-001
OP4    1
IP1  50 1 800 1.00000000e-004 1.00000000e-004 1
IP2  40 400 1.00000000e-002
IP3  10 5.00000000e-001 1.00000000e-002 5.00000000e-002
PT1  1   1   1   2
TC1  1.46018250e+004
TC2  0  1.8250
OC1  0   0   0  100
OC2  1   1
OC3  1   0  100
OC4  1   1
MP1  0
MP3  1.00000000e+003 1.12000000e+002 7.32000000e+010 5.89000000e-020
MP4  1.0000000e+000 0.0000000e+000 0.0000000e+000 0.0000000e+000
1.0000000e+000 0.0000000e+000 0.0000000e+000 0.0000000e+000
XY1 1 2 0 0 0 0.0 "dense_sand_mc"
-10.0 0.25
  0.0 0.25
XY1 2 2 0 0 0 0.0 "stiff_till_mc"
-10.0 0.38
  0.0 0.38
XY1 3 2 0 0 0 0.0 "plastic_clay_mc"
-10.0 0.40
  0.0 0.40
XY1 4 2 0 0 0 0.0 "rc"
-10.0 1.0
  0.0 1.0
XY1 5 2 0 0 0 0.0 "wc"
-10.0 0.0
  0.0 0.0
MP2   1 8.64e-00 8.64e-00 8.64e-00 0.0 0.0 0.0 2.50e-18 2.50e-01 1.00
MP5   1 0.0 0.0 0.0 0.0 0.0 1.00 0.0 0.0 0.0 0.0
SP1   1   1   4   5
MP2   2 8.64e-04 8.64e-04 8.64e-04 0.0 0.0 0.0 2.50e-17 3.80e-01 1.00
MP5   2 0.0 0.0 0.0 0.0 0.0 1.00 0.0 0.0 0.0 0.0
SP1   2   2   4   5
MP2   3 8.64e-05 8.64e-05 8.64e-05 0.0 0.0 0.0 5.00e-16 4.00e-01 1.00
MP5   3 0.0 0.0 0.0 0.0 0.0 1.00 0.0 0.0 0.0 0.0
SP1   3   3   4   5
XY1 6 1 0 0 0 0.0 constant
0.000 3.0
XY1 7 1 0 0 0 0.0 constant
0.000 1.0
```

```
XY1 8 5 0 0 0 0.0  Load increments beneath berm (Series 8-54)
    0.00 0.0
  365.00 0.01316
  368.65 0.0
  372.30 0.0
  375.95 0.0
```

```
XY1 54 5 0 0 0 0.0
    0.00 0.0
  365.00 0.00602
  368.65 0.0
  372.30 0.0
  375.95 0.0
XY1 55 5 0 0 0 0.0 Load increments beneath pond (Series 55-101)
    0.00 0.0
  365.00 0.00770
  368.65 0.0
  372.30 0.0
  375.95 0.0
```

```
XY1 101 5 0 0 0 0.0
    0.00 0.0
  365.00 0.00347
  368.65 0.0
  372.30 0.0
  375.95 0.0
XY1 102 5 0 0 0 0.0 Load increments beneath Pile dip slope (Series 102-
1312)
 0.000   0.0
 7.300   0.08208
 9.125   0.0
 10.950  0.0
 12.750  0.0
```

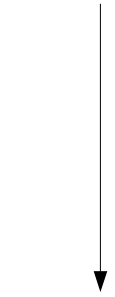

```
XY1 1312 5 0 0 0 0.0
0.000 0.0
4745.000    0.0
5104.525    0.11660
5475.000    0.12860
5476.825    0.0
XY1 1313 4 0 0 0 0.0 Load increments beneath pile scarp slope (Series
1313-1347)
0.000 0.0
5104.525    0.0
5475.000    0.04614
5476.825    0.0
```

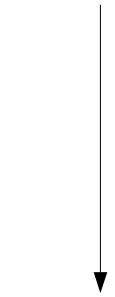

```
XY1 1347 4 0 0 0 0.0
   0.000    0.0
5104.525    0.0
5475.000    0.09106
5476.825    0.0
RS3 0.0  0.0
PS3 9390 8 (PS3- element number-XY1 series)
PS3 9358 8
PS3 9326 8
PS3 9294 9
PS3 9262 9
PS3 9230 10
PS3 9198 11
PS3 9166 12
PS3 9134 13
PS3 9102 14
```

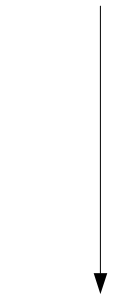

```
PS3 34842 1347
PS3 34843 1347
PS3 34844 1347
PS3 34845 1347
PS3 34846 1347
PS3 34847 1347
PS3 34848 1347
DB1     1     7   (Dirichlet boundaries)
DB1     2     7
DB1     3     7
DB1     4     7
DB1     5     7
DB1     6     7
DB1     7     7
DB1     8     7
DB1     9     7
DB1    10     7
```



```
DB1 47182     7
DB1 47183     7
DB1 47184     7
DB1 47185     7
DB1 47186     7
DB1 47187     7
DB1 47188     7
DB1 47189     7
DB1 47190     7
ICH  0 0.0
ICC  0 0.0
ICS  0
ICT  0.0
ICF  0   0   0
END
```

For berm and brine pond, a fixed loading rate is applied for the first year of the modelling period to simulate construction. A number of XY1 series are needed because of the variation of stress intensity factors throughout the model domain. In this particular example series 8 to 54 belong to berm. Series 55 to 101 belong to brine pond. For pile

region, loading rate varies with time. In addition stress intensity factors vary. Therefore, a large number of XY series are needed. In this problem, series numbers 102 to 1347 represent pile: (102-1312) dip slope, (1313-1347) scarp slope. The XY series are related to elements by means of PS3 cards. A detailed description of the 3bc file and abbreviations used in the file can be found in the FEMWATER User's Manual (Lin et al, 2001).